AD_____

AWARD NUMBER: W81XWH-12-1-0613

TITLE: HOXC9-Induced Differentiation in Neuroblastoma Development

PRINCIPAL INVESTIGATOR: Han-Fei Ding

RECIPIENT: Georgia Health Sciences University Research Institute, Inc.
Augusta, GA 30912

REPORT DATE: October 2014

TYPE OF REPORT: Annual Report

PREPARED FOR: U.S. Army Medical Research and Materiel Command
Fort Detrick, Maryland 21702-5012

REPORT DOCUMENTATION PAGE

Form Approved
OMB No. 0704-0188

1. REPORT DATE *(DD-MM-YYYY)*	2. REPORT TYPE	3. DATES COVERED *(From - To)*
October 2014	Annual	30 Sep 2013 – 29 Sep 2014

4. TITLE AND SUBTITLE
HOXC9-Induced Differentiation in Neuroblastoma Development

5a. CONTRACT NUMBER

5b. GRANT NUMBER
W81XWH-12-1-0613

5c. PROGRAM ELEMENT NUMBER

6. AUTHOR(S)
Han-Fei Ding, Ph.D.

email: hding@gru.edu

5d. PROJECT NUMBER

5e. TASK NUMBER

5f. WORK UNIT NUMBER

7. PERFORMING ORGANIZATION NAME(S) AND ADDRESS(ES)
Georgia Regents University Research Institute, Inc.
Augusta, GA 30912-4810

8. PERFORMING ORGANIZATION REPORT NUMBER

9. SPONSORING / MONITORING AGENCY NAME(S) AND ADDRESS(ES)
U.S. Army Medical Research and Materiel Command

FORT DETRICK MD 21702-5012

10. SPONSOR/MONITOR'S ACRONYM(S)

11. SPONSOR/MONITOR'S REPORT NUMBER(S)

12. DISTRIBUTION / AVAILABILITY STATEMENT

Approved for public release; distribution unlimited

13. SUPPLEMENTARY NOTES

14. ABSTRACT The overall objective of this project is to test the hypothesis that HOXC9 expression levels have a causal role in determining the differentiation states of neuroblastoma tumors, with higher levels of HOXC9 promoting differentiation. At the cellular level, HOXC9 promotes the differentiation of neuroblastoma stem cells. At the molecular level, HOXC9 activates the H3K4 demethylase KDM5B and the H3K27 demethylase KDM6B for global control of its differentiation program. During the second budget year of this grant, significant progress has been made in the proposed studies, which is described in detail in the **Overall Project Summary** section below. Briefly, we have 2 publications reporting our new findings on the molecular mechanism by which HOXC9 induces neuronal differentiation of neuroblastoma cells. We show that HOXC9 directly regulate a large number of genes involved in neuronal differentiation, upregulating neuronal genes and downregulating cell cycle and DNA repair genes. For Aim 1, we have completed the experiments proposed in MYCN mouse tumor development studies. For Aim 2, we have developed a culture system for enriching and long-term propagating neuroblastoma stem cell and shown that high Hoxc9 expression is essential for their differentiation induced by RA. For Aim 3, we have identified 3 modes of epigenetic regulation of transcription by HOXC9 that involve modulation of H3K4me3 and H3K27me3 levels, thereby providing a molecular basis for the role of KDM5B and KDM6B in the control of neuroblastoma differentiation. These findings significantly advance our molecular understanding of neuroblastoma differentiation and suggest new targets for neuroblastoma therapy.

15. SUBJECT TERMS
Cancer stem cells, Chromatin immunoprecipitation and sequencing (ChIP-seq), Epigenetics, Histone H3 methylation, Histone H3 demethylases (KDMs), HOXC9, Mouse model of neuroblastoma (MYCN mice), neuroblastoma differentiation; Retinoic acid (RA)

16. SECURITY CLASSIFICATION OF:			17. LIMITATION OF ABSTRACT	18. NUMBER OF PAGES	19a. NAME OF RESPONSIBLE PERSON
					USAMRMC
a. REPORT	b. ABSTRACT	c. THIS PAGE	UU	44	19b. TELEPHONE NUMBER *(include area code)*
U	U	U			

Standard Form 298 (Rev. 8-98)
Prescribed by ANSI Std. Z39.18

Table of Contents

INTRODUCTION:

Neuroblastoma is a common pediatric cancer of the sympathetic nervous system [1]. It is a heterogeneous group of tumors, ranging from tumors composed predominantly of poorly differentiated neuroblasts to those consisting largely of differentiated neurons. Patients with poorly differentiated neuroblastoma have a significantly poorer prognosis than those with differentiated neuroblastoma. The molecular mechanisms underpinning neuroblastoma heterogeneity are largely unknown [2-5]. Our hypothesis is that HOXC9 expression levels have a causal role in determining the differentiation states of neuroblastoma tumors, with higher levels of HOXC9 promoting differentiation [6, 7]. At the cellular level, HOXC9 promotes the differentiation and represses the self-renewal of neuroblastoma stem cells. At the molecular level, HOXC9 activates the H3K4 demethylase KDM5B and the H3K27 demethylase KDM6B for global control of its differentiation program. The study supported by this award has three specific aims: **1) to investigate the role of HOXC9 in neuroblastoma development; 2) to investigate the role of HOXC9 in neuroblastoma stem cell differentiation;** and **3) to investigate the molecular mechanism for global control of HOXC9-induced differentiation.** Identification and characterization of neuroblastoma stem cells will advance our understanding of neuroblastoma heterogeneity and provide a key cellular target for earlier detection of neuroblastoma, for better prediction of clinical outcomes, and for cancer stem cell-based drug discovery. A molecular understanding of HOXC9-induced differentiation will open new avenues for the development of more effective differentiation-based neuroblastoma therapies.

1. KEYWORDS:

Cancer stem cells, Chromatin immunoprecipitation and sequencing (ChIP-seq), Epigenetics, Histone H3 methylation, Histone H3 demethylases (KDMs), HOXC9, Mouse model of neuroblastoma (MYCN mice), neuroblastoma differentiation; Retinoic acid (RA)

2. OVERALL PROJECT SUMMARY:

Task 1. To investigate the role of HOXC9 in neuroblastoma development (months 3-26)

The goal of Task 1 is to test the hypothesis that HOXC9 expression levels have a causal role in determining the differentiation states of neuroblastoma tumors. We will examine the effects of Hoxc9 deficiency and heterozygosity on the differentiation states of neuroblastoma tumors developed in *MYCN* mice, an animal model of the human disease. As differentiation states affect tumor development, we will also examine the effects of Hoxc9 deficiency and heterozygosity on neuroblastoma initiation and progression in *MYCN* mice. A total of 492 mice will be used for breeding (n = 144) and for the proposed hyperplasia (n = 108) and tumor development (n = 240) studies.

The Task 1 experiments outlined in the approved SOW for the second budget year include tumor development studies and microarray analysis.

Task 1.2. Tumor development studies (months 13-24): 40 mice for each group (6 groups, n=240) will be monitored for tumor development. Animals that are moribund will be euthanized and subjected to full autopsy. Tumors will be removed, measured for weight and sectioned for H&E and immunofluorescence staining for nestin, Phox2B and TH. The stained sections will be examined with regular and confocal fluorescent microscopes and positive cells will be quantified from randomly selected fields. We will also quantify tumor cells expressing nestin, Phox2B and/or TH by immunoflow cytometry.

We have finished the collection, section and H&E staining of tumors developed in $Hoxc9^{+/+}$ and $Hoxc9^{+/-}$ mice with *MYCN*. We have also completed immunofluorescence staining and quantification of tumor cells that express nestin (stem cell marker), Phox2B (progenitor cell marker) and/or TH (differentiation marker). We are currently in the process of analyzing the data to determine the effects of Hoxc9 heterozygosity on neuroblastoma development and differentiation.

We have not been able to obtain tumors from $Hoxc9^{-/-}$ *MYCN* mice because most of them died within one month (~4 weeks) after birth. Necropsy revealed no overt tumor growth. In general, *MYCN* mice develop neuroblastoma tumors at a median age of ~14 weeks [8]. We are currently investigating the cause of the early death of $Hoxc9^{-/-}$ *MYCN* mice.

Task 1.3. Microarray analysis of tumor differentiation states (months 20-26): we will conduct gene profiling of Hoxc9$^{-/-}$, Hoxc9$^{+/-}$, and Hoxc9$^{+/+}$ tumors by microarray. Five tumor samples per genotype will be analyzed (total 15 microarrays). We will then analyze the microarray data using GO terms analysis, IPA and GSEA to gain a molecular view of tumor differentiation states, as well as genes regulated by Hoxc9.

We have collected Hoxc9$^{+/+}$ and Hoxc9$^{+/-}$ tumors samples and finished the preparation of RNA samples for microarray analysis. We are now conducting microarray assays. We anticipate the completion of microarray data analysis in the next two months.

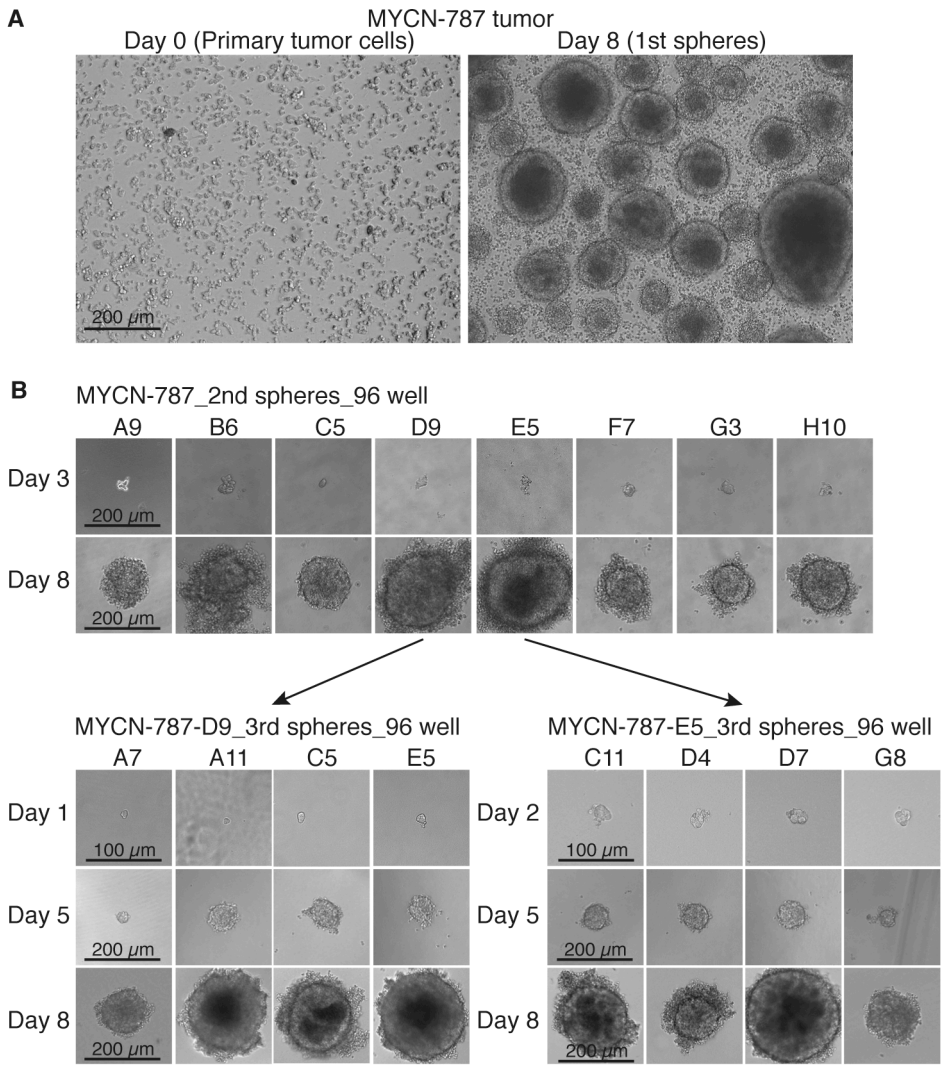

C

Primary tumor cells		
5 x 10^6	100%	(12/12)
5 x 10^5	36%	(5/14)
5 x 10^4	0%	(0/10)
Sphere-forming cells		
5 x 10^4	100%	(6/6)
5 x 10^3	50%	(3/6)
5 x 10^2	0%	(0/6)

Fig. 1. Isolation and functional characterization of MYCN neuroblastoma sphere-forming cells. **A-B,** Serial sphere formation assays of neuroblastoma cells from Hoxc9+/+ MYCN mice. Primary spheres were individually collected, dissociated into single cells and plated into 96-well plates with an average of one cell per well. **C,** Tumorigenic assays of primary and sphere-forming neuroblastoma cells.

Task 2. To investigate the role of HOXC9 in neuroblastoma stem cell differentiation (months 16-36)

The goal of Task 2 is to test the hypothesis that HOXC9 expression levels control the balance between the differentiation and self-renewal of neuroblastoma stem cells. We will examine the effects of Hoxc9 deficiency and heterozygosity on the abilities of nestin$^+$ neuroblastoma stem cells to self-renew and to differentiate in culture, and to generate tumors that recapitulate the heterogeneity of the original tumor in syngeneic mice. The Task 2 experiments outlined in the approved SOW for the second budget year include tumor cell sphere formation and differentiation assays.

Task 2.1. Self-renewal sphere or soft agar colony formation assays (months 16-21): Tumor samples from Task 1 will be used to isolate nestin-GFP$^+$ neuroblastoma cells (5 tumor samples per genotype, 3 genotypes, Hoxc9$^{+/+}$, Hoxc9$^{+/-}$, Hoxc9$^{-/-}$ mice with *MYCN* and *nestin-GFP*). The freshly isolated tumor cells will be plated at 1 cell/well (one 96-well plate per tumor sample) for sphere-formation assay or at 500 cells/well (one 6-well plate per tumor sample) for colony formation assay. This will be followed by secondary and tertiary sphere and/or colony formation assays with 5 randomly selected primary/secondary spheres or colonies for each tumor sample (5 tumor samples per genotype). Self-renewal will be quantified as the number of spheres or colonies generated from each previous sphere or colony.

We have performed all the assays proposed under this task for Hoxc9$^{+/+}$ and Hoxc9$^{+/-}$ MYCN tumors (as stated above, we have not been able to obtain Hoxc9$^{-/-}$ MYCN tumors).

We have developed a cell culture system that allowed us to propagate neuroblastoma sphere-forming cells (**Fig. 1A**). Through serial sphere formation assays with single cells, we were able to demonstrate that these sphere-forming cells possess self-renewal potential (**Fig. 1B**), an essential property of cancer stem cells. Compared to their parental primary tumor cells, these sphere-forming cells showed a marked (>100-fold) increase in the capacity to induce tumors in syngeneic wild-type 129/J mice (**Fig. 1C**). Together, these data indicate that we have isolated a minor population of mouse neuroblastoma cells with cancer stem cells properties.

Importantly, neuroblastoma tumors from Hoxc9$^{+/-}$ mice appeared to contain a higher number of sphere-forming cells (~1-5% of primary tumor cells) in comparison to Hoxc9$^{+/+}$ MYCN tumors (~0.01%), suggesting that a decrease in Hoxc9 expression enhances the production and/or maintenance of neuroblastoma stem cells, probably as a result of reduced differentiation. This finding is consistent with our model that HOXC9 has an important role in promoting neuroblastoma differentiation [6, 9].

Although Hoxc9$^{-/-}$ MYCN tumors are not available at the moment, we have developed an alternative approach to investigating the effect of Hoxc9 deficiency on the self-renewal and differentiation of neuroblastoma stem cells. We have begun the process of generating Hoxc9 knockout neuroblastoma sphere-forming cells using the RNA-guided CRISPR-Cas9 nuclease system [10]. Once generated, the Hoxc9$^{-/-}$ neuroblastoma sphere-forming cells will be examined for their ability to undergo self-renewal and differentiation, in comparison with their parental Hoxc9$^{+/+}$ sphere-forming cells.

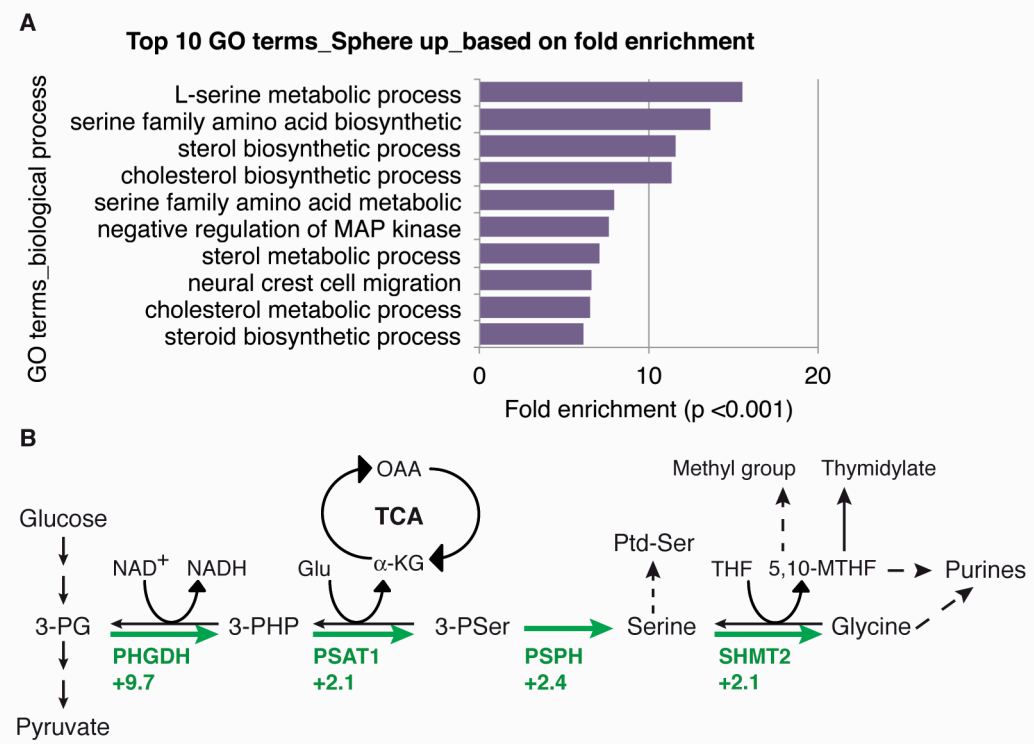

Fig. 2. Activation of the serine-glycine synthesis pathway in sphere-forming cells. **A**, GO analysis of genes upregulated in sphere-forming cells (enrichment fold > 2.0, p < 0.01). **B,** Serine-glycine synthesis pathway with the indicated fold changes in mRNA expression of the enzyme genes determined by microarray. 3-PG, 3-phosphoglycerate; 3-PHP, 3-phosphohydroxy-pyruvate; 3-PSer, 3-phosphoserine; OAA, oxaloacetate; Ptd-Ser, phosphatidylserine.

To characterize sphere-forming neuroblastoma cells at the molecular level, we performed microarray profiling of these cells from 3 Hoxc9$^{+/+}$ MYCN tumors in comparison with their parental primary cells. Gene Ontology (GO) analysis revealed that among the genes upregulated in sphere-forming cells, those within the serine-glycine synthesis pathway were significantly enriched (**Fig. 2A**), including phosphoglycerate dehydrogenase (PHGDH), phosphoserine aminotransferase 1 (PSAT1), phosphoserine phosphatase (PSPH), and serine hydroxymethyltransferase 2 (SHMT2) (**Fig. 2B**). It is known that increased activation of the serine-glycine biosynthetic pathway is an important part of cancer metabolism [11, 12]. In addition to generating serine and glycine for the biosynthesis of proteins, purines (via one-carbon units), and lipids (via phosphatidylserine), this pathway produces equimolar amounts of reduced nicotinamide adenine dinucleotide (NADH), α-ketoglutarate (α-KG), and 5,10-MTHF (**Fig. 2B**). These metabolites have critical roles in the control of cellular metabolism for cell proliferation and survival: NADH participates in ATP production and redox regulation [13]; α-KG supplies carbon to the tricarboxylic acid (TCA) cycle for the generation of many essential biosynthetic precursors [14]; and 5,10-methylenetetrahydrofolate (5,10-MTHF) is a coenzyme for the only cellular pathway of de novo thymidylate biosynthesis catalyzed by thymidylate synthase and a

major source of one-carbon units for purine synthesis [11, 15-17]. Our findings provide the first line of direct evidence for increased activation of this biosynthetic pathway in cancer stem cells.

Task 2.2. Differentiation assays (months 21-26):

a. For spontaneous differentiation assays, clonally derived secondary and tertiary spheres or colonies (n = 5 per tumor sample, 5 tumor sample per genotype, 3 genotypes, Hoxc9+/+, Hoxc9+/-, Hoxc9-/- mice with MYCN and nestin-GFP) will be cultured at 1 sphere or colony per coverslip. The spheres or colonies will be cultured for 8 days and then stained for Phox2B or TH (neuronal markers) and BLBP or S100 (both are glial markers). Percentages of spheres or colonies containing both neurons and glial cells or only neurons or glial cells will be determined.

b. For induced differentiation assays, clonally derived secondary and tertiary spheres or colonies will be cultured at 1 sphere or colony per coverslip in the presence of RA (neuronal differentiation). After 7 days, cells will be stained for Phox2B and TH. The percentage of neuron-only spheres/colonies will be determined. In parallel experiments, we will treat the cells with neuregulin (glial differentiation). After 7 days, cells will be stained for BLBP and S100. The percentage of glia-only spheres/colonies will be determined (months 21-26).

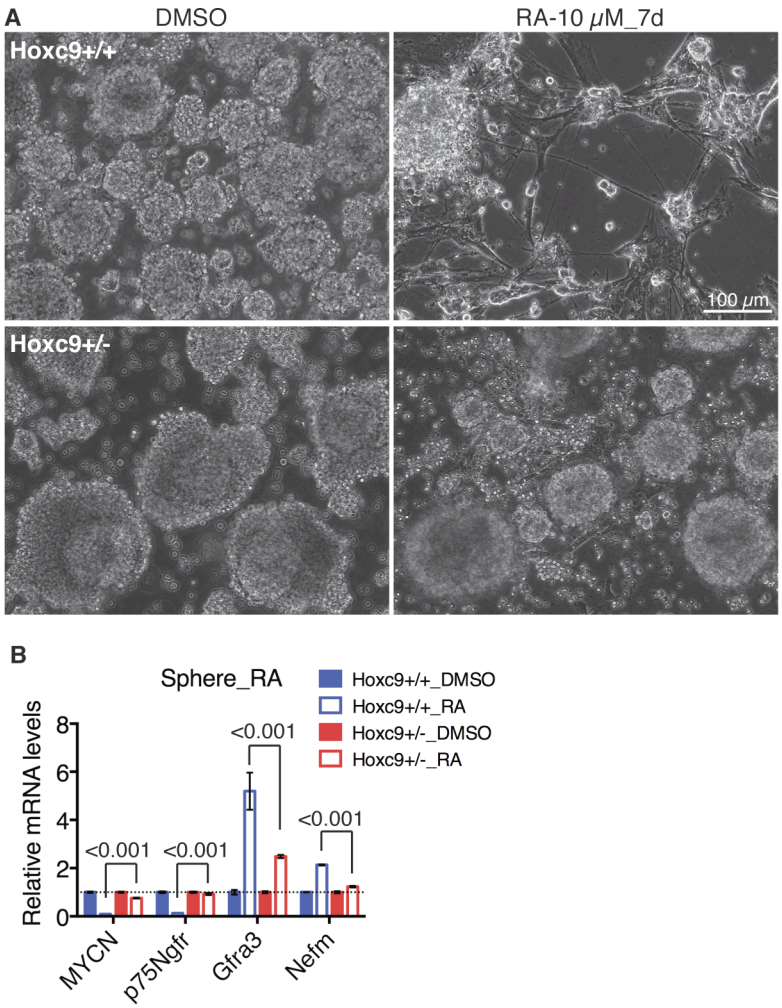

Fig. 3. Hoxc9+/- spheres are resistant to RA-induced differentiation. **A,** Morphological examination of Hoxc9+/+ and Hoxc9+/- spheres treated with DMSO or 10 μM RA for 7 days. **B,** Quantitative RT-PCR analysis of mRNA expression of the indicated genes in Hoxc9+/+ and Hoxc9+/- spheres following treatment with DMSO or 10 μM RA for 7 days. Data were analyzed by two-tailed Student's t-test with P values indicated.

We originally proposed to use Phox2B and TH as neuronal markers for assessing neuronal differentiation of neuroblastoma cells. However, our recent studies have shown that upregulation of the neuronal genes *GFRA3* and *NEFM* correlates better with neuroblastoma neuronal differentiation [6, 9] (see also Appendix 1). *GFRA3* encodes glial cell line-derived neurotrophic factor (GDNF) family receptor alpha 3 (GFRα3) and has a critical role in embryonic development of the sympathetic nervous system, promoting the differentiation and axonal outgrowth of sympathetic neurons [18]. NEFM (neurofilament, medium polypeptide 150kDa) is a common marker for differentiated neurons. Therefore, we have been using Gfrα3 and Nefm as markers for neuronal differentiation in both spontaneous and induced differentiation studies.

We have completed the spontaneous differentiation study. We found no significant levels of spontaneous differentiation for both Hoxc9$^{+/+}$ and Hoxc9$^{+/-}$ spheres following 8-day culture, as determined by immunofluorescent staining for neuronal (Gfrα3 and Nefm) and glial (BLBP and S100) markers, and by quantitative RT-PCR analysis of mRNA expression of these markers (data not shown).

We have also completed RA-induced differentiation study. Following RA treatment for 7 days, Hoxc9$^{+/+}$ spheres displayed morphologic features of neuronal differentiation, such as extensive neurite outgrowth (**Fig. 3A**, Hoxc9$^{+/+}$). By contrast, most of Hoxc9$^{+/-}$ spheres showed no obvious morphological changes following RA

treatment (**Fig. 3A**, Hoxc9$^{+/-}$). At the molecular level, Hoxc9 heterozygosity significantly inhibited the ability of RA to downregulate MYCN and p75Ngfr, and to upregulate Gfrα3 and Nefm (**Fig. 3B**). It has long been known that downregulation of MYCN by RA is critical for neuroblastoma cells to differentiate [19]. p75Ngfr is a marker for neural crest stem cells [20-22], which is generally thought to give rise to neuroblastoma stem cells [23, 24]. Together, these data suggest that high Hoxc9 expression is essential for RA-induced differentiation of mouse neuroblastoma stem cells.

Task 3. To investigate the molecular mechanism for global control of HOXC9-induced differentiation (months 3-32)

The goal of Task 3 is to test the hypothesis that HOXC9 transcriptionally activates the histone H3 demethylases KDM5B and KDM6B for global control of its differentiation program. It is well established that histone H3 methylation at specific lysine residues is a major mechanism for global control of development and differentiation programs by regulating the active and silent states of genes [25-27]. H3K4me3 maintains genes in an active state, whereas H3K27me3 keeps genes in a silent state. KDM5B catalyzes demethylation at H3K4, whereas KDM6B catalyzes demethylation at H3K27 [28, 29]. We proposed that KDM5B upregulation by HOXC9 leads to a decrease in H3K4me3 levels at cell cycle-promoting genes, whereas KDM6B upregulation by HOXC9 results in a decrease in H3K27me3 levels at the genes required for differentiation.

The Task 3 experiments outlined in the approved SOW for the second budget year include KDM6B knockdown studies and ChIP-seq assays.

Task 3.2. <u>KDM5B and KDM6B knockdown studies (months 9-20)</u>:

a. To examine the effects of KDM5B and KDM6B knockdown on the induction of the HOXC9-induced differentiation program, we will infect BE(2)-C/Tet-Off/HOXC9 cells cultured in the presence of doxycycline (Doxy) with pLKO.1 lentiviral constructs expressing shRNAs to human *KDM5B* or *KDM6B*. To examine the effects of KDM5B and KDM6B knockdown on the maintenance of the differentiation program, BE(2)-C/Tet-Off/HOXC9 cells will be cultured in the absence of Doxy for 6 days to induce HOXC9 and differentiation, followed by the lentiviral infection. pLKO.1-GFP shRNA will be used as negative control.
b. Microarray assays will be conducted for assessing the effects of KDM5B and KDM6B knockdown on the ability of HOXC9 to regulate gene expression. There will be a total of 18 microarrays: 9 (GFP-, KDM5B- and KDM6B-shRNA, 3 independent samples/shRNA) x 2 (Doxy+/Doxy-) = 18.
c. Functional analyses will be conducted for assessing the effects of KDM5B and KDM6B knockdown on the ability of HOXC9 to induce cell cycle exit and neuronal differentiation.

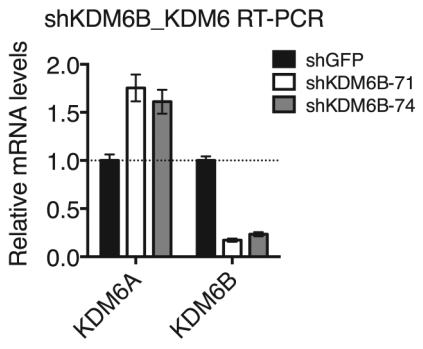

Fig. 4. Compensatory upregulation of KDM6A by KDM6B knockdown. Quantitative RT-PCR analysis of KDM6A and KDM6B mRNA levels in BE(2)-C/TetOff/HOXC9 cells infected with lentiviruses expressing shRNA to GFP or KDM6B.

As summarized in my last annual report, we have completed the study to examine the effect of KDM5B knockdown on the ability of HOXC9 to induce differentiation.

During the last budget year, we have completed the study to examine the effect of KDM6B knockdown on the ability of HOXC9 to induce differentiation. We infected BE(2)-C/Tet-Off/HOXC9 cells cultured in the presence of doxycycline (Doxy) with lentiviral constructs expressing shRNA to GFP (control) or human KDM6B. The cells were then cultured in the absence of Doxy for 6 days to induce HOXC9. So far, we have observed no significant effects of KDM6B knockdown on the ability of HOXC9 to induce cell cycle arrest, to repress cell cycle genes (i.e., CCNA2, CCNB1 and CCNE2), and to induce neuronal genes (*GFRA3* and *NENM*) (data not shown). However, we noticed that in cells with KDM6B knockdown the expression of KDM6A was upregulated (**Fig. 4**). It is known that KDM6A and KDM6B share the same substrate specificity [29]. Thus, it is possible that KDM6A upregulation masked the effect of KDM6B knockdown. We have developed two alternative strategies to address the issue.

First, as proposed in my original application, we have begun co-knockdown experiments by sequential infection of BE(2)-C/Tet-Off/HOXC9 cells with lentiviral constructs expressing shRNA to KDM6A and KDM6B. After verification by RT-PCR and immunoblotting, we will examine the effects of KDM6A and KDM6B co-knockdown on the ability of HOXC9 to induce differentiation.

Second, we have taken the advantage of recent progress on the development of small-molecule KDM inhibitors and obtained a small-molecule inhibitor (GSK-J4) that specifically targets both KDM6A and KDM6B [30]. We will treat BE(2)-C/Tet-Off/HOXC9 cells with GSK-J4 and then examine its effect on HOXC9-induced differentiation.

For microarray assays, we have already collected RNA samples from the KDM5B knockdown study. We will perform the assays once we obtain RNA samples from the KDM6 co-knockdown and inhibition studies.

Task 3.3. Anti-KDM5B, -KDM6B, -H3K4me3, and -H3K27me3 ChIP-Seq assays (months 21-32):

a. ChIP-Seq assays will be conducted with BE(2)-C/Tet-Off/HOXC9 cells before (Doxy+) and after HOXC9 induction (Doxy- 6 days) using ChIP-quality antibodies against KDM5B, KDM6B, H3K4me3, and H3K27me3, followed by massively parallel DNA sequencing (Illumina).

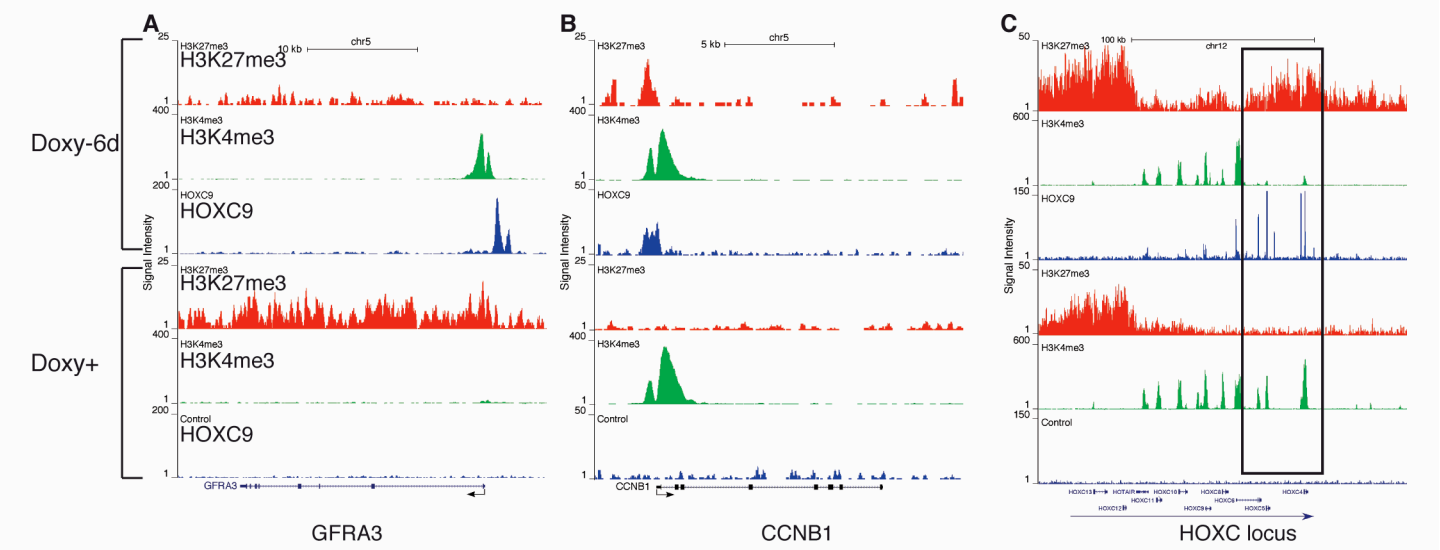

Fig. 5. Epigenetic regulation of transcription by HOXC9. ChIP-seq tag profiles showing HOXC9 binding to representative target genes, leading to changes in H3K4me3 and/or H3K27me3 levels at their loci (**A**, GFRA3; **B**, CCNB1; **C**, HOXC locus).

We have performed the proposed anti-H3K4me3 and anti-H3K27me3 ChIP-seq assays. H3K4me3 maintains genes in an active state, whereas H3K27me3 keeps genes in a silent state. Our ChIP-seq data revealed 3 modes of epigenetic regulation of transcription by HOXC9 (**Fig. 5**). First, HOXC9-mediated transcriptional activation of *GFRA3* is associated with a marked increase in H3K4me3 levels at the *GFRA3* promoter and a significant reduction in H3K27me3 levels at the *GFRA3* genomic locus (**Fig. 5A**). Second, HOXC9-mediated transcriptional repression of *CCNB1* (coding for cyclin B1) is associated with a significant increase in H3K27 levels at the *CCNB1* promoter but with no significant change in H3K4me3 levels (**Fig. 5B**). Third, HOXC9 repression of anterior HOXC genes is characterized by a significant increase in H2K27me3 levels and a marked reduction in H3K4me3 levels at their genomic loci (**Fig. 5C**, inset). These findings provide evidence in support of our hypothesis that HOXC9 transcriptionally activates the H3K4 demethylase KDM5B and the H3K27 demethylase KDM6B for global control of its differentiation program.

3. KEY RESEARCH ACCOMPLISHMENTS:

- We have completed the experiments proposed in MYCN mouse tumor development studies and we are in the final stage of data analysis to determine the effects of Hoxc9 heterozygosity on neuroblastoma development and differentiation.

- We have developed a cell culture system for enriching and long-term propagating mouse neuroblastoma sphere-forming cells that possess cancer stem cell properties.

- We have obtained evidence that Hoxc9 heterozygosity increases the population of sphere-forming cells in mouse neuroblastoma, suggesting a potential tumor suppressor function of Hoxc9 in mouse neuroblastoma development.

- We have performed microarray gene expression profiling of mouse neuroblastoma sphere-forming cells and identified key metabolic pathways that are activated in these cells, thereby providing a molecular rational for targeting these pathways for neuroblastoma therapy.

- We have completed the study of RA-induced differentiation of mouse neuroblastoma sphere-forming cells and obtained evidence for an important role of Hoxc9 in promoting neuroblastoma stem cell differentiation.

- We have completed anti-H3K4me3 and anti-H3K27me3 ChIP-seq assays with BE(2)-C/Tet-Off/HOXC9 cells before (Doxy+) and after HOXC9 induction (Doxy- 6 days) and identified 3 modes of epigenetic regulation of transcription by HOXC9.

4. CONCLUSION:

Neuroblastoma is a common childhood malignant tumor of the sympathetic nervous system. Differentiation status in neuroblastoma strongly affects clinical outcomes and inducing differentiation is a treatment strategy in this disease [1-5]. We have recently shown that HOXC9 is a key regulator of neuroblastoma cell differentiation and a prognostic marker for survival in neuroblastoma patients [6]. Neuroblastoma differentiation is characterized at the molecular level by repression of cell cycle genes and activation of neuronal differentiation markers. Our research during the second budget year of this award has significantly advanced our understanding of the role and the mechanism of HOXC9 action in neuroblastoma. We developed a cell culture system for enriching and long-term propagating mouse neuroblastoma sphere-forming cells that possess cancer stem cell properties. With this culture system, we were able to show that high Hoxc9 expression is essential for RA-induced differentiation of neuroblastoma stem cells. Moreover, we identified 3 modes of epigenetic regulation of transcription by HOXC9 that involve modulation of H3K4me3 and H3K27me3 levels, thereby providing a molecular basis for the role of KDM5B and KDM6B in the control of neuroblastoma differentiation. Finally, through microarray gene expression profiling, we obtained evidence for selective activation of the serine-glycine synthesis pathway in mouse neuroblastoma stem cells. These findings provide the first line of direct evidence for the presence of a minor population of neuroblastoma stem cells within primary tumors and suggest that pharmacological inactivation of the serine-glycine synthesis pathway is a promising therapeutic strategy for neuroblastoma.

5. PUBLICATIONS, ABSTRACTS, AND PRESENTATIONS:

a) Manuscripts and abstracts

(1) Wang, X., Choi, J., Ding, J., Yang, L., Lee, E.J., Ngoka, Zha, Y., Jin, B., Ren, M., Huang, S., Cowell, J., Shi, H., Cui, H. **Ding, H.-F.** HOXC9 directly regulates distinct sets of genes to coordinate diverse cellular processes during differentiation. BMC Genomics 14:830. 2013. PMID: 24274069

(2) Wang, X., Yang, L., Choi, J., Kitamura, E., Chang, C., Ding, J., Lee, E., Cui, H., **Ding, H.-F.** Genome-wide analysis of HOXC9-induced neuronal differentiation of neuroblastoma cells. Genomics Data 2:50-52, 2014

(3) Ding, J., Li, T., Wang, X., Zhao, E., Choi, J., Yang, L., Zha, Y., Dong, Z., Huang, S., Asara, J.M., Cui, H., **Ding, H.-F.** The histone H3 methyltransferase G9A epigenetically activates the serine-glycine synthesis pathway to sustain cancer cell survival and proliferation. Cell Metab. 18:896-907. 2013. PMID: 24315373; PMCID: PMC3878056

b) Presentations

(1) Poster Presentation: "Histone H3 methyltransferase G9A epigenetically activates the serine synthesis pathway to sustain cancer cell survival and proliferation", Advances in Neuroblastoma Research, Cologne, Germany. May 13-16, 2014

6. INVENTIONS, PATENTS AND LICENSES: None

7. REPORTABLE OUTCOMES: None

8. OTHER ACHIEVEMENTS: None

9. REFERENCES:

1. Brodeur GM: **Neuroblastoma: biological insights into a clinical enigma.** *Nat Rev Cancer* 2003, **3:**203-216.
2. Beckwith JB, Martin RF: **Observations on the histopathology of neuroblastomas.** *J Pediatr Surg* 1968, **3:**106-110.
3. Hughes M, Marsden HB, Palmer MK: **Histologic patterns of neuroblastoma related to prognosis and clinical staging.** *Cancer* 1974, **34:**1706-1711.
4. Shimada H, Chatten J, Newton WA, Jr., Sachs N, Hamoudi AB, Chiba T, Marsden HB, Misugi K: **Histopathologic prognostic factors in neuroblastic tumors: definition of subtypes of ganglioneuroblastoma and an age-linked classification of neuroblastomas.** *J Natl Cancer Inst* 1984, **73:**405-416.
5. Ambros IM, Hata J, Joshi VV, Roald B, Dehner LP, Tuchler H, Potschger U, Shimada H: **Morphologic features of neuroblastoma (Schwannian stroma-poor tumors) in clinically favorable and unfavorable groups.** *Cancer* 2002, **94:**1574-1583.
6. Mao L, Ding J, Zha Y, Yang L, McCarthy BA, King W, Cui H, Ding HF: **HOXC9 Links Cell-Cycle Exit and Neuronal Differentiation and Is a Prognostic Marker in Neuroblastoma.** *Cancer Res* 2011, **71:**4314-4324.
7. Zha Y, Ding E, Yang L, Mao L, Wang X, McCarthy BA, Huang S, Ding HF: **Functional dissection of HOXD cluster genes in regulation of neuroblastoma cell proliferation and differentiation.** *PLoS One* 2012, **7:**e40728.
8. Weiss WA, Aldape K, Mohapatra G, Feuerstein BG, Bishop JM: **Targeted expression of MYCN causes neuroblastoma in transgenic mice.** *Embo J* 1997, **16:**2985-2995.
9. Wang X, Choi JH, Ding J, Yang L, Ngoka LC, Lee EJ, Zha Y, Mao L, Jin B, Ren M, et al: **HOXC9 directly regulates distinct sets of genes to coordinate diverse cellular processes during neuronal differentiation.** *BMC Genomics* 2013, **14:**830.
10. Mali P, Esvelt KM, Church GM: **Cas9 as a versatile tool for engineering biology.** *Nat Methods* 2013, **10:**957-963.
11. Kalhan SC, Hanson RW: **Resurgence of serine: an often neglected but indispensable amino Acid.** *J Biol Chem* 2012, **287:**19786-19791.
12. Locasale JW: **Serine, glycine and one-carbon units: cancer metabolism in full circle.** *Nat Rev Cancer* 2013, **13:**572-583.
13. Corkey BE, Shirihai O: **Metabolic master regulators: sharing information among multiple systems.** *Trends Endocrinol Metab* 2012, **23:**594-601.
14. DeBerardinis RJ, Lum JJ, Hatzivassiliou G, Thompson CB: **The biology of cancer: metabolic reprogramming fuels cell growth and proliferation.** *Cell Metab* 2008, **7:**11-20.
15. Teperino R, Schoonjans K, Auwerx J: **Histone methyl transferases and demethylases; can they link metabolism and transcription?** *Cell Metab* 2010, **12:**321-327.
16. Tibbetts AS, Appling DR: **Compartmentalization of Mammalian folate-mediated one-carbon metabolism.** *Annu Rev Nutr* 2010, **30:**57-81.
17. Touroutoglou N, Pazdur R: **Thymidylate synthase inhibitors.** *Clin Cancer Res* 1996, **2:**227-243.
18. Ernsberger U: **The role of GDNF family ligand signalling in the differentiation of sympathetic and dorsal root ganglion neurons.** *Cell Tissue Res* 2008, **333:**353-371.

19. Thiele CJ, Israel MA: **Regulation of N-myc expression is a critical event controlling the ability of human neuroblasts to differentiate.** *Exp Cell Biol* 1988, **56:**321-333.
20. Bixby S, Kruger GM, Mosher JT, Joseph NM, Morrison SJ: **Cell-intrinsic differences between stem cells from different regions of the peripheral nervous system regulate the generation of neural diversity.** *Neuron* 2002, **35:**643-656.
21. Molofsky AV, Pardal R, Iwashita T, Park IK, Clarke MF, Morrison SJ: **Bmi-1 dependence distinguishes neural stem cell self-renewal from progenitor proliferation.** *Nature* 2003, **425:**962-967.
22. Morrison SJ, White PM, Zock C, Anderson DJ: **Prospective identification, isolation by flow cytometry, and in vivo self-renewal of multipotent mammalian neural crest stem cells.** *Cell* 1999, **96:**737-749.
23. Ross RA, Spengler BA, Domenech C, Porubcin M, Rettig WJ, Biedler JL: **Human neuroblastoma I-type cells are malignant neural crest stem cells.** *Cell Growth Differ* 1995, **6:**449-456.
24. Cui H, Ma J, Ding J, Li T, Alam G, Ding HF: **Bmi-1 regulates the differentiation and clonogenic self-renewal of I-type neuroblastoma cells in a concentration-dependent manner.** *J Biol Chem* 2006, **281:**34696-34704.
25. Schuettengruber B, Chourrout D, Vervoort M, Leblanc B, Cavalli G: **Genome regulation by polycomb and trithorax proteins.** *Cell* 2007, **128:**735-745.
26. Natoli G: **Maintaining cell identity through global control of genomic organization.** *Immunity* 2010, **33:**12-24.
27. Mills AA: **Throwing the cancer switch: reciprocal roles of polycomb and trithorax proteins.** *Nat Rev Cancer* 2010, **10:**669-682.
28. Swigut T, Wysocka J: **H3K27 demethylases, at long last.** *Cell* 2007, **131:**29-32.
29. Mosammaparast N, Shi Y: **Reversal of histone methylation: biochemical and molecular mechanisms of histone demethylases.** *Annu Rev Biochem* 2010, **79:**155-179.
30. Kruidenier L, Chung CW, Cheng Z, Liddle J, Che K, Joberty G, Bantscheff M, Bountra C, Bridges A, Diallo H, et al: **A selective jumonji H3K27 demethylase inhibitor modulates the proinflammatory macrophage response.** *Nature* 2012, **488:**404-408.

10. APPENDICES:

(1) Wang, X., Choi, J., Ding, J., Yang, L., Lee, E.J., Ngoka, Zha, Y., Jin, B., Ren, M., Huang, S., Cowell, J., Shi, H., Cui, H. **Ding, H.-F.** HOXC9 directly regulates distinct sets of genes to coordinate diverse cellular processes during differentiation. BMC Genomics 14:830. 2013. PMID: 24274069

(2) Wang, X., Yang, L., Choi, J., Kitamura, E., Chang, C., Ding, J., Lee, E., Cui, H., **Ding, H.-F.** Genome-wide analysis of HOXC9-induced neuronal differentiation of neuroblastoma cells. Genomics Data 2:50-52, 2014

(3) Ding, J., Li, T., Wang, X., Zhao, E., Choi, J., Yang, L., Zha, Y., Dong, Z., Huang, S., Asara, J.M., Cui, H., **Ding, H.-F.** The histone H3 methyltransferase G9A epigenetically activates the serine-glycine synthesis pathway to sustain cancer cell survival and proliferation. Cell Metab. 18:896-907. 2013. PMID: 24315373; PMCID: PMC3878056

BMC Genomics

RESEARCH ARTICLE Open Access

HOXC9 directly regulates distinct sets of genes to coordinate diverse cellular processes during neuronal differentiation

Xiangwei Wang[1†], Jeong-Hyeon Choi[2,3†], Jane Ding[2,4†], Liqun Yang[6†], Lambert C Ngoka[2], Eun J Lee[2,5], Yunhong Zha[7], Ling Mao[8], Bilian Jin[2,5], Mingqiang Ren[2,4], John Cowell[2,4], Shuang Huang[2,5], Huidong Shi[2,5], Hongjuan Cui[6*] and Han-Fei Ding[2,4,5*]

Abstract

Background: Cellular differentiation is characterized by the acquisition of specialized structures and functions, cell cycle exit, and global attenuation of the DNA damage response. It is largely unknown how these diverse cellular events are coordinated at the molecular level during differentiation. We addressed this question in a model system of neuroblastoma cell differentiation induced by HOXC9.

Results: We conducted a genome-wide analysis of the HOXC9-induced neuronal differentiation program. Microarray gene expression profiling revealed that HOXC9-induced differentiation was associated with transcriptional regulation of 2,370 genes, characterized by global upregulation of neuronal genes and downregulation of cell cycle and DNA repair genes. Remarkably, genome-wide mapping by ChIP-seq demonstrated that HOXC9 bound to 40% of these genes, including a large number of genes involved in neuronal differentiation, cell cycle progression and the DNA damage response. Moreover, we showed that HOXC9 interacted with the transcriptional repressor E2F6 and recruited it to the promoters of cell cycle genes for repressing their expression.

Conclusions: Our results demonstrate that HOXC9 coordinates diverse cellular processes associated with differentiation by directly activating and repressing the transcription of distinct sets of genes.

Keywords: Neuronal differentiation, Cell cycle arrest, DNA damage response, E2F6, HOXC9, Neuroblastoma

Background

Cellular differentiation is an essential process of normal development by which a stem or progenitor cell becomes a post-mitotic, specialized cell with unique morphology and function. In addition, it has long been recognized that differentiated cells of both normal and tumor origin are defective in the DNA damage response and repair at the global level, displaying a marked increase in sensitivity to ionizing radiation and other DNA damaging agents [1-3]. Consistent with these observations, recent studies have shown that brain and breast cancer stem cells, a small subpopulation of tumor cells thought to be responsible for initiating and sustaining tumor growth [4-6], are more resistant to irradiation and chemotherapy than bulk tumor cells [7-10]. Particularly interesting is the observation that inhibition of DNA damage checkpoint kinases can reverse the radioresistance of glioma stem cells [7]. Thus, a molecular understanding of cellular differentiation may suggest new therapeutic strategies that target both cell proliferation and the DNA damage response.

Among the genes that have a critical role in the control of cellular differentiation are the *HOX* gene family members. *HOX* genes encode a family of transcription factors that function as master regulators of morphogenesis and cell fate specification [11-13]. Dysregulation of *HOX* gene expression has been implicated in the pathogenesis of cancers of different tissue types. In most tumor types, *HOX* genes function as oncogenes to promote cancer development such as

* Correspondence: hcui@swu.edu.cn; hding@gru.edu
†Equal contributors
[6]State Key Laboratory of Silkworm Genome Biology, Institute of Sericulture and System Biology, Southwest University, Chongqing, China
[2]Cancer Center, Georgia Regents University, Augusta, GA 30912, USA
Full list of author information is available at the end of the article

HOXA9 in leukemia and *HOXB13* in ovarian and breast cancers [13,14]. However, in neuroblastoma, a common childhood malignant tumor of the sympathetic nervous system [15,16], there is evidence suggesting that *HOX* genes may function as tumor suppressors [13]. Particularly, downregulation of HOXC9 expression is significantly associated with poor prognosis in neuroblastoma patients [17,18].

Neuroblastoma cells can be induced to undergo neuronal differentiation by serum deprivation [19], nerve growth factor [20] or retinoic acid (RA) [21]. RA-induced neuronal differentiation of neuroblastoma cells is a well-established model for molecular investigation of neuronal differentiation [22]. We recently reported that RA-induced differentiation of neuroblastoma cells required the activation of several *HOX* genes [18,23]. Among them, HOXC9 appeared to be a major mediator of RA action in neuroblastoma cells. HOXC9 expression was upregulated by RA, and silencing HOXC9 expression conferred resistance to RA-induced differentiation. Importantly, ectopic HOXC9 expression alone was sufficient to induce growth arrest and morphologic differentiation in neuroblastoma cells, fully recapitulating the neuronal differentiation phenotype induced by RA [18].

Differentiated neuroblastoma cells morphologically and functionally resemble mature peripheral neurons characterized by G1 arrest, extensive neurite outgrowth, and significant resting potential. It has long been observed that differentiated neuroblastoma cells are highly sensitive to UV and X-ray radiation with a significantly reduced rate of DNA damage repair [20,24-27]. The molecular basis for the differentiation-induced radiosensitivity is not well understood. The biological functions of RA are mediated by multiple isotypes of RA receptors (RARs) and retinoid X receptors (RXRs), which form RAR/RXR heterodimers that bind RA response elements in the regulatory regions of RA target genes and regulate their transcription [28]. The complexity of multiple RARs and RXRs involved in the action of RA presents a daunting challenge to dissect the molecular mechanism that coordinates the diverse cellular events associated with differentiation. Thus, the finding that HOXC9 alone is able to initiate a robust transcriptional program that drives neuronal differentiation provides a unique experimental system for this investigation. In this study, we conducted genome-wide profiling of the HOXC9-initiated transcriptional program. Our investigation reveals that HOXC9 directly regulates the expression of three major sets of genes that separately control neuronal differentiation, cell cycle progression, and the DNA damage response.

Results

Gene expression profiling of HOXC9-induced neuronal differentiation

To gain a molecular understanding of HOXC9-induced differentiation, we conducted microarray gene expression profiling of human neuroblastoma BE(2)-C/Tet-Off/myc-HOXC9 cells, which express myc-tagged human HOXC9 and undergo neuronal differentiation in the absence of doxycycline [18] (Figure 1A). The profiling analysis identified a total of 2,370 genes that were differentially expressed ($\geq +1.5$ and ≤ -1.5 fold, $P < 0.01$), with 879 genes being upregulated and 1,491 genes downregulated (Additional file 1: Table S1). Gene annotation enrichment analysis revealed that HOXC9-induced differentiation is characterized by a genome-wide coordination in transcriptional regulation of genes that control neuronal differentiation, cell cycle progression, and the DNA damage response.

Global upregulation of neuronal genes

Gene Ontology (GO) analysis of the 879 HOXC9-upregulated genes by DAVID [29,30] revealed that they were significantly enriched for genes that control nervous system development such as neuron generation and differentiation, axonogenesis, and synapse formation and organization (Figure 1B and Additional file 2: Table S2, enrichment fold ≥ 2.0, false discovery rate (FDR) ≤1%). A total of 105 HOXC9-responsive genes were involved in nervous system development (Figure 1B), accounting for approximately 12% of the 879 genes upregulated by HOXC9. We obtained similar results with Gene Set Enrichment Analysis (GSEA), which showed significant enrichment of gene sets involved in synaptogenesis and neuron differentiation among the genes upregulated by HOXC9 (Figure 1C). Particularly significant was the activation of *ASCL1*, *GFRA3*, *RET*, and *NTN3* (Figure 1D). ASCL1, a member of the basic helix-loop-helix (bHLH) family of transcription factors, is a master regulator in the generation and differentiation of sympathetic neurons [31,32]. *GFRA3* encodes the glial cell line-derived neurotrophic factor (GDNF) family receptor alpha 3 (GFRα3), which forms a receptor complex with RET that preferentially binds the GDNF family ligand Artemin. This receptor signaling has a critical role in embryonic development of the sympathetic nervous system, promoting the survival, differentiation, axonal outgrowth, and target innervation of sympathetic neurons [33]. NTN3 (netrin 3) belongs to a family of extracellular proteins that promote axon growth and migration during the development of the nervous system [34]. Ingenuity Pathways Analysis (IPA) further revealed a network of HOXC9-upregulated genes relevant to the development and function of sympathetic neurons (Additional file 3: Figure S1). Together, these analyses demonstrate that HOXC9 activates a large number of neuronal genes, providing the molecular mechanism for its ability to induce neuronal differentiation of neuroblastoma cells.

Global downregulation of cell cycle and DNA repair genes

GO analysis of the 1,491 HOXC9-downregulated genes revealed that they were remarkably enriched for genes

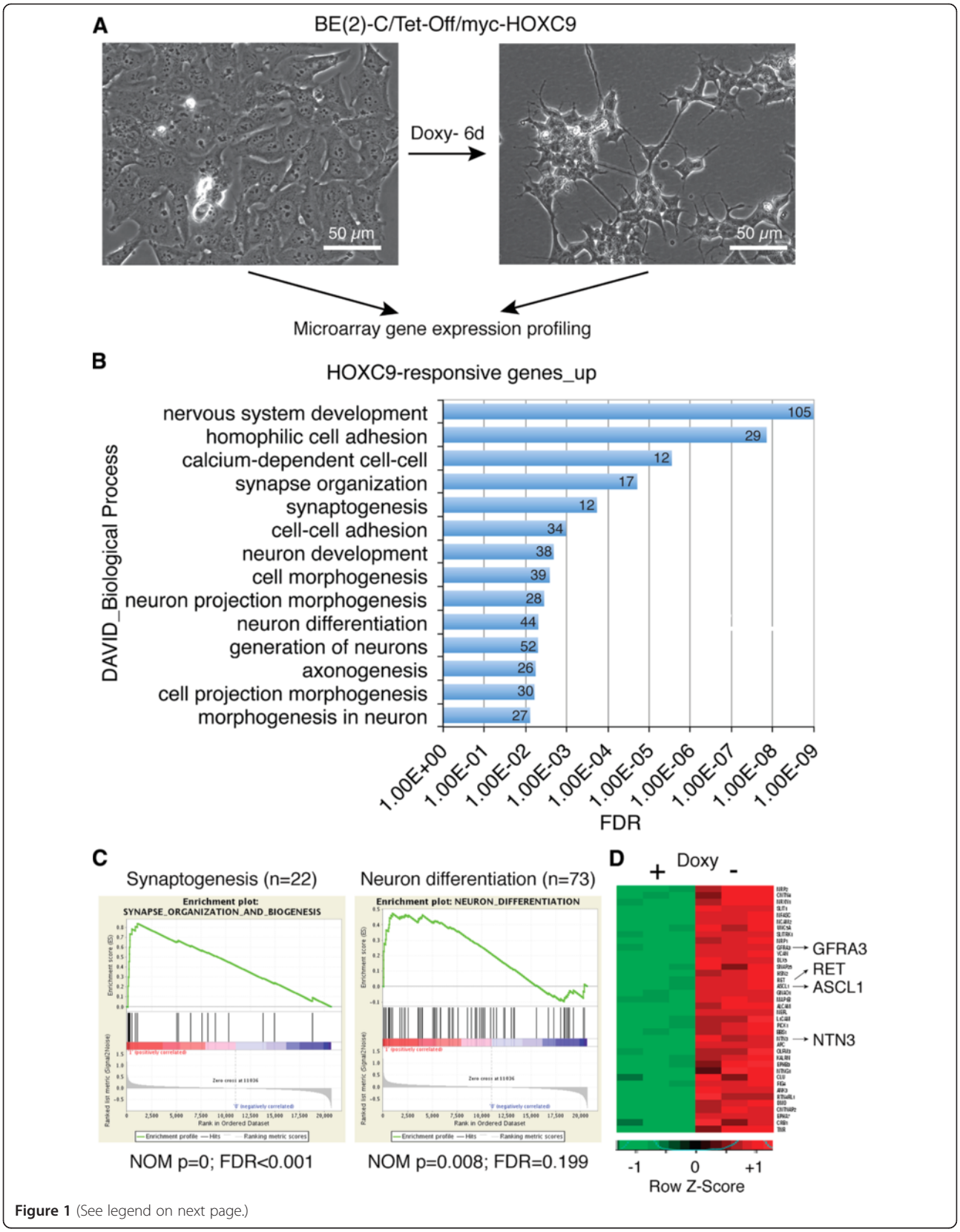

Figure 1 (See legend on next page.)

(See figure on previous page.)
Figure 1 Global upregulation of neuronal genes by HOXC9. (A) Schematic of experiment. Doxy, doxycycline. **(B)** DAVID analysis of upregulated HOXC9-responsive genes for enriched GO biological process categories (enrichment fold > 2.0; FDR <1%). The number of genes for each biological process category is indicated. **(C)** GSEA showing significant enrichment of gene sets involved in synapse organization and biogenesis and neuron differentiation among the genes upregulated by HOXC9. **(D)** Heatmap of select neuronal genes activated by HOXC9.

that control cell cycle progression and the DNA damage response (Figure 2A and Additional file 4: Table S3, enrichment fold ≥ 2.0; FDR ≤1%). The analysis identified 206 genes involved in cell cycle regulation and 98 genes in the DNA damage response (Figure 2A). Similarly, GSEA showed that among the genes downregulated by HOXC9, those regulating mitotic cell cycle, DNA replication and DNA repair were significantly enriched (Figure 2B). IPA further revealed that the downregulated genes include most of cyclin (CCN) and cyclin-dependent kinase (CDK) genes, and genes that control DNA replication, mitosis, double-strand break (DSB) repair, base excision repair (BER), nucleotide excision repair (NER), mismatch repair (MMR), and Fanconi anemia (FA)-mediated repair (Additional file 3: Figures S2A-S2E and Additional file 4: Table S3). These findings suggest that global downregulation of cell cycle and DNA repair genes is the primary cause of the cell cycle arrest and attenuation of the DNA damage response associated with neuronal differentiation.

Genome-wide mapping of HOXC9-binding sites

We next asked how HOXC9 coordinates the expression of distinct sets of genes: the upregulation of genes critical for nervous system development and the downregulation of genes essential for cell cycle progression and the DNA damage response. Mechanistically, HOXC9 could function through a few master transcription factors, which in turn regulate their own subsets of target genes that work together to drive differentiation. Alternatively, HOXC9 could directly regulate distinct sets of genes to coordinate the cellular events associated with differentiation. To test these models, we conducted two independent anti-HOXC9 chromatin immunoprecipitation assays followed by massively parallel sequencing of the enriched DNA fragments (ChIP-seq) for genome-wide mapping of HOXC9-binding sites. We identified a total of 29,221 HOXC9-binding peaks with FDR less than 1% (Figure 3A and Additional file 5: Table S4). Scatter plot analysis (Figure 3B, R = 0.93, correlation coefficient) and ChIP-seq tag profiles (Figure 3C) demonstrated that the mapping data were highly reproducible between the two independent HOXC9 ChIP-seq samples. We next analyzed the distribution of HOXC9-binding peaks within the genome that was classified into functional categories including promoters (within 5 kb upstream of the transcription start site, TSS), 5'-untranslated regions (5'-UTRs), exons, introns, 3'-UTRs, downstream (within 5-kb downstream of the gene), and intergenic regions (outside −5 ~ +5 kb of genes). The analysis revealed that a majority of HOXC9-binding peaks were localized in introns (41.2%) and intergenic regions (43.4%) (Figure 3D). However, after normalization to the size of these functional regions, it became clear that HOXC9-binding peaks were highly enriched in gene promoters and 5'-UTRs (Figure 3E and F). Analysis of the sequences covered by HOXC9-binding peaks with the motif-finding program MEME revealed that the most enriched binding motif (T/ATTTAT, E value = 1.6e-35) corresponds to the *Drosophila* Abd-B motif (MA0165.1, Figure 3G) and is highly homologous to the mouse Hoxc9-binding motif (ATTTAT) [35]. HOXC9 is a mammalian ortholog of the *Drosophila* Hox protein Abd-B. Thus, myc-tagged HOXC9 binds to cognate sequences in human neuroblastoma cells.

Genome-wide identification of HOXC9 target genes

The ChIP-seq assay revealed that a total of 4,992 genes contained at least one HOXC9-binding peak within 5-kb upstream or downstream of their genomic loci (Figure 3A and Additional file 6: Table S5). We next combined the anti-HOXC9 ChIP-seq data with the HOXC9 microarray data to generate a list of genes that were bound by HOXC9 and whose expression levels were significantly changed as a result of HOXC9 induction (≥ +1.5 and ≤ −1.5 fold, P <0.01). The analysis revealed that 954 genes or 40.3% of the 2,370 HOXC9-responsive genes are direct targets of HOXC9, with 445 and 509 genes being upregulated and downregulated, respectively (Additional file 7: Table S6). GO analysis of HOXC9 direct target genes revealed a transcriptional program characterized by coordinated regulation of genes critical for neuron differentiation, cell cycle progression, and the DNA damage response.

HOXC9 directly induces a large number of neuronal genes

The only sets of genes that were significantly enriched among the upregulated HOXC9 direct target genes are those exclusively involved in nervous system development, particularly the generation and differentiation of neurons and axonogenesis (Figure 4A and Additional file 8: Table S7, enrichment fold ≥ 2.0, FDR ≤ 5%). The 57 HOXC9 direct target genes account for 54.3% (57/105) of the HOXC9-responsive genes involved in nervous system development (Figure 1B). Among them are *ASCL1*,

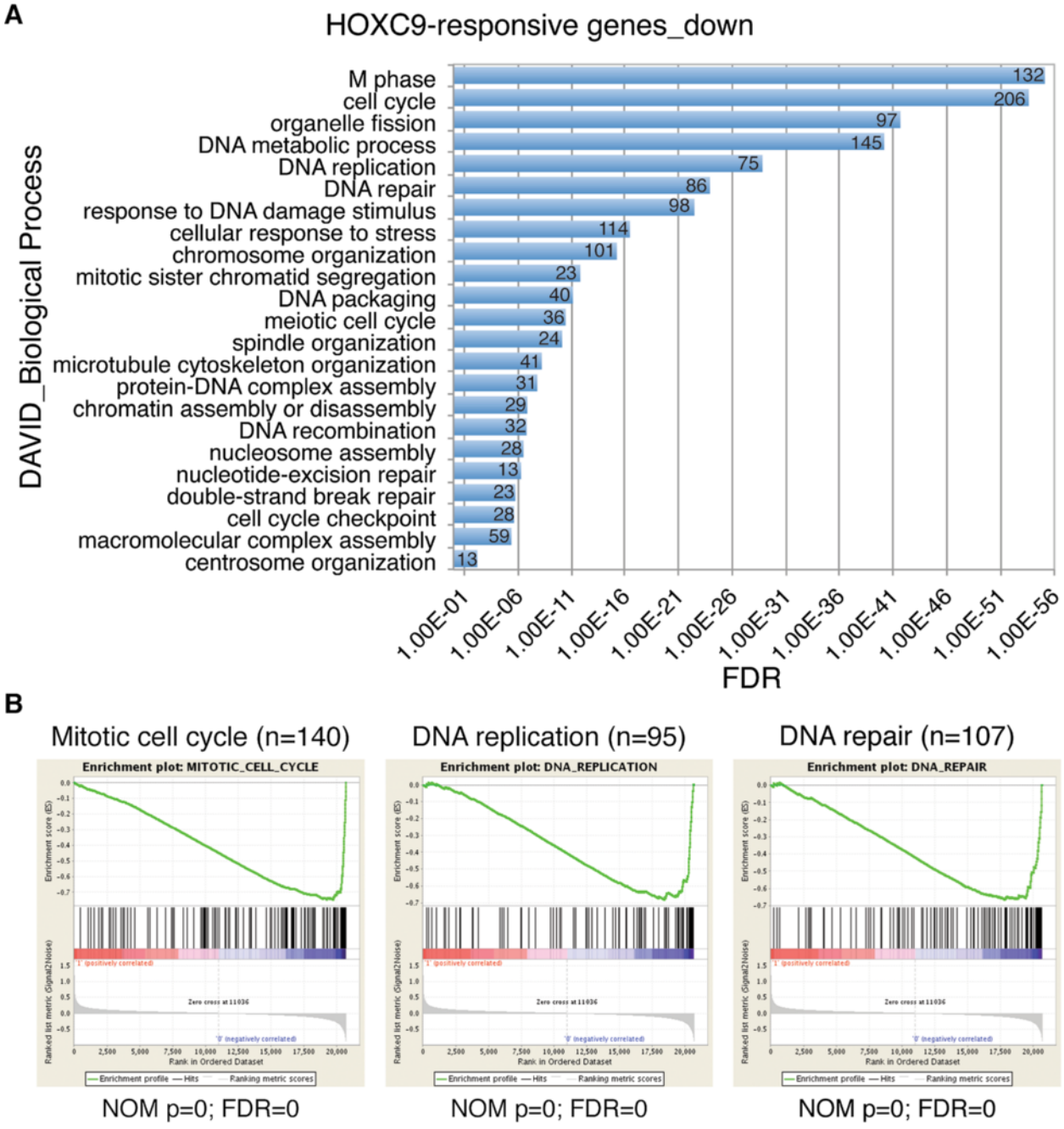

Figure 2 Global downregulation of cell cycle and DNA repair genes by HOXC9. (A) DAVID analysis of downregulated HOXC9-responsive genes for enriched GO biological process categories (enrichment fold > 2.0; FDR <1%). The number of genes for each biological process category is indicated. **(B)** GSEA showing significant enrichment of gene sets involved in mitotic cell cycle, DNA replication and DNA repair among the genes downregulated by HOXC9.

GFRA3, *RET*, and *NTN3*. Figure 4B shows the ChIP-seq tag profiles of HOXC9 binding to the promoter regions of *GFRA3*, *RET*, and *NTN3*. As discussed above, these genes have a critical role in sympathetic neurogenesis and axonogenesis.

HOXC9 directly represses a large number of genes essential for cell cycle progression and the DNA damage response

GO analysis of the downregulated HOXC9 direct target genes revealed that they were significantly enriched for

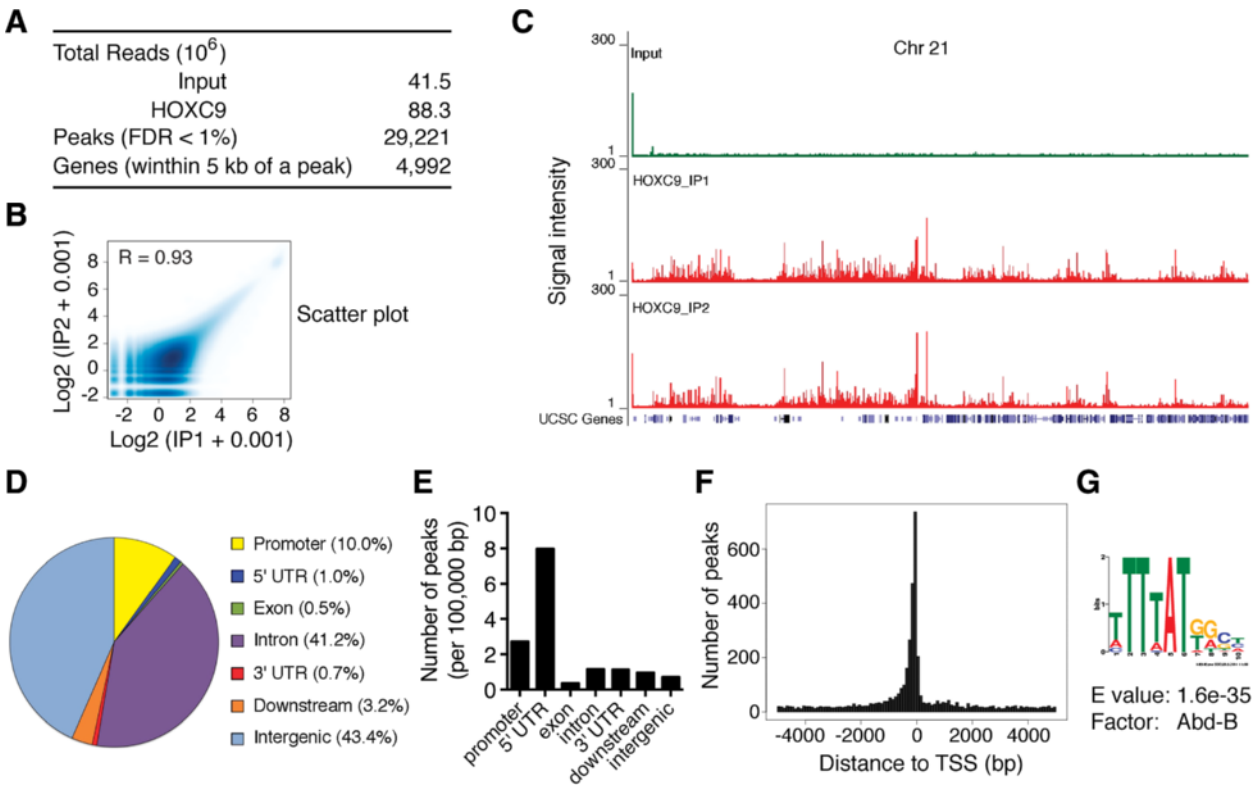

Figure 3 ChIP-seq analysis of HOXC9 genomic distribution. (A) Summary of HOXC9-binding peaks and genes identified by ChIP-seq. **(B-C)** Scatter plot analysis **(B)** and ChIP-seq tag profiles of chromosome 21 **(C)** showing a high correlation between two independent HOXC9 ChIP-seq samples. **(D)** Pie chart showing genomic distribution of HOXC9-binding peaks relative to RefSeq functional categories including promoters (within 5 kb upstream of TSS), 5′ UTRs, exons, introns, 3′ UTRs, downstream (within 5 kb downstream of the gene), and intergenic regions (outside −5 ~ +5 kb of genes). **(E)** Bar graph showing the distribution of HOXC9-binding peaks relative to the functional categories after normalization to the size of each category in 100 kb. **(F)** Histogram showing the distribution of HOXC9-binding peaks relative to the nearest TSS. Peaks were combined in 100 bp. **(G)** Web logo showing the top enriched motif present in HOXC9 ChIP-seq peaks, which corresponds to the binding site for Abd-B, the *Drosophila* ortholog of mammalian HOX9-13 paralogs.

genes that control cell cycle progression and the DNA damage response (Figure 5A and Additional file 9: Table S8), enrichment fold ≥ 2.0, FDR ≤ 1%). The analysis identified 52 cell cycle genes that were directly repressed by HOXC9 (Figure 5A), accounting for 25.2% (52/206) of the HOXC9-responsive genes involved in cell cycle regulation (Figure 2A). It was particularly striking that the vast majority of the HOXC9-repressed cell cycle genes are involved in the control of the M phase (n = 25) and DNA replication (n = 21) (Figure 5A). Figure 5B and C show the association of HOXC9 with the promoter regions of representative cell cycle genes, including *CDC45L* and *MCM3* (DNA replication), and *CCNB1* and *CDCA8* (M phase). CDC45L and MCM3 are components of the replicative complex that catalyzes DNA replication during the S phase [36], while CDCA8, also known as BOREALIN, is a component of the chromosomal passenger complex essential for mitosis and cell division [37].

We also identified 32 genes associated with the DNA damage response that were directly repressed by HOXC9 (Figure 5A), accounting for 32.7% (32/98) of the HOXC9-responsive genes involved in the DNA damage response. Figure 5D shows the binding of HOXC9 to the promoter of *FANCM* and to both the promoter and 3′ region of *FEN1*. FANCM is a component of the FANCM–FAAP24–MHF protein complex that binds to DNA with interstrand cross-links and is responsible for recruiting the FA core complex to the damaged site [38]. FEN1 (flap endonuclease 1) is essential for DNA replication and repair by removing RNA and DNA 5′ flaps [39].

Collectively, these findings suggest that HOXC9 directly regulates the expression of distinct sets of genes to coordinate the molecular and cellular processes characteristic of neuronal differentiation.

HOXC9 targets E2F6 to the promoters of cell cycle genes

We next sought to determine the molecular basis for HOXC9 regulation of gene expression by identifying HOXC9-interacting proteins. We used a myc-tag antibody to isolate myc-HOXC9 and its associated proteins from

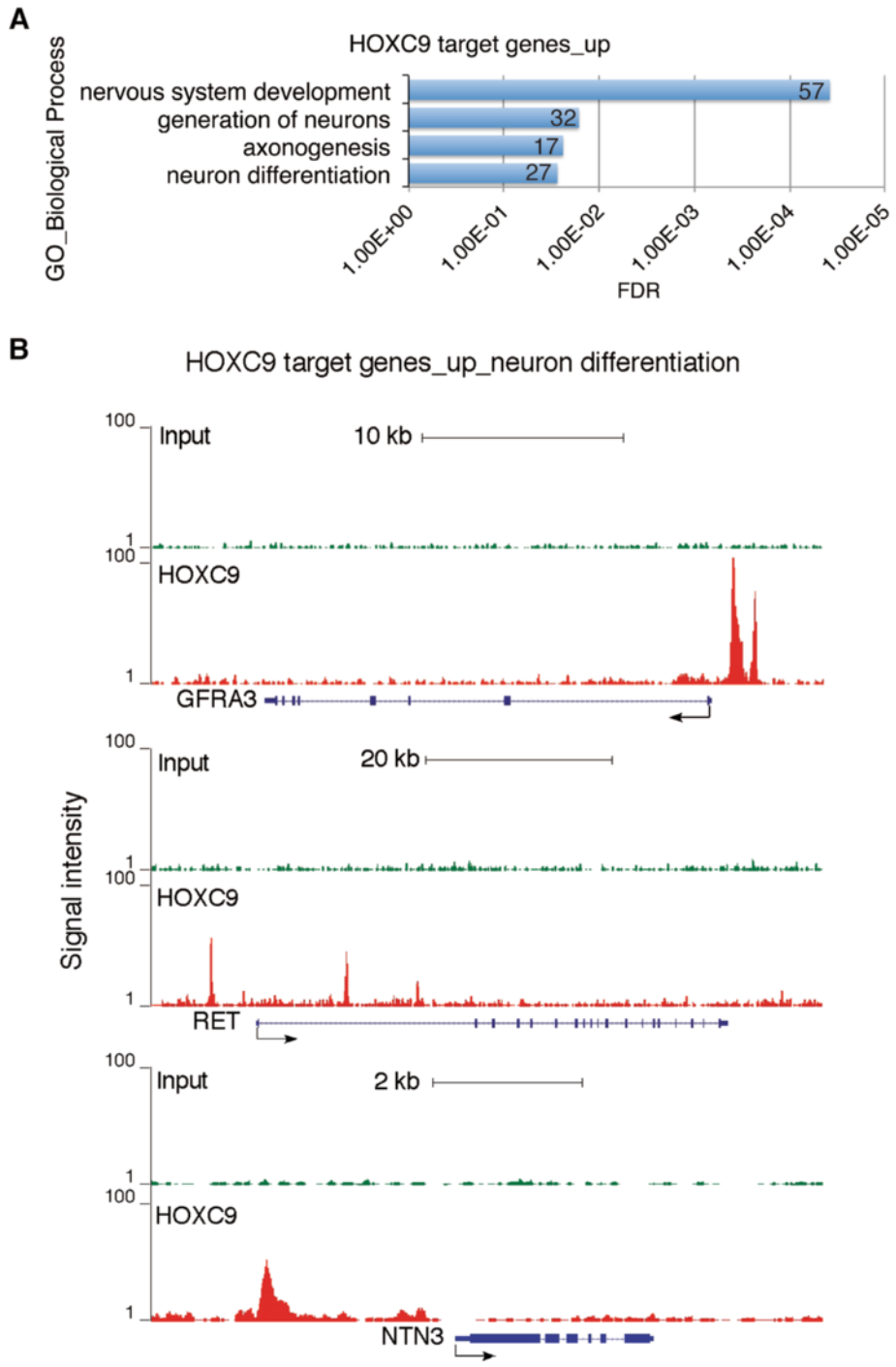

Figure 4 HOXC9 directly induces a large number of neuronal genes. (A) DAVID analysis of upregulated HOXC9 target genes for enriched GO biological process categories (enrichment fold > 2.0; FDR < 5%). The number of genes for each biological process category is indicated. **(B)** ChIP-seq tag profiles showing HOXC9 binding to representative upregulated HOXC9 target genes involved in nervous system development (*GFRA3*, top; *RET*, middle; *NTN3*, bottom).

nuclear extracts of BE(2)-C/Tet-Off/myc-HOXC9 cells cultured in the absence of doxycycline for 6 days (Additional file 3: Figure S3A). Mass spectrometric analysis of two independent samples identified E2F6 as a HOXC9-interacting protein (Additional file 3: Figure S3B), a well characterized transcriptional repressor that plays a major role in repressing E2F-responsive genes essential for cell proliferation [40]. It is known that E2F family proteins

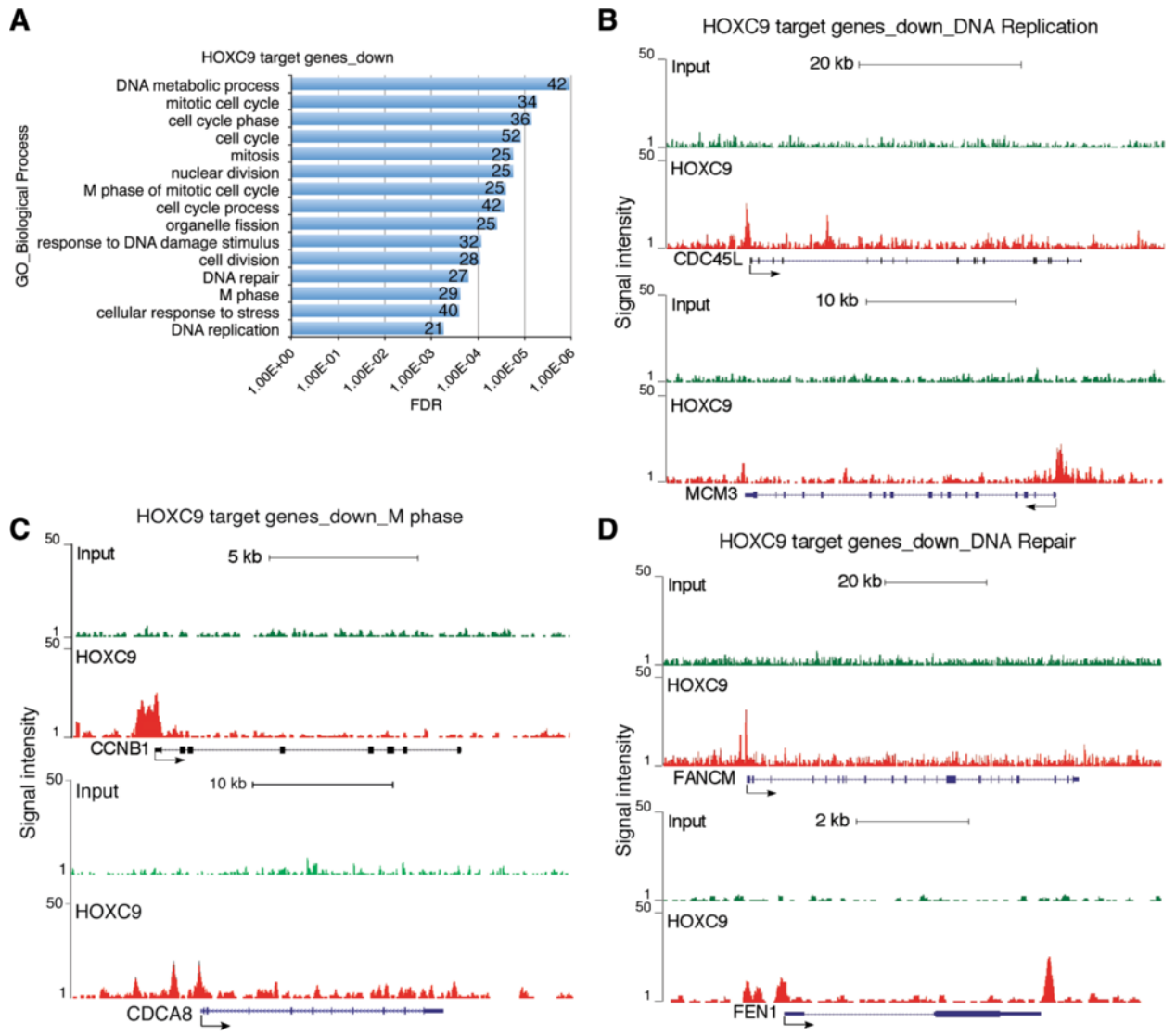

Figure 5 HOXC9 directly represses a large number of cell cycle and DNA repair genes. (A) DAVID analysis of downregulated HOXC9 target genes for enriched GO biological process categories (enrichment fold > 2.0; FDR <1%). The number of genes for each biological process category is indicated. **(B-D)** ChIP-seq tag profiles showing HOXC9 binding to representative downregulated HOXC9 target genes involved in DNA replication **(B)**, mitosis **(C)**, and DNA repair **(D)**.

(E2F1-6) share the same core consensus G/CTTTG/C binding site [41]. Interestingly, GSEA revealed significant enrichment of the E2F-binding motif among the genes downregulated by HOXC9 (Additional file 3: Figure S3C). Taken together, these observations suggest that E2F6 has an important role in HOXC9-mediated repression of cell cycle genes.

To corroborate the finding of mass spectrometry, we performed co-immunoprecipitation (Co-IP) experiments using nuclear extracts from BE(2)-C/Tet-Off/myc-HOXC9 cells cultured in the absence of doxycycline for 6 days. The myc-tag antibody, but not control IgG, precipitated myc-HOXC9 and E2F6 (Figure 6A, left panel). Reciprocally, an E2F6 antibody precipitated E2F6 and myc-HOXC9 (Figure 6A, right panel). We next performed size-exclusion chromatography using the same nuclear extracts. Immunoblot analysis revealed the presence of HOXC9 (~31 kDa) in two complexes: the larger complex (peak at fraction 20) had an estimated molecular mass of ~1,800 kDa and the other (peak at fraction 34) of ~250 kDa (Figure 6B). A significant amount of endogenous E2F6 (~36 kDa) co-eluted with the 1,800-kDa HOXC9 complex, whereas MEIS2 (~37-49 kDa), which interacts with HOX proteins and functions as a HOX cofactor [12], exclusively co-eluted with the 250 kDa-HOXC9 complex (Figure 6B). Co-IP experiments using pooled fractions confirmed the association

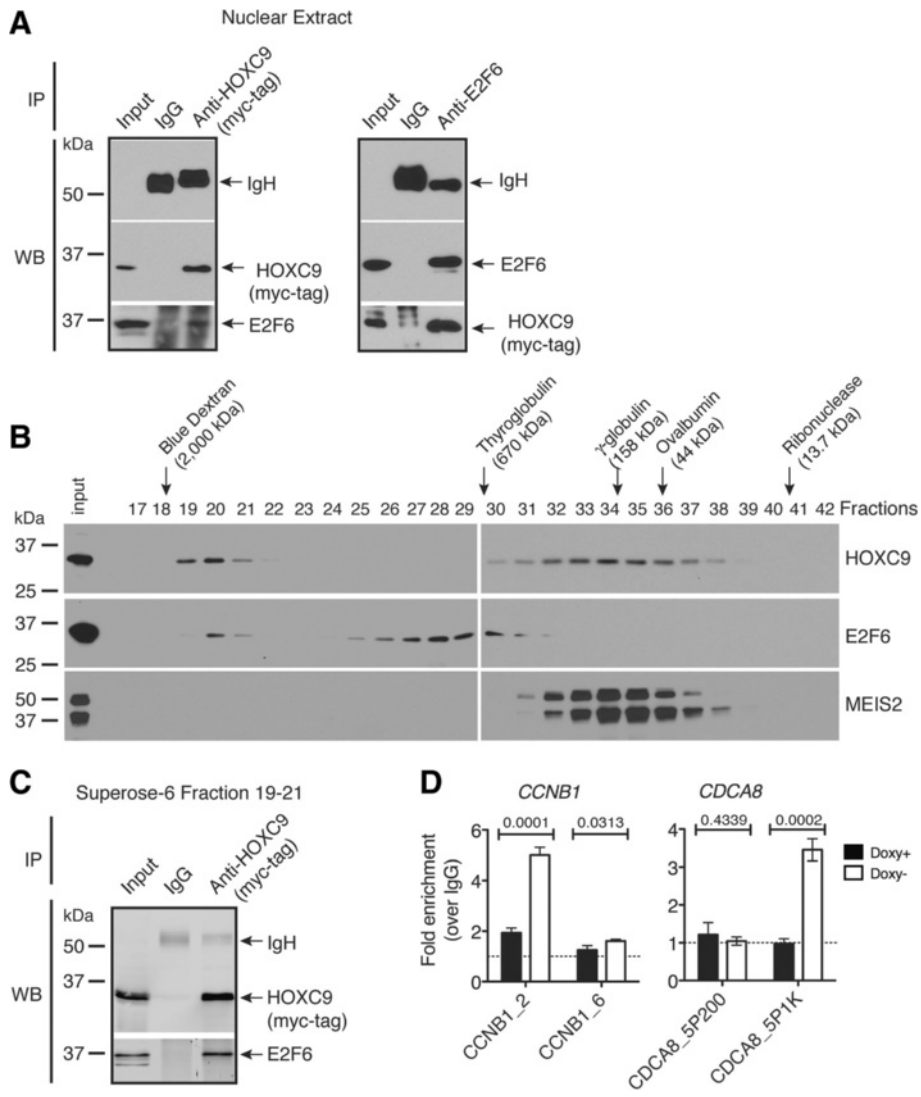

Figure 6 HOXC9 interacts with E2F6 and recruits it to cell cycle genes. (A) Reciprocal Co-IP of myc-HOXC9 and E2F6 in nuclear extracts from BE(2)-C/Tet-Off/myc-HOXC9 cells cultured in the absence of doxycycline (Doxy) for 6 days. **(B)** Size-exclusion chromatography analysis of complexes containing myc-HOXC9, E2F6 or MEIS2 in nuclear extracts of BE(2)-C/Tet-Off/myc-HOXC9 cells cultured in the absence of Doxy for 6 days. **(C)** Co-IP of myc-HOXC9 and E2F6 in pooled Superose-6 fractions 19–21. **(D)** ChIP-qPCR analysis showing E2F6 binding to specific promoter regions of the cell cycle genes *CCNB1* and *CDCA8* in BE(2)-C/Tet-Off/myc-HOXC9 cells before (Doxy+) and after (Doxy-) HOXC9 induction. Dashed lines indicate IgG control. Error bars represent SD (n = 3). Data were analyzed with unpaired, two-tailed Student's *t*-test and *p* values are indicated.

of HOXC9 with E2F6 within the larger complex (Figure 6C).

To determine whether the HOXC9-E2F6 interaction plays a role in recruiting E2F6 to HOXC9 target genes in vivo, we performed anti-E2F6 ChIP using BE(2)-C/Tet-Off/myc-HOXC9 cells before and after HOXC9 induction. HOXC9 induction had no apparent effect on E2F6 expression as determined by microarray gene expression profiling (−1.003 fold). ChIP-qPCR assay revealed that E2F6 was recruited to specific promoter regions of the cell cycle genes *CCNB1* and *CDCA8* only after HOXC9 induction (Figure 6D). By contrast, no significant binding of E2F6 to the *NEFM* promoter was observed before and after HOXC9 induction (Additional file 3: Figure S4A). As reported previously, *NEFM* is a neuronal gene directly activated by HOXC9 during differentiation [18] (See also Additional file 3: Figure S4B). Together, these data suggest that elevated levels of HOXC9 facilitate the formation of a repressive complex with E2F6, which is then recruited to cell cycle but not neuronal genes during differentiation.

E2F6 is essential for HOXC9-induced cell cycle arrest and transcriptional repression of cell cycle genes

To determine the functional significance of the HOXC9-E2F6 interaction, we examined the effect of E2F6 knockdown on HOXC9-induced growth arrest. We

depleted E2F6 using short hairpin RNA (shRNA) sequences targeting different coding regions of the human *E2F6* gene (Figure 7A). Cells with E2F6 knockdown were highly resistant to HOXC9-induced G1 arrest, showing continued cell proliferation (Figure 7B) and cell cycle progression (Figure 7C) following HOXC9 induction. This was accompanied by a marked decrease in the population of cells in the G1 phase and a significant increase in the population of cells in the S phase (Figure 7D). In addition, E2F6 knockdown largely abrogated the ability of HOXC9 to repress cyclin A2 and B1 expression, but had no significant effect on HOXC9 induction of NEFM (Figure 7E and F), a finding consistent with the observation of no significant E2F6 binding to the *NEFM* promoter during HOXC9-induced differentiation (Additional file 3: Figure S4A). Together, these findings identify an essential and specific role for E2F6 in HOXC9 induction of growth arrest and repression of cell cycle genes.

Discussion

In this report, we present evidence for a master regulator of development with the capacity to coordinate diverse cellular events characteristic of neuronal differentiation by simultaneously and directly regulating distinct sets of genes (Figure 8). Through gene expression profiling, we show that HOXC9-induced neuronal differentiation is characterized at the molecular level by transcriptional regulation of 2,370 genes, with global activation of genes that promote nervous system development and repression of genes that are essential for cell cycle progression and the DNA damage response. Moreover, through a combination of genome-wide mapping of HOXC9 binding sites and gene expression profiling, we show that HOXC9 directly regulates the expression of 954 genes, ~40% of the 2,370 HOXC9-responsive genes, including a large number of genes required for neuronal differentiation, cell cycle progression and the DNA damage response. Finally, we identify an essential role for E2F6 in HOXC9 repression of cell cycle genes and induction of G1 arrest.

Our findings that HOXC9 can both activate and repress gene transcription are consistent with previous observations from the study of spinal cord development in chick and mouse embryos. In the developing spinal cord, Hoxc9 functions as a transcription activator to promote the fate of preganglionic motor column (PGC) neurons [42], most likely through its interaction with the transcription factor FoxP1 [43,44]. However, Hoxc9 can also specify the fate of hypaxial motor column (HMC) neurons by repressing the *Hox* genes that promote the switch of HMC neurons to the lateral motor column (LMC) neurons [35]. Importantly, our study further demonstrated that within the same population of neuroblastoma cells, HOXC9 could simultaneously activate the genes that promote neuronal differentiation and repress the genes that are essential for cell cycle progression and the DNA damage response. While the molecular basis for the transcription activator function of HOXC9 in neuroblastoma cells remain to be defined, we showed that the ability of HOXC9 to repress cell cycle genes depended on its interaction with the transcription repressor E2F6, a member of the E2F family of transcription factors that have a critical role in the control of cell proliferation [40].

Cellular differentiation is tightly linked to cell cycle exit, with the differentiated cell containing the G1 content of DNA. The molecular mechanism that couples cell cycle exit and differentiation is not well understood, although it is generally recognized that cell cycle regulators influence differentiation, and cell fate determinants influence the cell cycle [45-48]. A primary example is the CDK inhibitor $p27^{Kip1}$ as a key regulator that links cell cycle exit and differentiation during development. $p27^{Kip1}$ induces G1 arrest by associating with CDK/cyclin complexes and inhibits their kinase activity [49]. Overexpression of $p27^{Xic1}$, a *Xenopus* homolog of $p27^{Kip1}$, in *Xenopus* retina glial progenitor cells promotes both cell cycle exit and differentiation [50]. Knockout and overexpression studies also demonstrate an important role of $p27^{Kip1}$ in neuronal differentiation in the mouse cerebral cortex by stabilizing Neurogenin 2 [51], a proneural bHLH transcription factor with a central role in cortical neurogenesis [52]. On the other hand, cell fate determinants can also modulate the expression of $p27^{Kip1}$ for coordinated regulation of cell cycle exit and differentiation. For instance, *Drosophila* proneural bHLH proteins cooperate with epidermal growth factor signaling to directly activate the transcription of *Dapaco*, a homolog of $p21^{Cip}$/$p27^{Kip1}$, during the differentiation of photoreceptor cells [53].

Our findings suggest an alternative mechanism for coupling cell cycle exit and differentiation. HOXC9 does not regulate the expression of CDK inhibitors, including $p27^{Kip1}$ and $p21^{Cip}$, and overexpression of either $p27^{Kip1}$ or $p21^{Cip}$ fails to stop the proliferation of BE(2)-C cells [18]. Rather, HOXC9 induces G1 arrest by directly repressing a large number of genes essential for cell cycle progression through the S to M phases, including cyclin B1, CDCA3, CDCA8, BUB1B, MCM3 and MCM8. This transcriptional repression function of HOXC9 requires E2F6. We found that HOXC9 interacts with E2F6 and recruits it specifically to the promoters of cell cycle genes. E2F6 lacks a transactivation domain and functions as a transcriptional repressor for E2F-responsive genes that drive cell proliferation [54-58]. Mechanistically, E2F6 interacts with chromatin modifiers with transcription repressor activity to establish a repressive chromatin structure. These chromatin modifiers include the DNA methyltransferase Dnmt3b [59] and polycomb-group (PcG) proteins [60-63]. In our study, we identified HOXC9 and E2F6 within a complex of approximately 1,800 kDa. Whether this

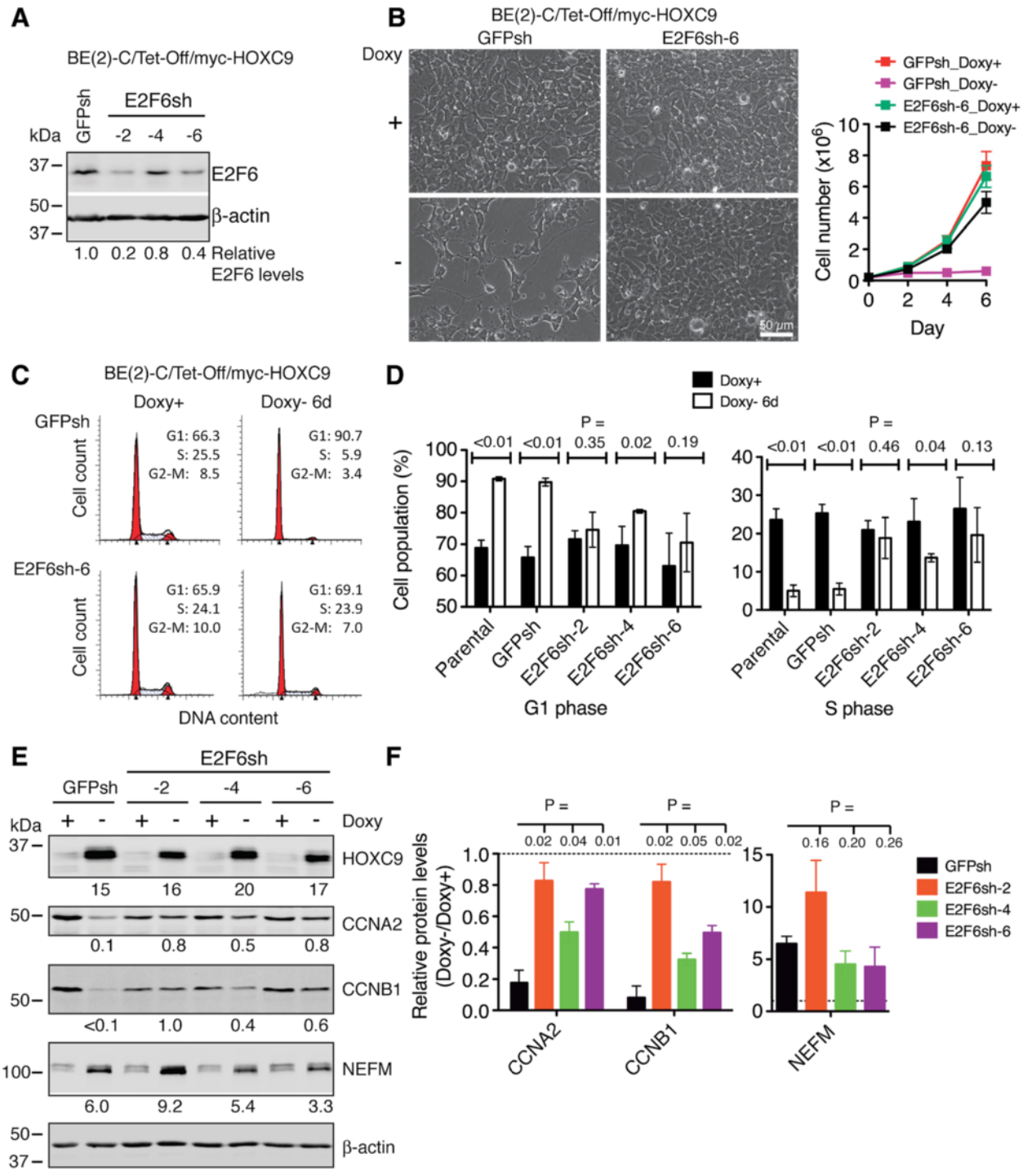

Figure 7 E2F6 is essential for HOXC9 induction of G1 arrest and repression of cell cycle genes. (A) Immunoblot analysis of E2F6 levels in BE(2)-C/Tet-Off/myc-HOXC9 cells infected with lentiviruses expressing shRNA against *GFP* or various coding regions of *E2F6*. E2F6 levels were quantified against β-actin. **(B-D)** Phase contrast imaging and growth assay **(B)** and cell cycle analysis **(C, D)** showing E2F6 knockdown abrogated HOXC9-induced growth arrest. Error bars, SD (n = 4). **(E-F)** Immunoblot analysis **(E)** and quantification **(F)** showing that E2F6 knockdown abrogated HOXC9 repression of cyclins, but not HOXC9 induction of NEFM. HOXC9, CCNA2, CCNB1 and NEFM levels were quantified against β-actin with the protein levels in GFPsh-expressing cells cultured in the presence of doxycycline (Doxy+) were defined as 1.0 (dashed lines). Error bars, SD (n = 3). Data in **(D)** and **(F)** were analyzed with unpaired, two-tailed Student's *t*-test and *p* values are indicated.

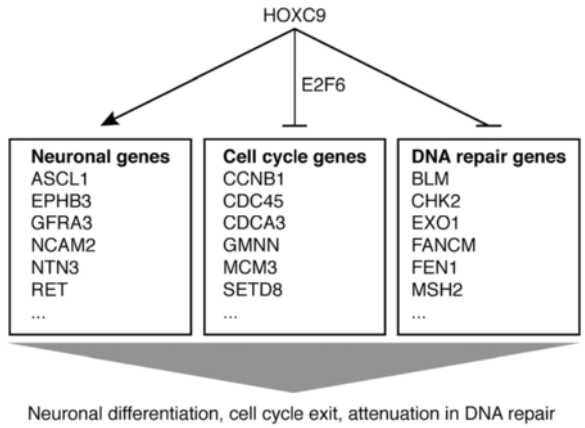

Figure 8 HOXC9 directly regulates the expression of distinct sets of genes to coordinate diverse cellular events associated with neuronal differentiation.

complex contains chromatin modifiers is currently under investigation.

Terminal cell differentiation is also tightly associated with a global reduction in DNA damage repair activities [1-3]. The underlying molecular mechanism is not well understood. It has been reported that E1 ubiquitin-activating enzyme can complement nucleotide-excision repair deficiency in extracts from differentiated macrophages, suggesting a role of ubiquitination in the control of the DNA damage response during differentiation [64]. Our study revealed that in HOXC9-induced neuronal differentiation, attenuation of the DNA damage response resulted from global transcriptional repression of DNA repair genes. This finding provides a molecular mechanism for the long observed differentiation-induced radiosensitivity in neuroblastoma cells [20,24-27]. For HOXC9-induced differentiation, a total of 98 genes with functions in the DNA damage response were significantly downregulated. These genes are involved in all types of DNA damage checkpoints and repair pathways. Importantly, we show that 32 of the 98 genes are direct targets of HOXC9. Thus, to a large extent, HOXC9 coordinates neuronal differentiation and attenuation of DNA repair activities by simultaneously activating neuronal genes and repressing DNA repair genes. Since the DNA damage response and DNA replication machineries share many components, we speculate that the downregulation of DNA repair genes during differentiation is a consequence of repression of cell cycle genes, particularly those involved in DNA replication.

The stem cell model of cancer attributes cancer growth to a subpopulation of cancer stem cells. It has been shown recently that cancer stem cells are intrinsically resistant to ionizing radiation and chemotherapy, as a result of enhanced checkpoint activation and more effective DNA damage repair [7-10]. Since differentiation is associated with global downregulation of DNA repair activities, a combination of differentiation-inducing agents and irradiation or chemotherapy may prove to be a more effective therapeutic strategy for targeting cancer stem cells.

Conclusions

Using neuroblastoma cell differentiation as an experimental system, we delineate a molecular mechanism by which HOXC9 coordinates diverse cellular processes associated with differentiation by directly activating and repressing the transcription of distinct sets of genes.

Methods

Cell culture and growth assays

The human neuroblastoma cell line BE(2)-C (CRL-2268, ATCC) with Tet-Off inducible expression of myc-tagged human HOXC9 has been described previously [18]. For E2F6 knockdown, BE(2)-C/Tet-Off/myc-HOXC9 cells were infected with lentiviruses expressing shRNA against E2F6 (TRCN013819, E2F6sh-2, TTTCGAGTTAAATAAACCAGC; TRCN013821, E2F6sh-4, ATTGGTGATGTCATACACTCT; TRCN018201, E2F6sh-6, ATCCAAAGCATCTTCCATTGC; Thermo Fisher Scientific). Cells were cultured in a 1:1 mixture of DMEM and Ham's nutrient mixture F12 supplemented with 10% fetal bovine serum (Invitrogen-Gibco) in the presence or absence of doxycycline. Cells were examined and phase contrast images captured using an Axio Observer microscope and AxioVision software (Carl Zeiss MicroImaging), and viable cell numbers were determined by trypan blue exclusion assay. For cell cycle analysis, cells were fixed in 70% ethanol, incubated with ribonuclease A (Sigma-Aldrich), and stained with 20 μg/ml propidium iodide (Invitrogen-Gibco). Samples were analyzed using a FACSCalibur system and ModFitLT V3.2.1 software (BD Bioscience).

Microarray gene expression profiling

Total RNA was isolated using Trizol (Invitrogen) from three independent samples of BE(2)-C/Tet-Off/myc-HOXC9 cells cultured in the presence or absence of doxycycline for 6 days. RNA was measured and quality assessed by a NanoDrop spectrophotometer and an Agilent 2100 Bioanalyzer (Agilent Technologies). Affymetrix microarray analysis was performed using the Human Gene 1.0 ST microarray chip. Data were normalized, significance determined by ANOVA, and fold change calculated with the Partek Genomics Suite (Partek Inc.). Gene annotation enrichment analysis was performed with DAVID v6.7 [30], GSEA [65], and IPA (Ingenuity® Systems www.ingenuity.com) for all significantly changed genes (≥ +1.5 and ≤ −1.5 fold, $P < 0.01$).

ChIP-seq and ChIP-qPCR

Two independent preparations of BE(2)-C/Tet-Off/myc-HOXC9 cells cultured in the presence or absence of doxycycline for 6 days were used for ChIP. Cross-linked chromatin DNA was sheared through sonication and immunoprecipitated using mouse anti-myc tag (clone 4A6, Millipore) or mouse anti-E2F6 (sc-53273, Santa Cruz Biotechnologies) according to the published procedure [66]. For ChIP-seq, libraries were generated from ChIP genomic DNA samples according to the Illumina ChIP-seq library construction procedure, and sequenced using Illumina Genome Analyzer IIx with a read length of 36 or 76 bp. For ChIP-qPCR, ChIP genomic DNA samples were assayed in triplicate by PCR using an iQ5 real-time PCR system (Bio-Rad) and the following primer sets that cover the promoter regions of *CCNB1* (CCNB1_2 and CCNB1_6), *CDCA8* (CDCA8_5P200 and CDCA8_5P1K), and *NEFM* (NEFM_5P1 and NEFM_5P2): CCNB1_2: CCAGAGAGTTGTTGCAACGAT, CTGGAGAGCAGT GAAGCCAGT; CCNB1_6: GGAAGGATTGATCAAACC CAG, AGTCACGGATCCGAAAGAAGG; CDCA8_5P200: GGTATTGCAGAGCCGCCA, CCTCCCCACCAACCCAC C; CDCA8_5P1K: TGGTGCCCATCAGGAGCC, GGCT ATGGGAGTGATAATC; NEFM_5P1: GCAGAAAGTAA TAAGCAACAA, CCTGCCTTCTGTAAAGTATTG; NEFM_ 5P2: CCTTTCCTGATTACTTACTGA, AGGGACTCCAGA CCGAAATAG.

ChIP-seq data analysis

Raw Illumina sequencing reads from the two independent ChIP replicates (rep1, GEO GSM848788 and rep2, GEO GSM848789) in the FASTQ format were cleaned using in-house scripts by trimming sequencing adaptors and low quality bases in both ends ($Q < 67$ in Illumina 1.5). Cleaned sequences were then mapped to the human genome (hg19) using Novoalign v2.07 for identifying the reads that were mapped uniquely to a single genomic locus. The identified reads from the rep1 ChIP sample (GEO GSM848788) were used for peak calling with Model-based Analysis of ChIP-Seq (MACS v1.4) [67], and only those peaks with FDR <1% were compared with RefSeq genes in the UCSC genome browser and classified into functional categories such as promoters, 5'-UTRs, exons, introns, 3'-UTRs, downstream, and intergenic regions. To measure the correlation of two HOXC9 replicates, we used 200 bp non-overlapping windows where a tag density is defined as the number of reads in a window. We calculated Pearson correlation coefficient with $R > 0.9$ being highly correlated. For motif analysis, we extracted 100 bp flanking sequences from predicted peak summits and ran MEME for identifying statistically overrepresented motifs. We performed MAST to search motifs in the peaks using the model built by MEME.

Identification of HOXC9 target genes

Genes with HOXC9-binding peaks that are non-intergenic (i.e., within $-5 \sim +5$ kb of genes) were defined as HOXC9 target genes. To correlate HOXC9 binding to gene expression, we combined the HOXC9 ChIP-seq data with the HOXC9 microarray data using in-house scripts to generate a list of the genes whose regulatory elements are bound by HOXC9 and whose expression levels are significantly changed ($\geq +1.5$ and ≤ -1.5 fold, $P < 0.01$) as the result of HOXC9 induction. The significantly up- and down-regulated HOXC9 target genes were then subjected to gene annotation enrichment analysis with DAVID v6.7, GSEA, and IPA.

Immunoprecipitation and mass spectrometric analyses

BE(2)-C/Tet-Off/myc-HOXC9 cells were cultured in the absence of doxycycline for 6 days and nuclear extracts were prepared following the Dignam protocol [68] except that buffer C contained 300 mM NaCl. Extracts from 1×10^7 cells were incubated with Protein A/G beads (Invitrogen) coated with 4 μg mouse anti-Myc tag (clone 4A6, Millipore) or mouse IgG for overnight at 4°C. The beads were washed 3 times with buffer C containing 150 mM NaCl, dried in a SpeedVac, re-suspended in a buffer containing 8M urea, 5 mM DTT and 100 mM ammonium bicarbonate, and alkylated with 15 mM iodoacetamide for 1 hour. After alkylation, unreacted iodoacetamide was removed by 15 mM DTT and the urea concentration was diluted to ~1M with a buffer containing 50 mM ammonium bicarbonate and 2 mM $CaCl_2$. Immunoprecipitated proteins were digested with 14 ng/μl sequencing grade trypsin (Promega) for 24 hours at 37°C. The digests were desalted with a Micro Trap desalting cartridge (Michrom BioResources), and tryptic peptides eluted with LC-MS Solvent B (90/10/0.05%: Acetonitrile/water/heptafluorobutyric acid) and dried in a SpeedVac. The digests were analyzed by Nano-HPLC using a Nano Trap column (CL5/61241/00, Michrom BioResources) and an Agilent 1200 Series Nano pump (Agilent Technologies) equipped with a refrigerated autosampler. An Agilent 1200 Series Capillary LC loading pump was used to introduce the sample onto a Captrap cartridge for sample concentration and de-salting.

Data-dependent MS and MS/MS spectra were acquired on an LTQ Orbitrap Discovery (Thermo Fisher Scientific) using 2 micro-scans, with a maximum injection time of 200 ms with 2 Da peak isolation width. Six scan events were recorded for each data acquisition cycle. The first scan event, acquired by the FTMS, was used for full scan MS acquisition from 300–2000 m/z. Data were recorded in the Centroid mode only. The remaining five scan events were used for collisionally activated dissociation (CAD): the five most abundant ions in each peptide MS

were selected and fragmented to produce product-ion mass spectra.

Database searching and protein identification

All MS/MS data were analyzed using BioWorks Rev.3.3.1 SP1 (Thermo Fisher Scientific) and X!Tandem (thegpm.org). SEQUEST was set up to search NCBInr_Homosapiens_05262011.fasta (221863 entries) and the human.protein_RefSeq_01192012 database (33376), and X!Tandem was set up to search subsets of the databases. SEQUEST and X!Tandem were searched with a fragment ion mass tolerance of 0.80 Da and a parent ion tolerance of 10.0 PPM. Scaffold (Proteome Software) was used to validate MS/MS-based peptide and protein identifications. Peptide identifications were accepted if they could be established at greater than 95.0% probability as specified by the Peptide Prophet algorithm [69]. Protein identifications were accepted if they could be established at greater than 90.0% probability and contained at least 1 identified peptide. Protein probabilities were assigned by the Protein Prophet algorithm [70]. Proteins that contained similar peptides and could not be differentiated based on MS/MS analysis alone were grouped to satisfy the principles of parsimony. Single-peptide protein identification was accepted only if the protein was independently identified by both SEQUEST and X!Tandem.

Size-exclusion chromatography

Size-exclusion chromatography was performed with a Superose-6 10/300 GL column (24 ml bed volume) and an AKTA purifier (GE Healthcare). Nuclear extracts (0.5 ml) were loaded onto the column equilibrated with PBS, and 0.5 ml fractions were collected and analyzed.

Co-immunoprecipitation

Nuclear extracts or pooled Sepharose-6 fractions were incubated with protein A/G beads coated with mouse anti-Myc tag (clone 4A6), mouse anti-E2F6, or control mouse IgG for 2 hours at 4°C. After washing 3 times with PBS, the beads were suspended in standard SDS sample buffer and analyzed by immunoblotting.

Immunoblotting

Unless indicated, all antibodies were from Santa Cruz Biotechnologies. Samples were suspended in SDS sample buffer and boiled. Proteins were separated on SDS-polyacrylamide gels, transferred to nitrocellulose membranes, and probed with the following primary antibodies: rabbit anti-cyclin A2 (sc-751, 1:200), rabbit anti-cyclin B1 (sc-752, 1:200), mouse anti-myc-tag (9E10, hybridoma supernatant, 1:10), rabbit anti-E2F6 (sc-22823, 1:200), mouse anti-MEIS2 (63-T, sc-81986, 1:400), mouse anti-NEFM (NF-09, sc-51683, 1:200), and rabbit anti-β-actin (600-401-886, Rockland Immunochemicals, 1:2000). Horseradish peroxidase-conjugated goat anti-mouse and goat anti-rabbit IgG were used as secondary antibodies. Proteins were visualized using a SuperSignal West Pico chemiluminescence kit (Pierce, Thermo Fisher Scientific) and quantified with ImageJ (National Institutes of Health). For visualization and quantification with the Odyssey system, goat anti-mouse IRDye 800, anti-rabbit IRDye 800, anti-mouse IRDye 680, and anti-rabbit IRDye 680 were used as secondary antibodies (LI-COR Biosciences).

Statistics

All quantitative data were analyzed and presented with GraphPad Prism 5.0f for Mac using unpaired, two-tailed Student's *t*-test.

Additional files

Additional file 1: Table S1. HOXC9-responsivel genes.

Additional file 2: Table S2. GO analysis of upregulated HOXC9-responsive genes.

Additional file 3: Supplemental Figures S1-S4.

Additional file 4: Table S3. GO analysis of downregulated HOXC9-responsive genes.

Additional file 5: Table S4. HOXC9-binding peaks.

Additional file 6: Table S5. HOXC9-binding genes.

Additional file 7: Table S6. HOXC9-target genes.

Additional file 8: Table S7. GO analysis of upregulated HOXC9 direct target genes.

Additional file 9: Table S8. GO analysis of downregulated HOXC9 direct target genes. The microarray and ChIP-seq data have been deposited in the NCBI Gene Expression Omnibus (GEO) with the accession number GSE34422 (http://0-www.ncbi.nlm.nih.gov.elis.tmu.edu.tw/geo/query/acc.cgi?acc=GSE34422).

Abbreviations

BER: Base excision repair; CCN: Cyclin; CDK: Cyclin-dependent kinase; ChIP-seq: Chromatin immunoprecipitation and sequencing; Co-IP: Co-immunoprecipitation; DAVID: Database for annotation visualization and integrated discovery; DMEM: Dulbecco's modified eagle medium; DSB: Double-strand break; FA: Fanconi anemia; FDR: False discovery rate; FoxP1: Forkhead box protein P1; GSEA: Gene set enrichment analysis; HMC: Hypaxial motor column; IPA: Ingenuity pathways analysis; LC-MS: Liquid chromatography; Mass: Spectrometry; LMC: lateral motor column; MMR: Mismatch repair; NEFM: Neurofilament medium; NER: Nucleotide excision repair; PBS: Phosphate buffered saline; PGC: Preganglionic motor column; RA: Retinoic acid; TSS: Transcription start site; UTR: Untranslated region.

Competing interests

The authors declare that they have no competing interests.

Authors' contributions

XW, JD, LY and H-FD performed experiments with the assistance of HC and LM in establishing and characterizing inducible HOXC9 expression cells, LM in microarray sample preparation, BJ and MR in ChIP, EJL in ChIP-seq library preparation, and LCN in mass spectrometry. J-HC YZ, and H-FD performed microarray and ChIP-seq data analyses. XW, JD, HC, and H-FD designed the study with the assistance of HS, JC, and SH H-FD wrote the manuscript with contributions from JD, J-HC, LCN and EJL. All authors read and approved the final manuscript.

Acknowledgements
We thank Drs. LesleyAnn Hawthorn and Sam Chang at the Georgia Regents University Cancer Center Genomics Core for assistance in Microarray and ChIP-seq. This work was supported by grants from the National Institutes of Health (CA124982) and Department of Defense (W81XWH-12-1-0613) to H.-F. D., the National Basic Research Program of China (No. 2012cb114603) to H.C., and the National Natural Science Foundation of China (No. 81172443) to X. W. H.-F.D., H.S., and J.C. are Georgia Cancer Coalition Distinguished Scholars.

Author details
[1]Department of Urology, Second Affiliated Hospital, Third Military Medical University, Chongqing, China. [2]Cancer Center, Georgia Regents University, Augusta, GA 30912, USA. [3]Department of Biostatistics and Epidemiology, Medical College of Georgia, Georgia Regents University, Augusta, GA 30912, USA. [4]Department of Pathology, Medical College of Georgia, Georgia Regents University, Augusta, GA 30912, USA. [5]Department of Biochemistry and Molecular Biology, Medical College of Georgia, Georgia Regents University, Augusta, GA 30912, USA. [6]State Key Laboratory of Silkworm Genome Biology, Institute of Sericulture and System Biology, Southwest University, Chongqing, China. [7]Department of Neurology, First Hospital of Yichang, Three Gorges University College of Medicine, Yichang, China. [8]Department of Neurology, Union Hospital, Tongji Medical College, Huazhong University of Science and Technology, Wuhan, China.

Received: 26 July 2013 Accepted: 20 November 2013
Published: 25 November 2013

References

1. Nouspikel T, Hanawalt PC: **DNA repair in terminally differentiated cells.** *DNA Repair (Amst)* 2002, **1**(1):59–75.
2. Simonatto M, Latella L, Puri PL: **DNA damage and cellular differentiation: more questions than responses.** *J Cell Physiol* 2007, **213**(3):642–648.
3. Fortini P, Dogliotti E: **Mechanisms of dealing with DNA damage in terminally differentiated cells.** *Mutat Res* 2010, **685**(1–2):38–44.
4. Reya T, Morrison SJ, Clarke MF, Weissman IL: **Stem cells, cancer, and cancer stem cells.** *Nature* 2001, **414**(6859):105–111.
5. Clarke MF, Dick JE, Dirks PB, Eaves CJ, Jamieson CH, Jones DL, Visvader J, Weissman IL, Wahl GM: **Cancer stem cells–perspectives on current status and future directions: AACR workshop on cancer stem cells.** *Cancer Res* 2006, **66**(19):9339–9344.
6. Visvader JE, Lindeman GJ: **Cancer stem cells in solid tumours: accumulating evidence and unresolved questions.** *Nat Rev Cancer* 2008, **8**(10):755–768.
7. Bao S, Wu Q, McLendon RE, Hao Y, Shi Q, Hjelmeland AB, Dewhirst MW, Bigner DD, Rich JN: **Glioma stem cells promote radioresistance by preferential activation of the DNA damage response.** *Nature* 2006, **444**(7120):756–760.
8. Phillips TM, McBride WH, Pajonk F: **The response of CD24(−/low)/CD44+ breast cancer-initiating cells to radiation.** *J Natl Cancer Inst* 2006, **98**(24):1777–1785.
9. Eramo A, Ricci-Vitiani L, Zeuner A, Pallini R, Lotti F, Sette G, Pilozzi E, Larocca LM, Peschle C, De Maria R: **Chemotherapy resistance of glioblastoma stem cells.** *Cell Death Differ* 2006, **13**(7):1238–1241.
10. Liu G, Yuan X, Zeng Z, Tunici P, Ng H, Abdulkadir IR, Lu L, Irvin D, Black KL, Yu JS: **Analysis of gene expression and chemoresistance of CD133+ cancer stem cells in glioblastoma.** *Mol Cancer* 2006, **5**:67.
11. Pearson JC, Lemons D, McGinnis W: **Modulating Hox gene functions during animal body patterning.** *Nat Rev Genet* 2005, **6**(12):893–904.
12. Moens CB, Selleri L: **Hox cofactors in vertebrate development.** *Dev Biol* 2006, **291**(2):193–206.
13. Shah N, Sukumar S: **The Hox genes and their roles in oncogenesis.** *Nat Rev Cancer* 2010, **10**(5):361–371.
14. Argiropoulos B, Humphries RK: **Hox genes in hematopoiesis and leukemogenesis.** *Oncogene* 2007, **26**(47):6766–6776.
15. Brodeur GM: **Neuroblastoma: biological insights into a clinical enigma.** *Nat Rev Cancer* 2003, **3**:203–216.
16. Maris JM: **Recent advances in neuroblastoma.** *N Engl J Med* 2010, **362**(23):2202–2211.
17. Kocak H, Ackermann S, Hero B, Kahlert Y, Oberthuer A, Juraeva D, Roels F, Theissen J, Westermann F, Deubzer H, *et al*: **Hox-C9 activates the intrinsic pathway of apoptosis and is associated with spontaneous regression in neuroblastoma.** *Cell Death Dis* 2013, **4**:e586.
18. Mao L, Ding J, Zha Y, Yang L, McCarthy BA, King W, Cui H, Ding HF: **HOXC9 Links cell-cycle exit and neuronal differentiation and is a prognostic marker in neuroblastoma.** *Cancer Res* 2011, **71**(12):4314–4324.
19. Seeds NW, Gilman AG, Amano T, Nirenberg MW: **Regulation of axon formation by clonal lines of a neural tumor.** *Proc Natl Acad Sci USA* 1970, **66**(1):160–167.
20. Jensen L, Linn S: **A reduced rate of bulky DNA adduct removal is coincident with differentiation of human neuroblastoma cells induced by nerve growth factor.** *Mol Cell Biol* 1988, **8**(9):3964–3968.
21. Sidell N: **Retinoic acid-induced growth inhibition and morphologic differentiation of human neuroblastoma cells in vitro.** *J Natl Cancer Inst* 1982, **68**(4):589–596.
22. Abemayor E, Sidell N: **Human neuroblastoma cell lines as models for the in vitro study of neoplastic and neuronal cell differentiation.** *Environ Health Perspect* 1989, **80**:3–15.
23. Zha Y, Ding E, Yang L, Mao L, Wang X, McCarthy BA, Huang S, Ding HF: **Functional dissection of HOXD cluster genes in regulation of neuroblastoma cell proliferation and differentiation.** *PLoS One* 2012, **7**(8):e40728.
24. Byfield JE, Lee YC, Klisak I, Finklestein JZ: **Effect of differentiation on the repair of DNA single strand breaks in neuroblastoma cells.** *Biochem Biophys Res Commun* 1975, **63**(3):730–735.
25. McCombe P, Lavin M, Kidson C: **Control of DNA repair linked to neuroblastoma differentiation.** *Int J Radiat Biol* 1976, **29**(6):523–531.
26. Lavin MF, McCombe P, Kidson C: **DNA replication and post-replication repair in U.V.-sensitive mouse neuroblastoma cells.** *Int J Radiat Biol* 1976, **30**(1):31–40.
27. James M, Mansbridge J, Kidson C: **Ultraviolet radiation sensitivity of proliferating and differentiated human neuroblastoma cells.** *Int J Radiat Biol* 1982, **41**(5):547–556.
28. Duester G: **Retinoic acid synthesis and signaling during early organogenesis.** *Cell* 2008, **134**(6):921–931.
29. Dennis G Jr, Sherman BT, Hosack DA, Yang J, Gao W, Lane HC, Lempicki RA: **DAVID: Database for Annotation, Visualization, and Integrated Discovery.** *Genome Biol* 2003, **4**(5):3.
30. Huang DW, Sherman BT, Lempicki RA: **Systematic and integrative analysis of large gene lists using DAVID bioinformatics resources.** *Nat Protoc* 2008, **4**(1):44–57.
31. Francis NJ, Landis SC: **Cellular and molecular determinants of sympathetic neuron development.** *Annu Rev Neurosci* 1999, **22**:541–566.
32. Goridis C, Rohrer H: **Specification of catecholaminergic and serotonergic neurons.** *Nat Rev Neurosci* 2002, **3**(7):531–541.
33. Ernsberger U: **The role of GDNF family ligand signalling in the differentiation of sympathetic and dorsal root ganglion neurons.** *Cell Tissue Res* 2008, **333**(3):353–371.
34. Rajasekharan S, Kennedy T: **The netrin protein family.** *Genome Biol* 2009, **10**(9):239.
35. Jung H, Lacombe J, Mazzoni EO, Liem KF Jr, Grinstein J, Mahony S, Mukhopadhyay D, Gifford DK, Young RA, Anderson KV, *et al*: **Global control of motor neuron topography mediated by the repressive actions of a single hox gene.** *Neuron* 2010, **67**(5):781–796.
36. Bell SP, Dutta A: **DNA replication in eukaryotic cells.** *Annu Rev Biochem* 2002, **71**(1):333–374.
37. Carmena M, Wheelock M, Funabiki H, Earnshaw WC: **The chromosomal passenger complex (CPC): from easy rider to the godfather of mitosis.** *Nat Rev Mol Cell Biol* 2012, **13**(12):789–803.
38. Kee Y, D'Andrea AD: **Expanded roles of the Fanconi anemia pathway in preserving genomic stability.** *Genes Dev* 2010, **24**(16):1680–1694.
39. Liu Y, Kao H-I, Bambara RA: **FLAP ENDONUCLEASE 1: a central component of DNA metabolism.** *Annu Rev Biochem* 2004, **73**(1):589–615.
40. Trimarchi JM, Lees JA: **Sibling rivalry in the E2F family.** *Nat Rev Mol Cell Biol* 2002, **3**(1):11–20.
41. Xu X, Bieda M, Jin VX, Rabinovich A, Oberley MJ, Green R, Farnham PJ: **A comprehensive ChIP-chip analysis of E2F1, E2F4, and E2F6 in normal and tumor cells reveals interchangeable roles of E2F family members.** *Genome Res* 2007, **17**(11):1550–1561.
42. Dasen JS, Liu JP, Jessell TM: **Motor neuron columnar fate imposed by sequential phases of Hox-c activity.** *Nature* 2003, **425**(6961):926–933.
43. Rousso DL, Gaber ZB, Wellik D, Morrisey EE, Novitch BG: **Coordinated actions of the forkhead protein Foxp1 and Hox proteins in the columnar organization of spinal motor neurons.** *Neuron* 2008, **59**(2):226–240.

44. Dasen JS, De Camilli A, Wang B, Tucker PW, Jessell TM: **Hox repertoires for motor neuron diversity and connectivity gated by a single accessory factor, FoxP1.** *Cell* 2008, **134**(2):304–316.
45. Edlund T, Jessell TM: **Progression from extrinsic to intrinsic signaling in cell fate specification: a view from the nervous system.** *Cell* 1999, **96**(2):211–224.
46. Ohnuma S, Harris WA: **Neurogenesis and the cell cycle.** *Neuron* 2003, **40**(2):199–208.
47. Galderisi U, Jori FP, Giordano A: **Cell cycle regulation and neural differentiation.** *Oncogene* 2003, **22**(33):5208–5219.
48. Salomoni P, Calegari F: **Cell cycle control of mammalian neural stem cells: putting a speed limit on G1.** *Trends Cell Biol* 2010, **20**(5):233–243.
49. Sherr CJ, Roberts JM: **CDK inhibitors: positive and negative regulators of G1-phase progression.** *Genes Dev* 1999, **13**(12):1501–1512.
50. Ohnuma S, Philpott A, Wang K, Holt CE, Harris WA: **p27Xic1, a Cdk inhibitor, promotes the determination of glial cells in Xenopus retina.** *Cell* 1999, **99**(5):499–510.
51. Nguyen L, Besson A, Heng JI, Schuurmans C, Teboul L, Parras C, Philpott A, Roberts JM, Guillemot F: **p27kip1 independently promotes neuronal differentiation and migration in the cerebral cortex.** *Genes Dev* 2006, **20**(11):1511–1524.
52. Nieto M, Schuurmans C, Britz O, Guillemot F: **Neural bHLH genes control the neuronal versus glial fate decision in cortical progenitors.** *Neuron* 2001, **29**(2):401–413.
53. Sukhanova MJ, Deb DK, Gordon GM, Matakatsu MT, Du W: **Proneural basic helix-loop-helix proteins and epidermal growth factor receptor signaling coordinately regulate cell type specification and cdk inhibitor expression during development.** *Mol Cell Biol* 2007, **27**(8):2987–2996.
54. Morkel M, Wenkel J, Bannister AJ, Kouzarides T, Hagemeier C: **An E2F-like repressor of transcription.** *Nature* 1997, **390**(6660):567–568.
55. Gaubatz S, Wood JG, Livingston DM: **Unusual proliferation arrest and transcriptional control properties of a newly discovered E2F family member, E2F-6.** *Proc Natl Acad Sci USA* 1998, **95**(16):9190–9195.
56. Cartwright P, Muller H, Wagener C, Holm K, Helin K: **E2F-6: a novel member of the E2F family is an inhibitor of E2F-dependent transcription.** *Oncogene* 1998, **17**(5):611–623.
57. Trimarchi JM, Fairchild B, Verona R, Moberg K, Andon N, Lees JA: **E2F-6, a member of the E2F family that can behave as a transcriptional repressor.** *Proc Natl Acad Sci USA* 1998, **95**(6):2850–2855.
58. Giangrande PH, Zhu W, Schlisio S, Sun X, Mori S, Gaubatz S, Nevins JR: **A role for E2F6 in distinguishing G1/S- and G2/M-specific transcription.** *Genes Dev* 2004, **18**(23):2941–2951.
59. Velasco G, Hube F, Rollin J, Neuillet D, Philippe C, Bouzinba-Segard H, Galvani A, Viegas-Pequignot E, Francastel C: **Dnmt3b recruitment through E2F6 transcriptional repressor mediates germ-line gene silencing in murine somatic tissues.** *Proc Natl Acad Sci USA* 2010, **107**(20):9281–9286.
60. Ogawa H, Ishiguro K, Gaubatz S, Livingston DM, Nakatani Y: **A complex with chromatin modifiers that occupies E2F- and Myc-responsive genes in G0 cells.** *Science* 2002, **296**(5570):1132–1136.
61. Attwooll C, Oddi S, Cartwright P, Prosperini E, Agger K, Steensgaard P, Wagener C, Sardet C, Moroni MC, Helin K: **A novel repressive E2F6 complex containing the polycomb group protein, EPC1, that interacts with EZH2 in a proliferation-specific manner.** *J Biol Chem* 2005, **280**(2):1199–1208.
62. Deshpande AM, Akunowicz JD, Reveles XT, Patel BB, Saria EA, Gorlick RG, Naylor SL, Leach RJ, Hansen MF: **PHC3, a component of the hPRC-H complex, associates with E2F6 during G0 and is lost in osteosarcoma tumors.** *Oncogene* 2007, **26**(12):1714–1722.
63. Trojer P, Cao AR, Gao Z, Li Y, Zhang J, Xu X, Li G, Losson R, Erdjument-Bromage H, Tempst P, *et al*: **L3MBTL2 protein acts in concert with PcG protein-mediated monoubiquitination of H2A to establish a repressive chromatin structure.** *Mol Cell* 2011, **42**(4):438–450.
64. Nouspikel T, Hanawalt PC: **Impaired nucleotide excision repair upon macrophage differentiation is corrected by E1 ubiquitin-activating enzyme.** *Proc Natl Acad Sci USA* 2006, **103**(44):16188–16193.
65. Subramanian A, Tamayo P, Mootha VK, Mukherjee S, Ebert BL, Gillette MA, Paulovich A, Pomeroy SL, Golub TR, Lander ES, *et al*: **Gene set enrichment analysis: a knowledge-based approach for interpreting genome-wide expression profiles.** *Proc Natl Acad Sci USA* 2005, **102**(43):15545–15550.
66. Lee TI, Johnstone SE, Young RA: **Chromatin immunoprecipitation and microarray-based analysis of protein location.** *Nat Protoc* 2006, **1**(2):729–748.
67. Zhang Y, Liu T, Meyer CA, Eeckhoute J, Johnson DS, Bernstein BE, Nusbaum C, Myers RM, Brown M, Li W, *et al*: **Model-based analysis of ChIP-Seq (MACS).** *Genome Biol* 2008, **9**(9):R137.
68. Dignam JD, Lebovitz RM, Roeder RG: **Accurate transcription initiation by RNA polymerase II in a soluble extract from isolated mammalian nuclei.** *Nucleic Acids Res* 1983, **11**(5):1475–1489.
69. Keller A, Nesvizhskii AI, Kolker E, Aebersold R: **Empirical statistical model to estimate the accuracy of peptide identifications made by MS/MS and database search.** *Anal Chem* 2002, **74**(20):5383–5392.
70. Nesvizhskii AI, Keller A, Kolker E, Aebersold R: **A statistical model for identifying proteins by tandem mass spectrometry.** *Anal Chem* 2003, **75**(17):4646–4658.

doi:10.1186/1471-2164-14-830
Cite this article as: Wang *et al.*: HOXC9 directly regulates distinct sets of genes to coordinate diverse cellular processes during neuronal differentiation. *BMC Genomics* 2013 **14**:830.

Genomics Data 2 (2014) 50–52

Contents lists available at ScienceDirect

Genomics Data

journal homepage: http://www.journals.elsevier.com/genomics-data/

Genome-wide analysis of HOXC9-induced neuronal differentiation of neuroblastoma cells ☆

Xiangwei Wang [a,1], Liqun Yang [b,1], Jeong-Hyeon Choi [c,1], Eiko Kitamura [d], Chang-Sheng Chang [d], Jane Ding [c], Eun J. Lee [c], Hongjuan Cui [b,*], Han-Fei Ding [c,**]

[a] Department of Urology, Second Affiliated Hospital, Third Military Medical University, Chongqing, China
[b] State Key Laboratory of Silkworm Genome Biology, Institute of Sericulture and System Biology, Southwest University, Chongqing, China
[c] Cancer Center, Georgia Regents University, Augusta, GA 30912, USA
[d] Cancer Center, Integrated Genomics Core, Georgia Regents University, Augusta, GA 30912, USA

ARTICLE INFO

Article history:
Received 28 March 2014
Accepted 10 April 2014
Available online 18 April 2014

Keywords:
Neuroblastoma
differentiation
HOXC9

ABSTRACT

Induction of differentiation is a therapeutic strategy in neuroblastoma, a common pediatric cancer of the sympathetic nervous system. The homeobox protein HOXC9 is a key regulator of neuroblastoma differentiation. To gain a molecular understanding of the function of HOXC9 in promoting differentiation of neuroblastoma cells, we conducted a genome-wide analysis of the HOXC9-induced differentiation program by microarray gene expression profiling and chromatin immunoprecipitation in combination with massively parallel sequencing (ChIP-seq). Here we describe in detail the experimental system, methods, and quality control for the generation of the microarray and ChIP-seq data associated with our recent publication [1].

Specifications	
Organism/cell line/tissue	*Homo sapiens*
Strain(s)	Human neuroblastoma cell line BE(2)-C (CRL-2268, ATCC)
Sequencer or array type	Microarray: Affymetrix Human Gene 1.0 ST ChIP-seq: Illumina Genome Analyzer IIX
Data format	Microarray raw data: CEL files ChIP-seq raw data: FASTQ files
Experimental factors	BE(2)-C cells without or with HOXC9 overexpression
Experimental features	Microarray gene expression profiling to identify genes that are regulated by HOXC9 ChIP-seq to map genomic sites that are bound by HOXC9
Consent	N/A
Sample source location	N/A

Direct link to deposited data

Deposited data are available here: https://www.ncbi.nlm.nih.gov/geo/query/acc.cgi?acc=GSE34422.

☆ This work was supported by grants from the National Institutes of Health (CA124982) and U.S. Department of Defense (W81XWH-12-1-0613) to H.-F.D., and the National Natural Science Foundation of China (No. 81172443) to X.W.

* Corresponding author. Tel.: +86 15213460192.
** Corresponding author. Tel.: +1 706 721 4286; fax: +1 706 721 1670.
E-mail addresses: hcui@swu.edu.cn (H. Cui), hding@gru.edu (H.-F. Ding).
[1] These authors contributed equally to this work.

Experimental design, materials and methods

Cell line

The human neuroblastoma cell line BE(2)-C was obtained from ATCC (CRL-2268, ATCC). BE(2)-C cells carry *p53* mutation and *MYCN* amplification [2,3]. It has been shown previously that this cell line contains a subpopulation of neuroblastoma cells capable of self-renewal and multi-lineage differentiation [4,5]. BE(2)-C cells can differentiate into neurons following treatment with retinoic acid (RA) [4–7] or into Schwann-like cells when treated with bromodeoxyuridine [4,5,8]. As a result, BE(2)-C cells have been used as a model system for investigating agents and signaling pathways that control neuroblastoma cell differentiation, which represents a promising therapeutic strategy for neuroblastoma [9,10].

We have recently identified HOXC9 as a downstream target gene of RA and an essential mediator of RA action in neuroblastoma differentiation: HOXC9 expression is upregulated by RA and knockdown of HOXC9 expression confers resistance to RA-induced differentiation. Moreover, HOXC9 induction can fully recapitulate the phenotype of RA treatment [7]. To gain a molecular understanding of the mechanism by which HOXC9 induces the neuronal differentiation of neuroblastoma cells, we generated BE(2)-C-derived cells with inducible expression of myc-tagged human HOXC9 in the absence of doxycycline, using the Retro-X Tet-Off Advanced Inducible Gene Expression System (Clontech).

http://dx.doi.org/10.1016/j.gdata.2014.04.002

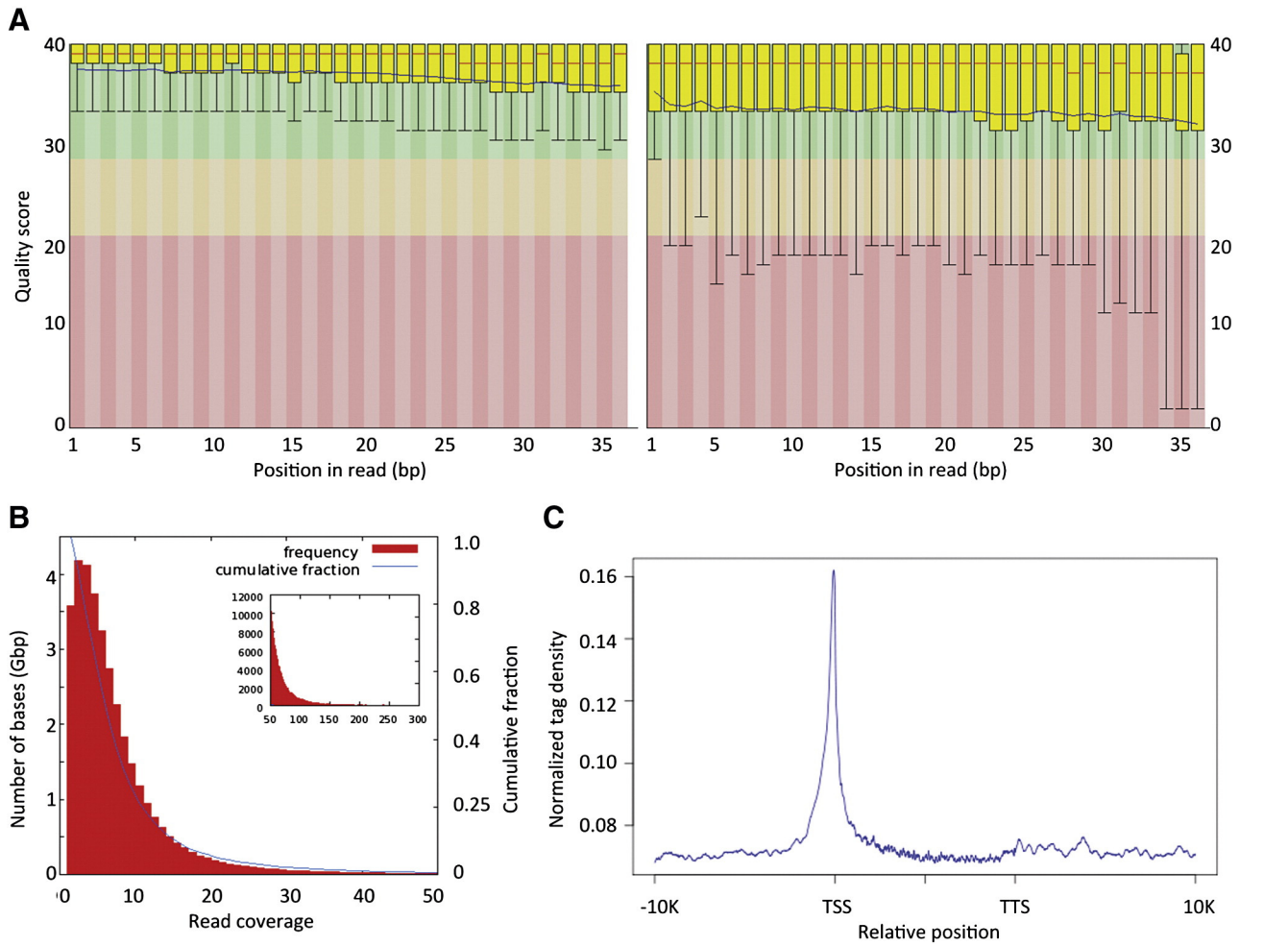

Fig. 1. Quality assessment of ChIP-seq data. (A) BoxWhisker type plot showing per-base sequence quality scores for read 1 (positive strand, left panel) and read 2 (negative strand, right panel). Higher score indicates better quality. (B) Quality assessment of sequencing sufficiency using histogram and cumulative fraction of base quality scores in peaks. (C) Tag density plot showing the average of the normalized tag densities for all RefSeq genes. HOXC9-binding sites are highly enriched around TSS. TTS, transcription termination sites.

Microarray and quality control

To identify the genes that are regulated by HOXC9, we isolated total RNA from three independent samples of BE(2)-C/Tet-Off/myc-HOXC9 cells cultured in the presence or absence of doxycycline for 6 days using Trizol (Invitrogen). The quantity and quality of the RNA samples were measured and assessed by a NanoDrop spectrophotometer and Agilent 2100 Bioanalyzer (Agilent Technologies). Affymetrix microarray analysis was performed using the Human Gene 1.0 ST microarray chip.

The quality of each CEL file was assessed using Affymetrix Expression Console Software according to the Affymetrix standard protocol (Quality Assessment of Exon and Gene 1.0 ST Arrays, Affymetrix White Paper, 2007). Relative log expression (RLE) was used to identify outlier samples. In order to monitor labeling and hybridization quality, we used polyA-control RNAs (*Lys*, *Phe*, *Thr* and *Dap*) and bacterial spike-in controls (*BioB*, *BioC*, *BioD* and *Cre*), respectively.

CEL files were imported into Partek Genomics Suit using RMA normalization. The probesets were annotated using the HuGene-1_0-st-v1 Probeset Annotations and Transcript Cluster Annotations. The differential expressions were calculated using ANOVA of the Partek package.

ChIP

To identify the genomic sites that are bound by HOXC9, we performed two independent ChIP-seq assays with BE(2)-C/Tet-Off/myc-HOXC9 cells cultured in the absence of doxycycline for 6 days according to the published procedure [11]. Briefly, 4×10^7 cells were fixed with 1% formaldehyde for 10 min and quenched with 0.125 M glycine for 5 min. After cell lysis, cross-linked chromatin DNA was sheared to approximately 250 bp by sonication (Model 150E ultrasonic dismembrator, Fisher Scientific), and immunoprecipitated with 10 μg of mouse anti-myc tag (clone 4A6, Millipore) and 80 μl Dynabeads Protein G (Invitrogen). The immunoprecipitated HOXC9–DNA complexes were washed extensively and eluted with SDS buffer, followed by incubation overnight at 65 °C to reverse cross-linking. The samples were then treated sequentially with RNase A and proteinase K to degrade associated RNA and proteins, and ChIP DNA was purified by phenol–chloroform extraction and ethanol precipitation. Input genomic DNA was purified from an aliquot of chromatin after sonication. DNA concentration was determined using a PicoGreen dsDNA quantitation assay kit (Invitrogen).

ChIP library and quality control

ChIP libraries were generated according to the Illumina ChIP-seq library construction procedure. Briefly, 10 ng of ChIP DNA was end repaired with T4 DNA polymerase, Klenow fragment and T4 polynucleotide kinase (all from Enzymatics), and an adenosine base was then added to the 3′ end of the blunt phosphorylated DNA fragments by Klenow fragment (3′ → 5′ exo-) (Enzymatics). This was followed by ligation of Illumina genomic adapters. Ligated DNA around the size of 250–300 bp was isolated by electrophoresis through a 3% NuSieve 3:1

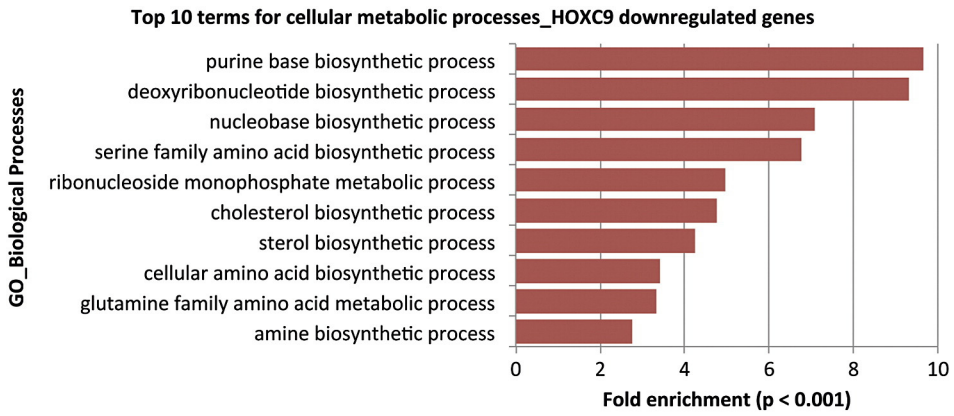

Fig. 2. HOXC9-induced neuroblastoma cell differentiation is characterized by reduced production of biosynthetic precursors. Gene ontology analysis of downregulated HOXC9-responsive genes reveals the enrichment of genes involved in the biosynthesis of nucleotides, sterol, and amino acids (enrichment fold >2.0, $p < 0.001$).

agarose gel and amplified by PCR using Phusion DNA Polymerase (Thermo Scientific). The PCR products were then purified using an Agencourt Ampure kit (Beckman Coulter) to remove primer dimmers.

Agilent 2100 Bioanalyzer was employed to examine the normal size distribution and possible primer or linker contamination of each library. The library concentration was measured using both Qubit dsDNA BR Assay Kit (Invitrogen) and real-time qPCR method. Real-time qPCR was performed on StepOne Plus Real-Time PCR systems (Applied Biosystems) using KAPA SYBR FAST universal qPCR kit (KAPA Biosystems). qPCR primers, 1.1 and 2.1, were designed based on Illumina Sequencing Library qPCR Quantification Guide. PhiX Control v3 (Illumina) was used in the reaction to plot the standard curve.

ChIP-seq data quality control

ChIP DNA was sequenced using Illumina Genome Analyzer IIX with a read length of 36 (paired-end). We performed several analyses to assess the quality of the sequencing data. Box whisker type plot analysis shows per base sequence quality scores for read 1 (Fig. 1A, left panel) and read 2 (Fig. 1A, right panel). Red and blue lines represent the median and mean value, respectively; the yellow box indicates the inter-quartile range (25–75%); and the upper and lower whiskers indicate the 10% and 90% points (FASTQC) [12]. Fig. 1B shows the quality assessment of sequencing sufficiency using histogram and cumulative fraction of base quality scores in peaks. We also analyzed tag density to visualize the quality of sequencing and mapping, and to examine the global profile of HOXC9 ChIP-seq based on genes, which shows that HOXC9-binding peaks are highly enriched around transcription start sites (TSS) (Fig. 1C).

Discussion

We described here a dataset composed of microarray gene expression profiling of HOXC9-responsive genes and ChIP-seq data for genome-wide mapping of HOXC9-binding sites in the human neuroblastoma BE(2)-C cells. With this dataset, we were able to demonstrate that HOXC9 directly controls and coordinates the expression of a large number of genes involved in neuron genesis and differentiation, cell cycle progression, and DNA damage repair [1]. We believe that this dataset would be particularly valuable for investigating the cellular processes associated with differentiation and underlying molecular mechanisms. For example, we found that HOXC9-induced differentiation is associated with a marked reduction in cellular metabolism, as a result of global downregulation of genes involved in the biosynthesis of nucleotides, sterol, and amino acids (Fig. 2). This finding sheds new light on the interplay between metabolic reprogramming and cancer cell differentiation, and suggests that reprogramming cellular metabolism may represent a promising strategy for promoting cancer cell differentiation.

Conflict of interest

The authors have no conflicts of interest.

References

[1] X. Wang, J.H. Choi, J. Ding, L. Yang, L.C. Ngoka, E.J. Lee, Y. Zha, L. Mao, B. Jin, M. Ren, J. Cowell, S. Huang, H. Shi, H. Cui, H.F. Ding, HOXC9 directly regulates distinct sets of genes to coordinate diverse cellular processes during neuronal differentiation. BMC Genomics 14 (2013) 830.
[2] D. Tweddle, A. Malcolm, N. Bown, A. Pearson, J. Lunec, Evidence for the development of p53 mutations after cytotoxic therapy in a neuroblastoma cell line. Cancer Res. 61 (2001) 8–13.
[3] N. Keshelava, J.J. Zuo, P. Chen, S.N. Waidyaratne, M.C. Luna, C.J. Gomer, T.J. Triche, C. P. Reynolds, Loss of p53 function confers high-level multidrug resistance in neuroblastoma cell lines. Cancer Res. 61 (2001) 6185–6193.
[4] H. Cui, J. Ma, J. Ding, T. Li, G. Alam, H.F. Ding, Bmi-1 regulates the differentiation and clonogenic self-renewal of I-type neuroblastoma cells in a concentration-dependent manner. J. Biol. Chem. 281 (2006) 34696–34704.
[5] R.A. Ross, B.A. Spengler, C. Domenech, M. Porubcin, W.J. Rettig, J.L. Biedler, Human neuroblastoma I-type cells are malignant neural crest stem cells. Cell Growth Differ. 6 (1995) 449–456.
[6] N. Sidell, Retinoic acid-induced growth inhibition and morphologic differentiation of human neuroblastoma cells in vitro. J. Natl. Cancer Inst. 68 (1982) 589–596.
[7] L. Mao, J. Ding, Y. Zha, L. Yang, B.A. McCarthy, W. King, H. Cui, H.F. Ding, HOXC9 links cell-cycle exit and neuronal differentiation and is a prognostic marker in neuroblastoma. Cancer Res. 71 (2011) 4314–4324.
[8] T. Sugimoto, T. Kato, T. Sawada, Y. Horii, J.T. Kemshead, T. Hino, H. Morioka, H. Hosoi, Schwannian cell differentiation of human neuroblastoma cell lines in vitro induced by bromodeoxyuridine. Cancer Res. 48 (1988) 2531–2537.
[9] C.P. Reynolds, K.K. Matthay, J.G. Villablanca, B.J. Maurer, Retinoid therapy of high-risk neuroblastoma. Cancer Lett. 197 (2003) 185–192.
[10] S.L. Volchenboum, S.L. Cohn, Progress in defining and treating high-risk neuroblastoma: lessons from the bench and bedside. J. Clin. Oncol. 27 (2009) 1003–1004.
[11] T.I. Lee, S.E. Johnstone, R.A. Young, Chromatin immunoprecipitation and microarray-based analysis of protein location. Nat. Protoc. 1 (2006) 729–748.
[12] S. Andrews, FastQC: a quality control tool for high throughput sequence data, http://www.bioinformatics.babraham.ac.uk/projects/fastqc/ 2011.

Cell Metabolism
Article

The Histone H3 Methyltransferase G9A Epigenetically Activates the Serine-Glycine Synthesis Pathway to Sustain Cancer Cell Survival and Proliferation

Jane Ding,[1,10] Tai Li,[1,6,10] Xiangwei Wang,[7] Erhu Zhao,[1,6] Jeong-Hyeon Choi,[1,2] Liqun Yang,[6] Yunhong Zha,[8] Zheng Dong,[3] Shuang Huang,[4] John M. Asara,[9] Hongjuan Cui,[6] and Han-Fei Ding[1,4,5,*]
[1]Cancer Center
[2]Department of Biostatistics and Epidemiology
[3]Department of Cellular Biology and Anatomy
[4]Department of Biochemistry and Molecular Biology
[5]Department of Pathology
Medical College of Georgia, Georgia Regents University, Augusta, GA 30912, USA
[6]State Key Laboratory of Silkworm Genome Biology, Institute of Sericulture and System Biology, Southwest University, Chongqing 400716, China
[7]Department of Urology, Second Affiliated Hospital, Third Military Medical University, Chongqing 400037, China
[8]Department of Neurology, The First Hospital of Yichang, Three Gorges University College of Medicine, Yichang 423000, China
[9]Division of Signal Transduction, Beth Israel Deaconess Medical Center, Harvard Medical School, Boston, MA 02115, USA
[10]These authors contributed equally to this work
*Correspondence: hding@gru.edu
http://dx.doi.org/10.1016/j.cmet.2013.11.004

SUMMARY

Increased activation of the serine-glycine biosynthetic pathway is an integral part of cancer metabolism that drives macromolecule synthesis needed for cell proliferation. Whether this pathway is under epigenetic control is unknown. Here we show that the histone H3 lysine 9 (H3K9) methyltransferase G9A is required for maintaining the pathway enzyme genes in an active state marked by H3K9 monomethylation and for the transcriptional activation of this pathway in response to serine deprivation. G9A inactivation depletes serine and its downstream metabolites, triggering cell death with autophagy in cancer cell lines of different tissue origins. Higher G9A expression, which is observed in various cancers and is associated with greater mortality in cancer patients, increases serine production and enhances the proliferation and tumorigenicity of cancer cells. These findings identify a G9A-dependent epigenetic program in the control of cancer metabolism, providing a rationale for G9A inhibition as a therapeutic strategy for cancer.

INTRODUCTION

Histone lysine methylation has a central role in the control of gene transcription. The histone lysine methylation state is controlled by histone lysine methyltransferases (KMTs) and demethylases (KDMs). The enzymatic reactions catalyzed by KMTs and KDMs depend on metabolic coenzymes including S-adenosylmethionine (SAM), flavin adenine dinucleotide (FAD), and α-ketoglutarate (α-KG). KMTs catalyze lysine methylation using SAM as the methyl group donor, whereas LSD (KDM1A and KDM1B) and JmjC domain-containing KDMs (KDM2-KDM8) require FAD and α-KG for demethylation, respectively (Black et al., 2012; Mosammaparast and Shi, 2010). Their dependence on metabolic coenzymes suggests that KMTs and KDMs could reprogram gene expression in response to changes in cellular metabolism. This notion has also led to the provocative hypothesis that KMTs and KDMs may contribute to metabolic control through transcriptional regulation (Teperino et al., 2010).

G9A, also known as EHMT2, is a H3K9 methyltransferase that has a primary role in catalyzing monomethylation and dimethylation of H3K9 (H3K9me1 and H3K9me2) in euchromatin (Peters et al., 2003; Rice et al., 2003; Shinkai and Tachibana, 2011; Tachibana et al., 2002), with H3K9me1 being associated with transcriptional activation and H3K9me2 with transcriptional repression (Black et al., 2012; Mosammaparast and Shi, 2010). Elevated levels of G9A expression have been observed in many types of human cancers, and G9A knockdown has been shown to inhibit the proliferation of cancer cell lines (Chen et al., 2010; Cho et al., 2011; Huang et al., 2010; Kondo et al., 2008). The molecular basis of G9A action in the control of cancer cell proliferation is not well understood. In this study, we identify an essential role of G9A in sustaining cancer cell survival and proliferation by transcriptional activation of the serine-glycine biosynthetic pathway. Our findings provide direct evidence for a G9A-dependent epigenetic program in the control of amino acid production and cancer metabolism.

RESULTS

G9A Is Essential for Sustaining Cancer Cell Proliferation and Survival

We examined the role of G9A in cell survival and proliferation in human cancer cell lines of different tissue origins, including the

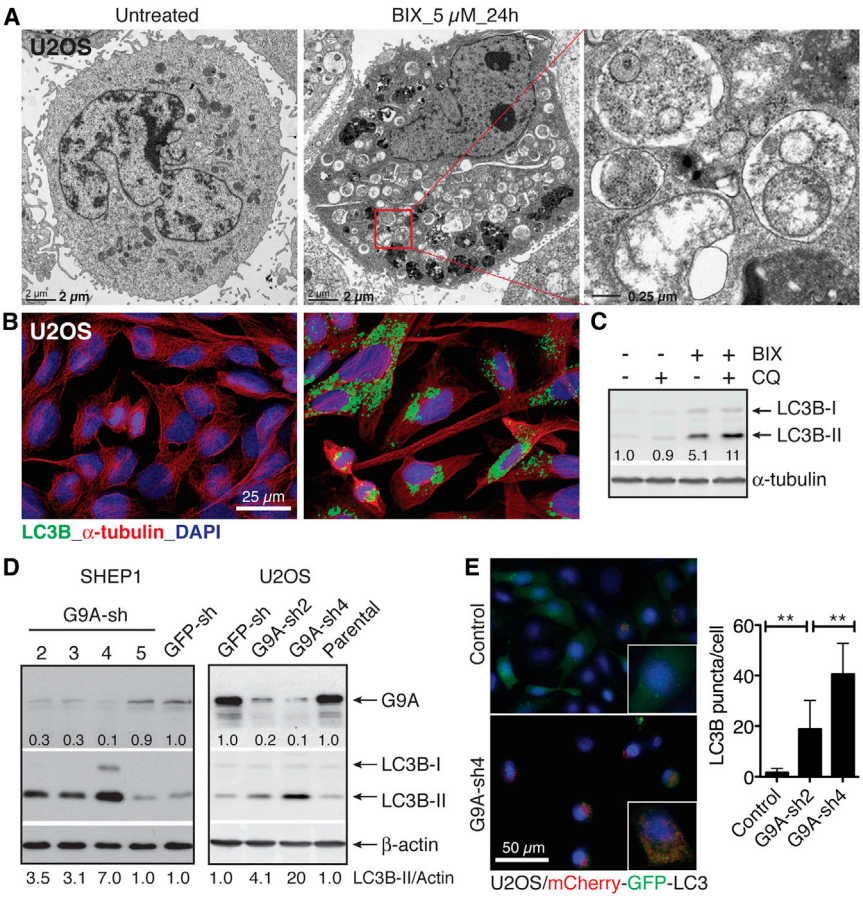

Figure 1. G9A Inhibition or Silencing Induces Autophagy

(A) Electron micrographs of U2OS cells with or without 5 μM BIX for 24 hr.

(B) Immunofluorescence of LC3B-positive autophagosomes in U2OS cells with or without 5 μM BIX for 24 hr.

(C) Immunoblotting of LC3B in U2OS cells with or without 5 μM BIX or 10 μM chloroquine (CQ) for 24 hr. LC3B-II levels were quantified against α-tubulin.

(D) Immunoblotting of G9A and LC3B in U2OS and SHEP1 cells expressing GFP shRNA (GFP-sh) or individual G9A-sh sequences. G9A and LC3B-II levels were quantified against β-actin.

(E) Fluorescence and quantification of LC3B-positive autophagosomes in U2OS/mCherry-EGFP-LC3B cells with or without G9A knockdown. Error bars represent SD (n = 100 cells). **$p < 0.001$. See also Figures S1 and S2.

bladder (J82), bone (U2OS), brain (U251), breast (MCF10A and MCF7), cervix (HeLa), colon (HCT116 and RKO), liver (Hep2G), lung (H1299), and sympathetic nervous system (BE(2)-C, SMS-KCNR, and SHEP1). We treated these cell lines with BIX01294 (BIX), a small molecule inhibitor of G9A (IC_{50} = 1.7 μM) (Kubicek et al., 2007). BIX at 2–5 μM significantly reduced the global levels of H3K9me1 and H3K9me2 (Figure S1A available online) and completely inhibited the proliferation of all the cancer cell lines examined (Figure S1B for representative cell lines). In addition, we observed a significant decrease in cell survival following BIX treatment (Figure S1C, BIX-5 μM_5d). To confirm that BIX targets G9A to inhibit cell proliferation and survival, we examined the effect of G9A silencing by small hairpin RNA (shRNA). G9A knockdown exerted a pronounced inhibitory effect on cell proliferation and survival (Figures S1D–S1G). Together, these findings indicate an essential role of G9A in sustaining cell proliferation and survival in a wide range of cancer cell lines.

G9A Inhibition or Silencing Induces Autophagy

An early and prominent morphological feature of the cells with G9A inhibition or silencing was the appearance of numerous cytoplasmic vesicles and vacuoles (Figures S1C and S1G) that morphologically resemble autophagosomes, a double-membraned structure that sequesters cellular organelles, proteins, and/or lipids during autophagy. Thus, we examined the possibility that G9A inhibition or silencing might induce autophagy by electron microscopy for ultrastructural morphology, by immunoblotting for detecting the lipidation of LC3 (microtubule-associated protein light chain 3), and by immunofluorescence for monitoring the formation of LC3-positive puncta. LC3 is the mammalian homolog of the yeast autophagy-related protein Atg8 and is proteolytically processed to LC3-I by the Atg4 protease following translation. Upon autophagy induction, LC3-I is converted to the lipidated LC3-II form, which is then incorporated into the autophagosomal membrane, resulting in the redistribution of LC3 from a diffuse pattern to a punctate pattern. Mammalian cells express three LC3 isoforms (LC3A, LC3B, and LC3C), with LC3B-II levels correlating with the steady-state levels of autophagosomes (Klionsky et al., 2008; Mizushima et al., 2010).

Electron microscopy revealed numerous double-membraned vacuoles in BIX-treated cells that contained fragments of the endoplasmic reticulum and other cytoplasmic components (Figure 1A). Immunofluorescence confirmed that these vesicles and vacuoles were LC3B positive (Figure 1B). To determine whether the accumulation of autophagosomes resulted from an increase in autophagosome formation or from a block in autophagosome turnover, we examined BIX-induced LC3B-II production in the presence or absence of chloroquine (CQ), which blocks lysosomal acidification and thus degradation of autophagosomal components. The presence of CQ further increased LC3B-II levels in BIX-treated cells (Figure 1C), indicating that BIX increased LC3B-II production rather than blocking its degradation.

Dose-titration and time course studies revealed that different tumor cell lines varied in their sensitivity to BIX. For the most sensitive SHEP1 and U2OS cells, BIX as low as 1 μM triggered significant levels of autophagy, as determined by LC3B-II production (Figure S2A). The maximal level of autophagy occurred at 6 hr (SHEP1 and U2OS) or 24 hr (HeLa) following 5 μM BIX

treatment (Figure S2B). We further confirmed the ability of BIX to induce autophagy with immortalized *Atg5*$^{+/+}$ and *Atg5*$^{-/-}$ mouse embryonic fibroblasts (MEFs). Atg5 is required for autophagosome formation (Kuma et al., 2004; Mizushima et al., 2001). BIX at the concentrations of 2–5 μM was able to induce LC3B-positive puncta in *Atg5*$^{+/+}$, but not in *Atg5*$^{-/-}$, MEFs (Figure S2C).

To verify that BIX targets G9A to induce autophagy, we examined the effect of BIX on cells with G9A overexpression. Both SHEP1 and U2OS cells overexpressing G9A were highly resistant to BIX-induced autophagy, as evidenced by a significant reduction in LC3B-II levels following BIX treatment compared to control cells (Figure S2D). Additionally, cells with G9A silencing fully recapitulated the autophagy phenotype induced by BIX, showing a significant increase in the production of LC3B-II (Figure 1D) and LC3B-positive puncta (Figure 1E). Collectively, these results demonstrate that G9A inhibition or silencing induces cell death with autophagy.

G9A Inhibition or Silencing Transcriptionally Represses Serine-Glycine Biosynthesis

To investigate the molecular basis of autophagy induction by G9A inhibition, we examined the kinase activity of the mammalian target of rapamycin complex 1 (mTORC1), which has a major role in the control of autophagy by integrating a wide range of signals including concentrations of nutrients and growth factors (He and Klionsky, 2009; Kim and Guan, 2011; Rabinowitz and White, 2010). mTORC1 inhibits autophagy by suppressing the autophagy-activating kinase ULK1. Nutrient or growth factor deprivation inhibits mTORC1 activity, thereby activating ULK1 and inducing autophagy. Immunoblotting revealed that BIX significantly inhibited mTORC1 kinase activity as demonstrated by a marked decrease in the phosphorylation of the ribosome protein S6 kinase (S6K) (Figure S3A), a key mTORC1 substrate. This finding suggests that G9A inhibition triggers autophagy by interfering with cell growth or survival signals upstream of mTORC1.

Given the role of G9A in epigenetic control of transcription, we performed microarray profiling to identify potential G9A targets involved in autophagy induction. A total of 615 BIX-responsive genes ($\geq \pm 1.50$-fold, $p < 0.01$) were identified, with 302 genes being upregulated and 313 downregulated (Table S1). Gene Ontology (GO) analysis revealed that among the genes downregulated by BIX, those within the serine-glycine biosynthetic pathway were significantly enriched (Figure 2A), including phosphoglycerate dehydrogenase (PHGDH), phosphoserine aminotransferase 1 (PSAT1), phosphoserine phosphatase (PSPH), and serine hydroxymethyltransferase 2 (SHMT2) (Figure 2B). We confirmed the ability of BIX to downregulate mRNA expression of these genes by quantitative reverse-transcription PCR (qRT-PCR) in four different cancer cell lines (Figures 2C and S3B). Time course studies revealed significant downregulation of these genes within 2 and 6 hr of BIX treatment in U2OS and HeLa cells, respectively (Figure 2C), which occurred at least several hours before most of the cells underwent autophagy (Figure S2B). We noticed that SHMT1, though downregulated in HeLa, SHEP1, and U2OS cells, was activated in BE(2)-C cells following BIX treatment (Figure S3B). The significance of this apparently cell-type-dependent regulation of SHMT1 expression is currently under investigation. In agreement with the microarray and qRT-PCR data, we observed a significant decrease in PHGDH protein levels in BIX-treated cells (Figure S3C). Similarly, G9A silencing resulted in marked downregulation of the same group of genes at both mRNA and protein levels (Figures 2D, S3D, and S3E).

Chromatin immunoprecipitation and quantitative PCR (ChIP-qPCR) assay revealed that BIX treatment significantly reduced the H3K9me1 levels around the transcriptional start sites (TSSs) of *PHGDH* and *PSAT1* (Figure 2E, H3K9me1). By contrast, H3K9me2 levels in the same regions were either unchanged or significantly increased following BIX treatment (Figure 2E, H3K9me2). Together, these results indicate that the serine-glycine biosynthetic pathway is under the direct transcriptional control of G9A, primarily through the regulation of H3K9me1 levels associated with the pathway enzyme genes.

Supplemental Serine Rescues the Cell Death Phenotype of G9A Inhibition

The serine-glycine biosynthetic pathway is an important source of precursors and coenzymes for the biosynthesis of amino acids, nucleotides, and lipids (de Koning et al., 2003; Kalhan and Hanson, 2012) and is crucial for cancer cell survival and proliferation (Locasale, 2013; Locasale et al., 2011; Pollari et al., 2011; Possemato et al., 2011). In addition, amino acid deprivation is a major trigger of autophagy (Kim and Guan, 2011). Thus, we investigated the possibility that suppression of this biosynthetic pathway might be a cause of the cell death phenotype induced by G9A inhibition or silencing. Gas chromatography-mass spectrometry (GC-MS) analysis revealed that only serine and glycine levels were significantly reduced in U2OS cells within 4 hr of BIX treatment (Figure 3A), demonstrating that G9A activity is essential for maintaining the intracellular steady-state levels of serine and glycine. We further assessed the activity of this biosynthetic pathway by [U-^{13}C] glucose flux analysis using liquid chromatography-tandem mass spectrometry (LC-MS/MS). BIX treatment significantly decreased the incorporation of [U-^{13}C] glucose into 3-phosphoserine and serine (Figure 3B). Importantly, addition of serine to the culture medium significantly diminished the effect of BIX (Figures 3C and 3D) or G9A silencing (Figure 3E) on cell proliferation and autophagy in all the cancer cell lines examined. By contrast, supplemental glycine had only a small protective effect on BIX-treated cells, and addition of both serine and glycine was no more effective than adding serine alone (Figures 3F, S4A, and S4B). We confirmed these findings with cell-permeable methyl-serine-ester and methyl-glycine-ester (Figure 3G). Other individual amino acid supplements all failed to prevent cell death with autophagy induced by BIX (Figures 3F, S4A, and S4C), providing further evidence for the specificity of serine action.

The observation that serine, but not glycine, was able to rescue the cell death phenotype suggests that the production of 5,10-methylenetetrahydrofolate (5,10-MTHF) might be crucial for cell survival and proliferation. The interconversion between serine and glycine is catalyzed by SHMT: serine conversion to glycine generates 5,10-MTHF, whereas glycine conversion to serine consumes 5,10-MTHF (Figure 3H). To test this idea, we generated SHEP1 cells overexpressing SHMT1, a cytoplasmic enzyme, or SHMT2, a predominantly mitochondrial enzyme (Figure 3I). Their overexpression alone had no significant effect

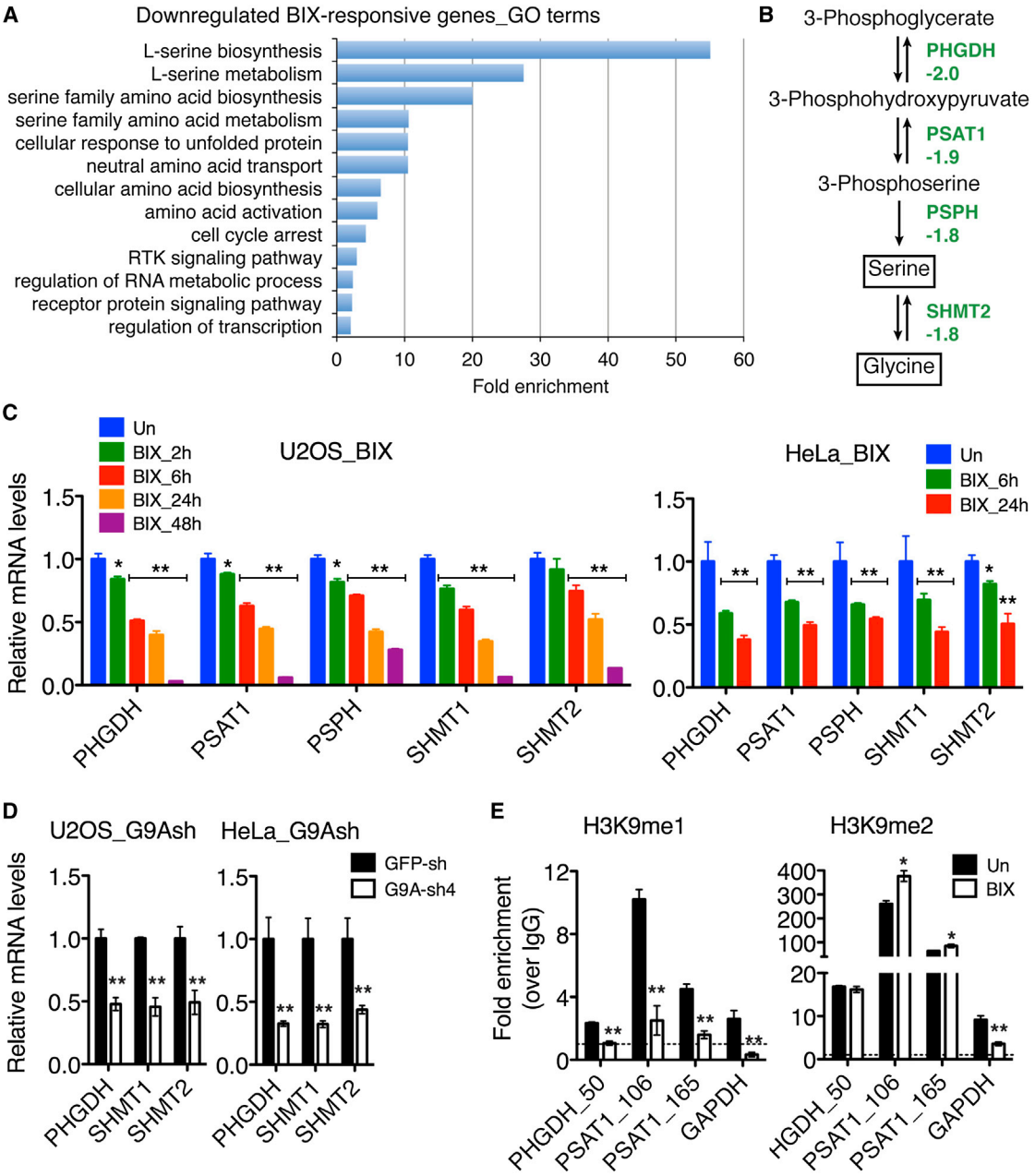

Figure 2. G9A Inhibition or Silencing Represses Serine-Glycine Biosynthesis

(A) GO analysis of downregulated BIX-responsive genes (enrichment fold >2.0, $p < 0.01$).

(B) Serine-glycine biosynthetic pathway with the indicated fold changes in mRNA expression determined by microarray.

(C and D) qRT-PCR analysis of mRNA expression of the pathway enzyme genes in U2OS and HeLa cells with or without 5 μM BIX (C) or G9A silencing (D). Error bars represent SD (n = 3).

(E) ChIP-qPCR analysis of H3K9me1 and H3K9me2 levels at the promoters of *PHGDH* and *PSAT1* in U2OS cells with or without 5 μM BIX for 4 hr. Data on the *GAPDH* coding region are shown as positive control. Dashed line indicates IgG control. Error bars represent SD of triplicate and are representatives of two independent experiments.

*$p < 0.01$, **$p < 0.001$. See also Figure S3, Table S1, and Table S3.

on BIX-induced cell death (Figure 3J). However, overexpression of SHMT2, but not SHMT1, synergized with supplemental serine to enhance cell survival and proliferation in the presence of BIX (Figure 3J). This observation is consistent with our model, since previous studies have suggested that SHMT2 has a major role in the conversion of serine to glycine and 5,10-MTHF, whereas SHMT1 primarily catalyzes the conversion of glycine to serine (Herbig et al., 2002; Narkewicz et al., 1996; Pfendner and Pizer, 1980; Stover et al., 1997; Tibbetts and Appling, 2010; Yoshida and Kikuchi, 1970). Collectively, these results indicate that

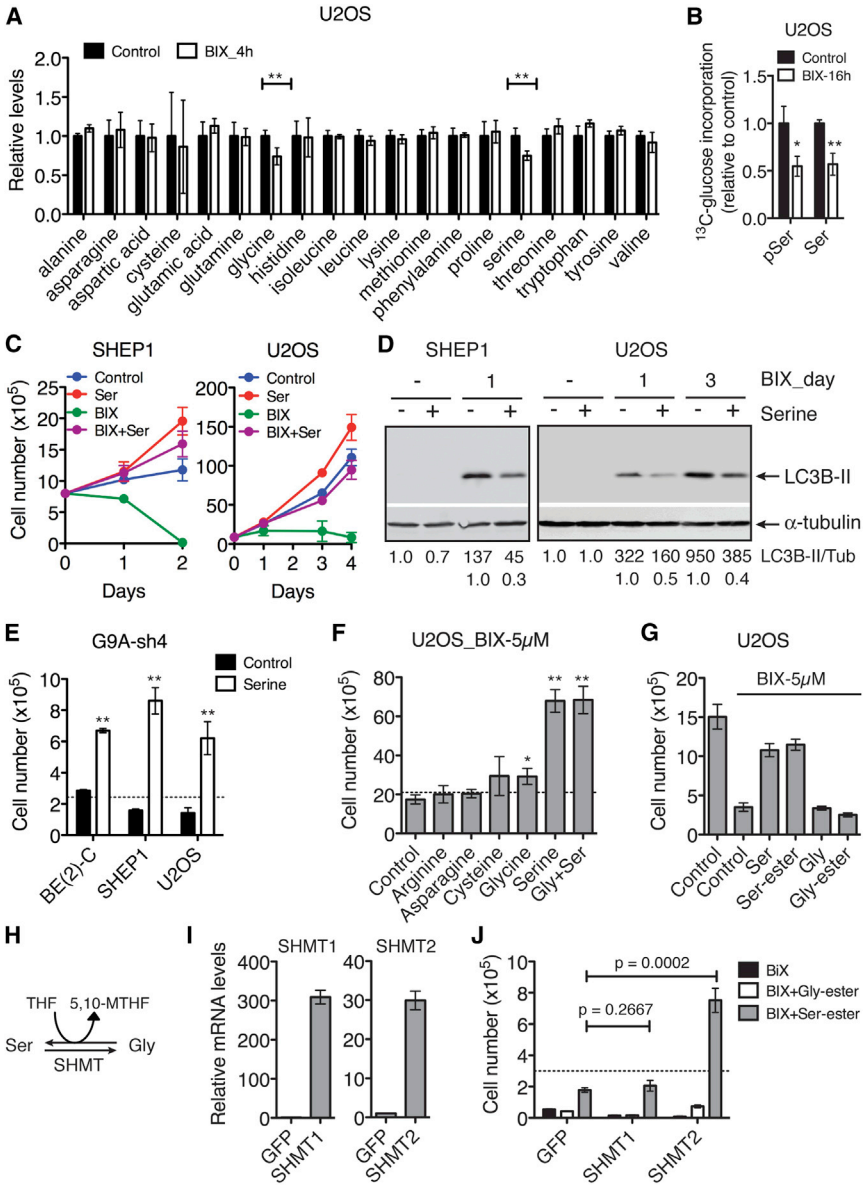

Figure 3. Supplemental Serine Rescues the Phenotype of G9A Inhibition or Silencing

(A) GC-MS analysis of amino acid levels in U2OS cells with or without 5 μM BIX for 4 hr. Error bars represent SD (n = 6).

(B) LC-MS/MS analysis of [U-^{13}C] glucose flux into 3-phosphoserine (pSer) and serine (Ser) biosynthesis in U2OS cells with or without 5 μM BIX for 16 hr. The fraction of labeled to total pSer and Ser, $^{13}C/(^{13}C + ^{12}C)$, was calculated and normalized to control. Error bars represent SD (n = 3).

(C) Growth assay of SHEP1 and U2OS cells with or without 5 μM BIX or supplemental serine (Ser). Error bars represent SD (n = 4).

(D) Immunoblotting of LC3B in the cell samples from (C). LC3B-II levels were quantified against α-tubulin.

(E) Growth assay of the indicated cell lines with G9A silencing in the presence or absence of supplemental serine for 4 days. Dashed line indicates the number of cells plated at time zero. Error bars represent SD (n = 4).

(F and G) Growth assay of U2OS cells in the presence of 5 μM BIX with or without the indicated supplemental amino acids for 2 days. Gly, glycine; Gly-ester, methyl-glycine-ester; Ser, serine; Ser-ester, methyl-serine-ester. Dashed line (F) indicates the number of cells plated at time zero. Error bars represent SD (n = 4).

(H) Schematic of the interconversion between serine and glycine. THF, tetrahydrofolate; 5,10-MTHF, 5,10-methylenetetrahydrofolate.

(I) qRT-PCR analysis of SHMT mRNA expression in SHEP1 cells overexpressing SHMT1 or SHMT2. Error bars represent SD (n = 3).

(J) Growth assay of SHEP1 cells expressing GFP, SHMT1, or SHMT2 in the presence of 5 μM BIX with or without supplemental Gly-ester or Ser-ester. Dashed line indicates the number of cells plated at time zero. Error bars represent SD (n = 3).

*p < 0.01, **p < 0.001. See also Figure S4.

maintaining the production of serine and its downstream metabolites, including 5,10-MTHF, is a major mechanism by which G9A sustains cancer cell survival and proliferation.

G9A Is a Key Component of the Serine Deprivation Response, Linking Serine Production, Ribosome Biogenesis, and Cell-Cycle Progression

It has been shown recently that serine deprivation leads to transcriptional activation of the serine biosynthetic pathway (Ye et al., 2012; Figure 4A). In light of our findings above, we asked whether G9A has a role in activation of this pathway in response to serine deprivation. Addition of BIX completely abrogated the induction of PHGDH and PSAT1 by serine deprivation (Figures 4B and 4C), supporting a physiological function of G9A in mediating the serine deprivation response.

Amino acid availability controls the rates of protein synthesis and cell growth (Kilberg et al., 2005), and it has been reported recently that G9A is required for activation of rRNA transcription (Yuan et al., 2007), a rate-limiting step in ribosome biogenesis. We therefore asked whether G9A has a role in linking serine metabolism to ribosome biogenesis and cell growth. To test this idea, we performed temporal transcriptome profiling of BIX-responsive genes by RNA sequencing (RNA-seq), which revealed distinctive patterns of gene expression in cells that were treated with BIX for 6 or 24 hr (Figure 4D). In agreement with the microarray data shown above (Figure 2A; Table S1), GO analysis of the genes downregulated by BIX at 6 hr revealed significant enrichment of genes within the serine biosynthetic pathway (Figure 4E; Table S2). However, cells treated with BIX for 24 hr displayed a gene expression pattern characterized by significant downregulation of genes that control cell-cycle progression (Figure 4F), including cyclins A2 and B2, and CDC25C (Table S2). We confirmed the RNA-seq result by qRT-PCR, which showed sequential downregulation of serine synthesis and cell-cycle genes following BIX treatment (Figure 4G). We also confirmed the time-dependent downregulation of cyclins

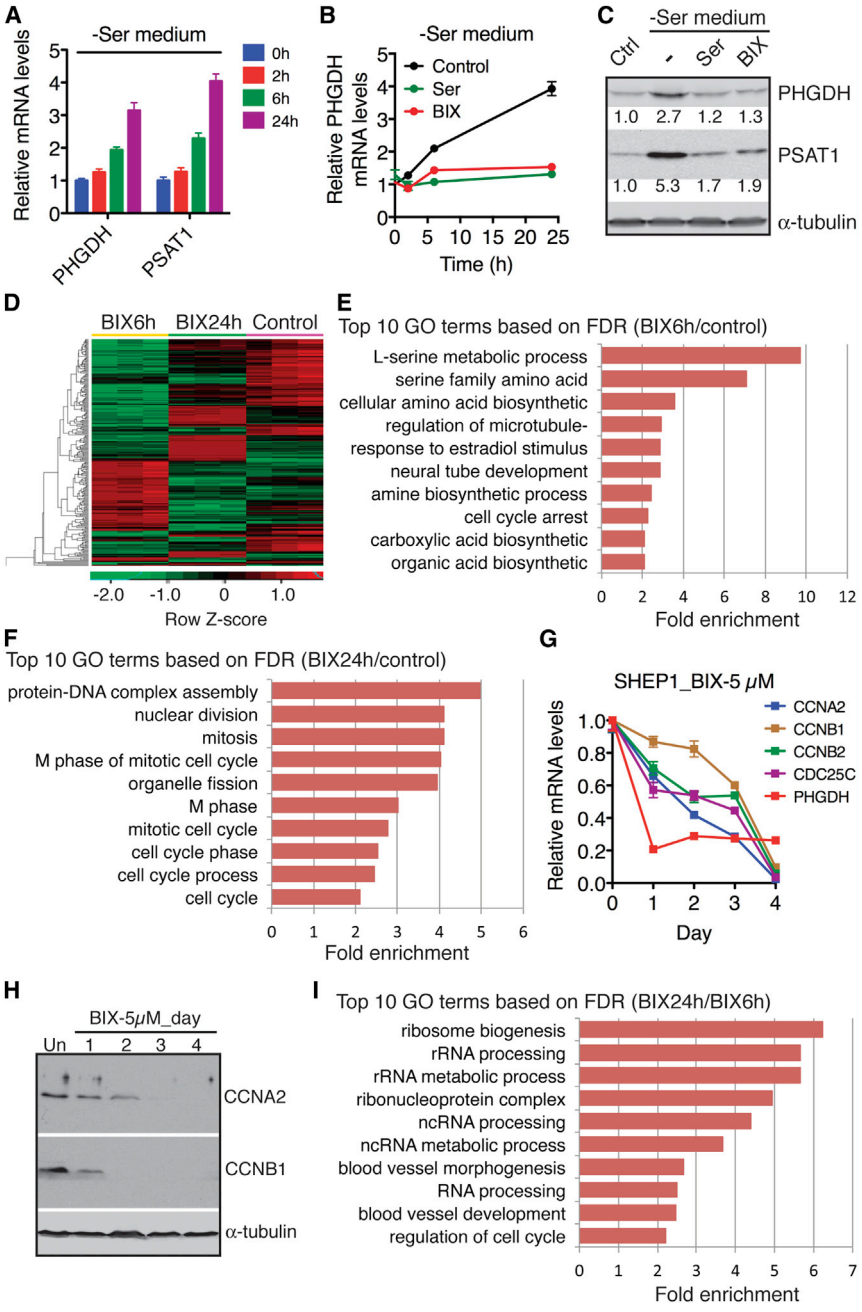

Figure 4. G9A Links Serine Production, Ribosome Biogenesis, and Cell Proliferation

(A) qRT-PCR analysis of PHGDH and PSAT1 mRNA levels in SHEP1 cells cultured in serine-deficient (−Ser) medium for 0, 2, 6, and 24 hr. Error bars represent SD (n = 3).

(B) qRT-PCR analysis of PHGDH mRNA levels in SHEP1 cells cultured in −Ser medium with or without 5 μM BIX or supplemental serine for 0, 2, 6, and 24 hr. Error bars represent SD (n = 3).

(C) Immunoblotting of PHGDH and PSAT1 in SHEP1 cells cultured in control (with serine) or −Ser medium with or without 5 μM BIX or supplemental serine for 24 hr. PHGDH and PSAT1 levels were quantified against α-tubulin.

(D) Heatmap showing differential gene expression in U2OS cells without (control) or with 5 μM BIX for 6 (BIX6h) or 24 hr (BIX24h).

(E and F) GO analysis of downregulated BIX-responsive genes at the 6 hr (E) or 24 hr (F) time point. Shown are top ten GO biological process terms.

(G and H) qRT-PCR (G) and immunoblot (H) analyses of cell-cycle genes in SHEP1 cells with or without 5 μM BIX for the indicated time. Error bars in (G) represent SD (n = 3).

(I) GO analysis of the genes downregulated by BIX at 24 hr versus 6 hr. Shown are top ten GO biological process terms.

See also Table S2 and Table S3.

A2 and B1 by immunoblotting (Figure 4H). Importantly, we found marked downregulation of genes involved in ribosome biogenesis in cells treated with BIX for 24 hr compared to those treated for 6 hr (Figure 4I; Table S2), a finding consistent with the reported role of G9A in activation of rRNA transcription (Yuan et al., 2007). Collectively, these results suggest a key role of G9A in coupling serine sensing to the transcription of genes that control protein synthesis and cell proliferation.

G9A Promotes Cell Proliferation and Tumorigenicity

G9A is overexpressed in various human cancers (Chen et al., 2010; Cho et al., 2011; Huang et al., 2010; Kondo et al., 2008), and it has been reported recently that elevated levels of G9A expression positively correlate with disease progression and poor prognosis in lung cancer (Chen et al., 2010). In line with these reports, we found that higher G9A expression was significantly associated with reduced overall survival in neuroblastoma patients (Figure 5A). These observations prompted us to investigate the functional consequence of high G9A expression. Ectopic expression of G9A in SHEP1 and U2OS cells significantly increased cell proliferation (Figure 5B) and the expression of genes that promote cell-cycle progression (Figure 5C), indicating that high G9A expression alone is sufficient to confer a growth advantage to cancer cells. Moreover, G9A overexpression markedly enhanced the anchorage-independent growth (Figure 5D) and tumorigenicity (Figures 5E and 5F) of SHEP1 and U2OS cells, demonstrating that G9A has transforming potential. Together, our results from both human primary tumors and cell lines suggest an oncogenic function of G9A in cancer development.

Activation of the Serine-Glycine Biosynthetic Pathway Is Essential for the Oncogenic Activity of G9A

Given the critical role of the serine-glycine biosynthetic pathway in sustaining cancer cell survival and proliferation (Locasale et al., 2011; Pollari et al., 2011; Possemato et al., 2011), we asked

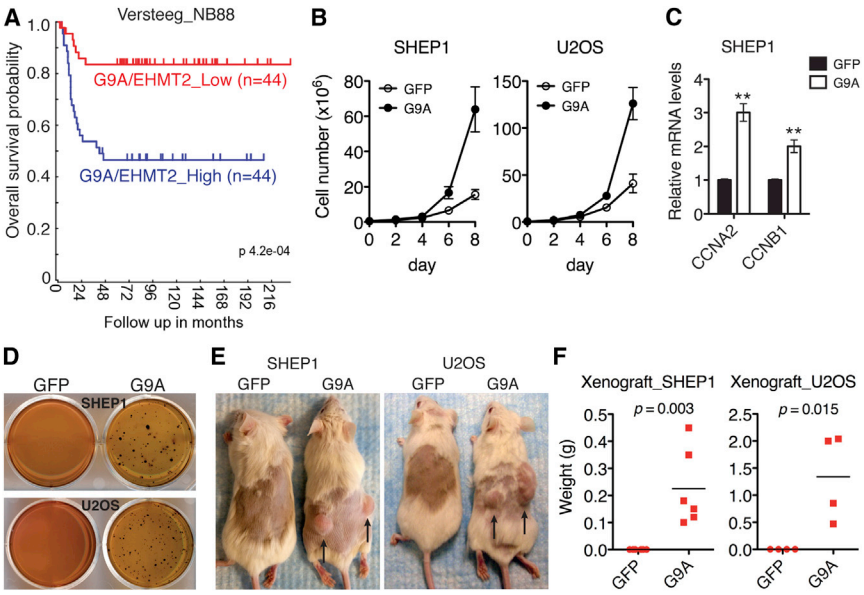

Figure 5. G9A Promotes Cell Proliferation and Tumorigenicity

(A) Kaplan-Meier overall survival for *G9A/EHMT2* expression in primary neuroblastoma tumors (Versteeg NB88 data set).

(B) Growth assay of SHEP1 and U2OS cells with or without G9A overexpression. Error bars represent SD (n = 4).

(C) qRT-PCR analysis of cyclin A2 and B1 mRNA levels in SHEP1 cells with or without G9A overexpression. Error bars represent SD (n = 3). **p < 0.001.

(D) Soft agar assay of SHEP1 and U2OS cells with or without G9A overexpression. Shown are representatives of three independent experiments.

(E and F) Xenograft assay of SHEP1 and U2OS cells with or without G9A overexpression. Images (E) were taken on day 42 after inoculation. Tumor weight (F) was analyzed by scatterplot with horizontal lines indicating the mean.

whether elevated levels of G9A lead to increased activation of this pathway and whether this is a major mechanism for the oncogenic activity of G9A. Ectopic expression of G9A in SHEP1 and U2OS cells markedly increased the mRNA (Figure 6A) and protein (Figure 6B) levels of the pathway enzyme genes. Moreover, ChIP in combination with DNA sequencing (ChIP-seq) revealed a significant increase in H3K9me1 levels at these gene loci (Figure 6C for *PHGDH* and *SHMT2*). We observed no significant change in H3K9me2 levels in the same regions (Figure 6C). These results suggest that G9A activates the expression of the pathway enzyme genes by increasing the H3K9me1 levels associated with their loci. As expected, G9A overexpression significantly increased the intracellular levels of serine and glycine (Figure 6D), and the flux of glucose into the serine biosynthetic pathway (Figure 6E).

To determine whether the oncogenic function of G9A depends on its ability to activate the serine-glycine pathway, we silenced the expression of PHGDH or PSAT1 in G9A-overexpressing U2OS cells by shRNA (Figures 7A and 7B). Knockdown of either PHGDH or PSAT1 abolished the ability of G9A to promote cell proliferation in a manner dependent on levels of PHGDH or PSAT1 downregulation (Figures 7C and 7D). In fact, G9A-overexpressing cells with more than 90% of PHGDH or PSAT1 knockdown failed to proliferate in the absence of supplemental serine (Figures 7C and 7D). We obtained essentially the same results with G9A-overexpressing SHEP1 (Figures S5A–S5D). Collectively, these data demonstrate that G9A promotes cell proliferation by transcriptionally activating the serine-glycine biosynthetic pathway.

The serine biosynthetic genes are direct transcriptional targets of activating transcription factor 4 (ATF4) (Adams, 2007; Seo et al., 2009; Ye et al., 2012), which is activated in response to amino acid deprivation (Kilberg et al., 2009). It has been shown that ATF4 knockdown or deficiency led to lower expression of serine biosynthetic enzymes (Ye et al., 2012), suggesting an essential role of ATF4 in maintaining transcriptional activation of this pathway. To examine the role of ATF4 in G9A action, we silenced ATF4 expression in G9A-overexpressing U2OS (Figure 7E) or SHEP1 cells (Figures S5E), which resulted in marked downregulation of PHGDH and PSAT1 at both mRNA and protein levels (Figures 7E and 7F and S5E and S5F). ATF4 silencing also significantly reduced the proliferation of G9A-overexpressing U2OS (Figure 7G) or SHEP1 cells (Figure S5G). Together, these results indicate that ATF4 is required for G9A to transcriptionally activate serine biosynthesis and to stimulate cell proliferation.

DISCUSSION

In this study, we show that the histone H3K9 methyltransferase G9A is essential for transcriptional activation of the serine-glycine biosynthetic pathway by specifically marking the pathway enzyme genes with H3K9me1, an epigenetic marker associated with active chromatin (Black et al., 2012; Mosammaparast and Shi, 2010). We further present evidence that G9A is a component of the molecular pathway that couples serine sensing to the transcriptional control of serine production, ribosome biogenesis, and cell proliferation. Finally, we provide evidence that G9A has an oncogenic function in cancer development by conferring survival and growth advantages to tumors through increasing the production of serine and its downstream metabolites. Our study uncovers an epigenetic mechanism for the control of amino acid metabolism and provides a molecular explanation for the functional significance of G9A overexpression observed in various human cancers (Chen et al., 2010; Cho et al., 2011; Huang et al., 2010; Kondo et al., 2008).

Cell growth and proliferation depend on protein synthesis, which must in turn match the cellular nutritional status including amino acid availability (Grummt and Ladurner, 2008; Kilberg et al., 2005). The mechanistic connection between these cellular processes remains to be clarified. Our study suggests an epigenetic mechanism for the control of ribosome biogenesis and cell proliferation in response to serine abundance. We show that G9A is essential for the serine deprivation response that leads

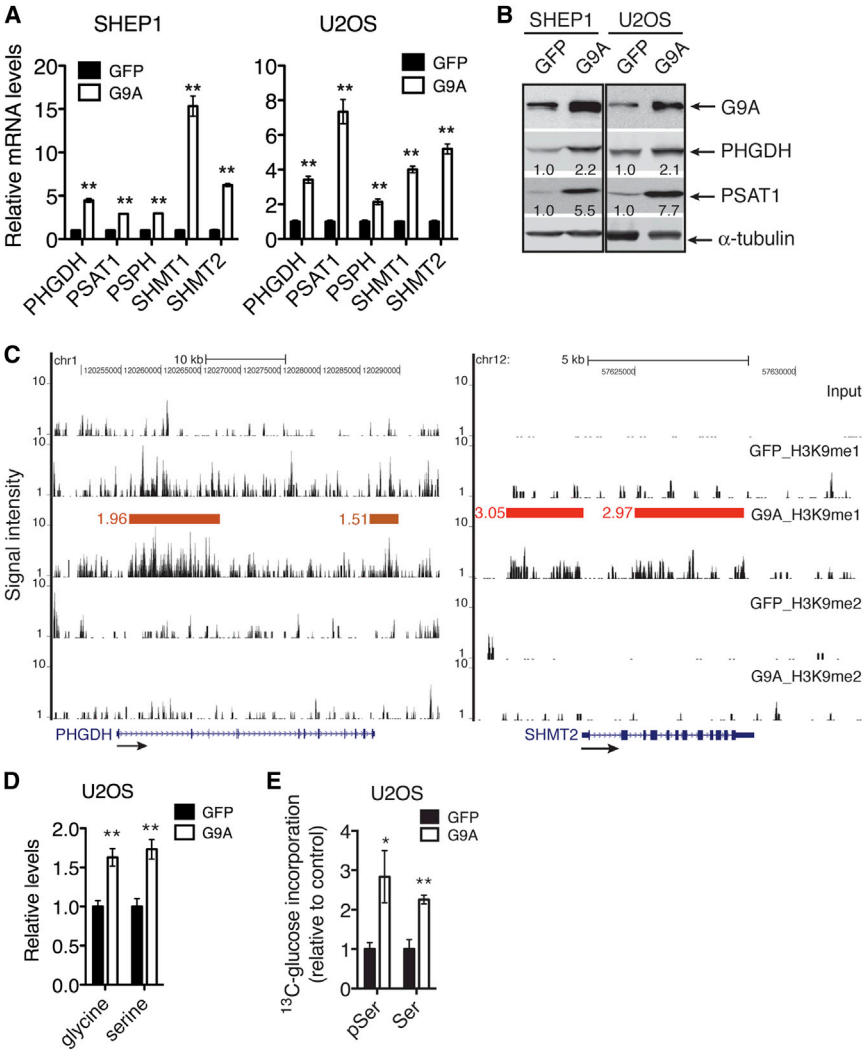

Figure 6. G9A Transcriptionally Activates Serine-Glycine Biosynthesis

(A) qRT-PCR analysis of mRNA levels of serine-glycine biosynthetic enzyme genes in SHEP1 and U2OS cells with or without G9A overexpression. Error bars represent SD (n = 3).

(B) Immunoblotting of PHGDH and PSAT1 in SHEP1 and U2OS cells with or without G9A overexpression. PHGDH and PSAT1 levels were quantified against α-tubulin.

(C) ChIP-seq tag profiles for H3K9me1 and H3K9me2 levels in the *PHGDH* and *SHMT2* loci in U2OS cells with or without G9A overexpression. Horizontal bars represent chromatin regions in which H3K9 methylation levels are significantly changed (G9A/GFP), and the numbers indicate fold enrichment.

(D) GC-MS analysis of serine and glycine levels in U2OS cells with or without G9A overexpression. Error bars represent SD (n = 6).

(E) LC-MS/MS analysis of [U-^{13}C] glucose flux into 3-phosphoserine (pSer) and serine (Ser) biosynthesis in U2OS cells with or without G9A overexpression. The fraction of labeled to total pSer and Ser, $^{13}C/(^{13}C + ^{12}C)$, was calculated and then normalized to GFP control. Error bars represent SD (n = 3).

*p < 0.05, **p < 0.001. See also Table S3.

to transcriptional activation of genes for serine biosynthesis. Moreover, we show that G9A activity or expression levels affect serine production and cell proliferation. Specifically, G9A inhibition initiated a transcriptional program that results in sequential repression of genes required for serine production, ribosome biogenesis, and cell-cycle progression, leading to lower levels of serine biosynthesis and cell growth arrest. Conversely, G9A overexpression activated genes for serine biosynthesis and cell-cycle progression, leading to higher levels of serine production and cell proliferation. These results are of particular interest in the context of recent work showing that G9A is required for activation of rRNA transcription (Yuan et al., 2007). Thus, we suggest that G9A-mediated H3K9 methylation serves as a key link between amino acid sensing and transcriptional control of ribosome biogenesis and cell proliferation.

Also importantly, we show that G9A requires ATF4 for transcriptional activation of the serine biosynthetic pathway and for stimulation of cell proliferation. ATF4 has a key role in the cellular response to amino acid limitation, which leads to increased ATF4 expression primarily at the translational level. ATF4 in turn transcriptionally activates a large number of genes including those for amino acid synthesis and transport (Harding et al., 2003; Kilberg et al., 2009; Ye et al., 2012). Although the mechanistic detail remains to be defined, the observed functional connection between G9A and ATF4 provides further evidence for G9A as a component of the signaling pathway that responds to amino acid abundance.

It is well documented that cancer cells alter cellular metabolism to meet the biosynthetic challenge of growth and proliferation (DeBerardinis et al., 2008). Cancer metabolism is characterized by aerobic glycolysis with a high rate of glucose consumption and lactate production (Warburg, 1956). It is now increasingly recognized that a major function of aerobic glycolysis is to divert glycolic intermediates for the biosynthesis of macromolecules needed for cell growth and proliferation (Cairns et al., 2011; Vander Heiden et al., 2009). Accumulated evidence suggests that increased activation of the serine-glycine biosynthetic pathway is an important part of cancer metabolism (Kalhan and Hanson, 2012; Locasale, 2013). In addition to generating serine and glycine for the biosynthesis of proteins, purines (via one-carbon units), and lipids (via phosphatidylserine), this pathway produces equimolar amounts of reduced nicotinamide adenine dinucleotide (NADH), α-KG, and 5,10-MTHF (Figure 7H). These metabolites have critical roles in the control of cellular metabolism for cell proliferation and survival: NADH participates in ATP production and redox regulation (Corkey and Shirihai, 2012); α-KG supplies carbon to the tricarboxylic acid (TCA) cycle for the generation of many essential biosynthetic precursors (DeBerardinis et al., 2008); and 5,10-MTHF is a coenzyme for

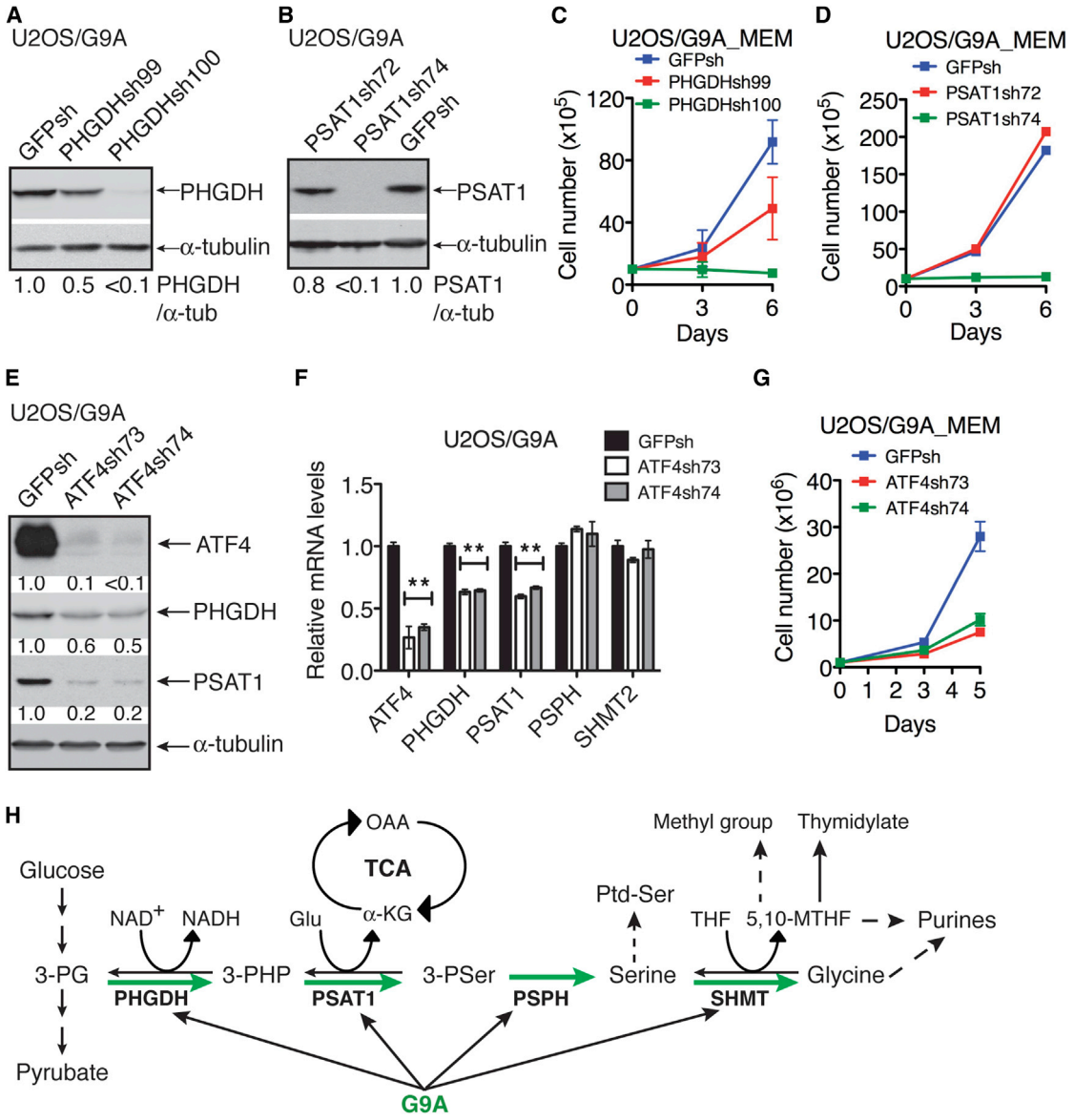

Figure 7. Activation of Serine-Glycine Biosynthesis Is Required for G9A to Promote Cell Proliferation

(A and B) Immunoblotting of PHGDH and PSAT1 in G9A-overexpressing U2OS cells with PHGDH (A) or PSAT1 (B) knockdown. PHGDH and PSAT1 levels were quantified against α-tubulin.

(C and D) Growth assay of G9A-overexpressing U2OS cells with PHGDH (C) or PSAT1 (D) knockdown. Error bars represent SD (n = 3).

(E and F) Immunoblot (E) and qRT-PCR (F) analysis of the expression of serine-glycine biosynthetic enzyme genes in G9A-overexpressing U2OS cells with ATF4 knockdown. **p < 0.001.

(G) Growth assay of G9A-overexpressing U2OS cells with ATF4 knockdown. Error bars represent SD (n = 3).

(H) Model for G9A regulation of serine metabolism. 3-PG, 3-phosphoglycerate; 3-PHP, 3-phosphohydroxypyruvate; 3-PSer, 3-phosphoserine; OAA, oxaloacetate; Ptd-Ser, phosphatidylserine.

See also Figure S5 and Table S3.

the only cellular pathway of de novo thymidylate biosynthesis catalyzed by thymidylate synthase and a major source of one-carbon units for purine synthesis and methyl group biogenesis, such as the generation of SAM, a coenzyme for histone and DNA methyltransferases (Kalhan and Hanson, 2012; Teperino et al., 2010; Tibbetts and Appling, 2010; Touroutoglou and Pazdur, 1996).

Importantly, we present evidence suggesting that the generation of 5,10-MTHF is crucial for the function of the serine-glycine biosynthetic pathway in promoting cancer cell survival and proliferation. We show that supplemental serine, but not glycine, is able to rescue the cell death phenotype induced by G9A inhibition or silencing. In addition, we show that supplemental serine synergizes with SHMT2 overexpression to enhance not

only cell survival but also cell proliferation under the condition of G9A inhibition. Since serine and glycine are interconvertible, the most obvious explanation for these observations is that the conversion of serine to glycine generates 5,10-MTHF, a metabolite essential for DNA replication and one-carbon metabolism. This model is also consistent with previous reports that the mitochondrial SHMT2 has a major role in the conversion of serine to glycine and 5,10-MTHF (Herbig et al., 2002; Narkewicz et al., 1996; Pfendner and Pizer, 1980; Stover et al., 1997; Tibbetts and Appling, 2010; Yoshida and Kikuchi, 1970). It should be pointed out that the mitochondrial enzyme glycine cleavage system catabolizes glycine into carbon dioxide, ammonia, and 5,10-MTHF (Tibbetts and Appling, 2010). Therefore, supplemental glycine could be a source of 5,10-MTHF when G9A is inhibited. However, G9A inhibition markedly reduces the steady-state levels of both serine and glycine. The demand for serine production from supplemental glycine would decrease the 5,10-MTHF pool. Thus, under the condition of G9A inhibition, 5,10-MTHF production from the cleavage of supplemental glycine might not be sufficient to sustain DNA synthesis and one-carbon metabolism.

Recent studies have identified a genetic mechanism for activating the serine-glycine biosynthetic pathway in breast cancer and melanoma through amplification of *PHGDH* (Locasale et al., 2011; Possemato et al., 2011). Our findings, coupled to the observation that G9A is overexpressed in various cancers (Chen et al., 2010; Cho et al., 2011; Huang et al., 2010; Kondo et al., 2008), suggest an epigenetic mechanism for activating this biosynthetic pathway in cancer cells. Thus, by increasing the amount of glycolic carbon diverted into macromolecule biosynthesis, G9A contributes to the generation of a metabolic microenvironment favorable for cancer cell survival and proliferation.

EXPERIMENTAL PROCEDURES

Cell Culture and Reagents

Cells were cultured in DMEM (HyClone SH30022, Thermo Scientific) or MEM (GIBCO 61100-061, Invitrogen) supplemented with 10% dialyzed FBS (GIBCO 26400-036). BIX01294 (B9311), CQ (C6628), and amino acids were purchased from Sigma-Aldrich. Stock solutions of 10 mM were made in DMSO (BIX) or H_2O (CQ). In all BIX experiments, DMSO was used as control (untreated). For rescue experiments, amino acids (100 mM stock in H_2O) were added to MEM at the final concentration of 0.4 mM (same as in DMEM). For serine deprivation assay, cells were cultured in MEM supplemented with nonessential amino acids (MEM-NEAA) and then transferred to serine-deficient MEM-NEAA. Phase contrast images were captured using an Axio Observer microscope and AxioVision software (Carl Zeiss MicroImaging). Trypan blue exclusion assay was used to assess cell growth and survival.

Immunoblotting

Cells were suspended in SDS sample buffer and protein concentrations determined using a protein assay kit (Bio-Rad). Proteins (20 μg) were separated on SDS-polyacrylamide gels, transferred to nitrocellulose membranes, and probed with primary antibodies detailed in Supplemental Experimental Procedures. Horseradish peroxidase-conjugated goat anti-mouse and anti-rabbit IgG (Santa Cruz Biotechnology) were used as secondary antibodies. Proteins were visualized using a SuperSignal West Pico chemiluminescence kit (Pierce) and quantified with ImageJ (version 1.47d). Films were exposed for various times for protein quantification within linear range of detection. For visualization and quantification with the Odyssey system, goat anti-mouse IRDye 800 or 680 and anti-rabbit IRDye 800 or 680 (LI-COR Biosciences) were used as secondary antibodies.

Immunofluorescence

Cells were fixed with 4% paraformaldehyde and costained with rabbit anti-LC3B (3868, Cell Signaling, 1:200) and mouse anti-α-tubulin (B-5-1-2, Sigma-Aldrich, 1:2000). All secondary fluorescence antibodies (Alexa Fluor 488 and 594) were from Molecular Probes and used at 1:1,000 dilution. Nuclei were stained with DAPI (D3571, Invitrogen) or Hoechst 33342 (H3570, Invitrogen). Fluorescent images were captured with an Axio Observer microscope and AxioVision software. For quantification of LC3B-positive puncta per cell, approximately 100 cells were counted from a random selection of four to six 630× fields independently by two investigators.

Microarray

Total RNA was isolated using Trizol (Invitrogen) from three independent samples of BE(2)-C cells with or without 5 μM BIX for 24 hr. Affymetrix microarray was performed using the Human Gene 1.0 ST microarray chip. Data were normalized, significance determined by ANOVA, and fold change calculated with the Partek Genomics Suite. GO analysis was performed with DAVID (Huang et al., 2009) for all differentially expressed genes ($\geq \pm 1.5$-fold, $p < 0.01$).

RNA-Seq

Total RNA was isolated using Trizol from three independent samples of U2OS cells either untreated or treated with 5 μM BIX for 6 or 24 hr. RNA-seq libraries were generated with an Illumina TruSeq RNA sample preparation kit (RS-122-2001) and sequenced using Illumina high-seq 2000 with a read length of 50 bp with pair ends. RNA-seq reads were mapped to the human genome (hg19) using TopHat (Trapnell et al., 2009). Only those reads mapped to unique genomic locations and with <5% mismatches were analyzed further. We used Cufflinks to measure gene transcripts, and Cuffdiff to identify differentially expressed genes with a RefSeq GTF file downloaded from Illumina iGenomes (Roberts et al., 2011). Deferentially expressed genes were fed into DAVID for functional annotation. Bioconductor (Gentleman et al., 2004) packages were used to generate heatmap.

qRT-PCR

Total RNA was isolated from three independent samples using Trizol. Reverse transcription was performed using SuperScript II Reverse Transcriptase (Invitrogen). Quantitative real-time PCR was performed using a RT^2 SYBR green/Fluorescein PCR master mix (SABiosciences) on an iQ5 real-time PCR system (Bio-Rad) with primers against *ATF4*, *CCNA2*, *CCNB1*, *CCNB2*, *CDC25C*, *PHGDH*, *PSAT1*, *PSPH*, *SHMT1*, *SHMT2*, and *B2M* (Table S3). All primer pairs were verified by melting curve analysis following qRT-PCR, with each primer pair showing a single desired amplification peak. All samples were normalized to β2 microglobulin mRNA levels.

ChIP-qPCR and ChIP-Seq

ChIP was performed as described (Lee et al., 2006), using 2×10^7 parental, GFP-overexpressing, or G9A-overexpressing U2OS cells with or without 5 μM BIX for the indicated times. Crosslinked chromatin was sheared through sonication and immunoprecipitated using ChIP grade mouse anti-H3K9me1 (17–680), rabbit anti-H3K9me2 (17–648), or control mouse IgG or rabbit IgG (all from Millipore). For qPCR, two independent ChIP samples were analyzed, and each sample was assayed in triplicate using primers that cover the promoter regions of *PHGDH* and *PSAT1*, and the coding region of *GAPDH* (detailed in Supplemental Experimental Procedures). For ChIP-seq, libraries were generated from ChIP samples using an Illumina TruSeq ChIP Sample Prep kit (IP-202-1012) and sequenced using Illumina high-seq 2000 with a read length of 50 bp with pair ends. Raw Illumina sequencing reads in the FASTQ format were cleaned using in-house scripts by trimming sequencing adaptors and low-quality bases in both ends (Q < 67 in Illumina 1.5). Cleaned sequences were then mapped to the human genome (hg19) using Novoalign v2.07. The reads that mapped uniquely to a single genomic locus were used for peak finding with MACS v1.4 (Zhang et al., 2008), and only those peaks with false discovery rate (FDR) <1% were compared with RefSeq genes in the UCSC genome browser.

Metabolite Analysis

GC-MS metabolomic analysis was performed in the University of Utah Metabolomics Core. Parental, GFP- or G9A-overexpressing U2OS cells

were cultured in MEM supplemented with 10% dialyzed FBS and were either untreated or treated with 5 μM BIX for 4 hr. Cells were washed with PBS, harvested by trypsin digestion, transferred to a microfuge tube, and frozen on dry ice. Metabolites were extracted by 80% methanol at −20°C and dried by vacuum centrifugation. Six biological replicate samples (5×10^6 cells/sample) were analyzed for each condition. GC-MS analysis was performed with a Waters GCT Premier mass spectrometer fitted with an Agilent 6890 gas chromatograph and a Gerstel MPS2 autosampler. Data were collected using MassLynx 4.1 software (Waters). Metabolites were identified and their peak area was recorded using QuanLynx. Data were normalized for extraction efficiency and analytical variation by mean centering the area of D4-succinate.

Flux Analysis

U2OS cells with or without overexpression of GFP or G9A were cultured in either glucose-deficient DMEM (11966-025, Invitogen) or MEM supplemented with 10% dialyzed FBS and 25 mM [U-^{13}C] glucose (CDLM-3813-1, Cambridge Isotope Laboratories) with or without 5 μM BIX for 16 hr before metabolite extraction with 80% methanol. Conversion of [U-^{13}C] glucose to other metabolites was analyzed by targeted LC-MS/MS using selected reaction monitoring (SRM) with a 5500 QTRAP mas spectrometer (Yuan et al., 2012). Three biological replicate samples were analyzed for each condition.

Analysis of Tumor Data Sets

The Versteeg NB88 data set contains 88 primary neuroblastoma tumors of all stages (Valentijn et al., 2012). Kaplan-Meier analysis was conducted online (http://r2.amc.nl), and the resulting survival curve and p value (log-rank test) were downloaded.

Statistics

Data are presented as mean ± SD. Statistics were determined with unpaired, two-tailed Student's t test using GraphPad Prism 6.01 for Mac.

ACCESSION NUMBERS

The NCBI Gene Expression Omnibus (GEO) accession number for the microarray data reported in this paper is GSE51512.

SUPPLEMENTAL INFORMATION

Supplemental Information includes five figures, three tables, and Supplemental Experimental Procedures and can be found with this article at http://dx.doi.org/10.1016/j.cmet.2013.11.004.

ACKNOWLEDGMENTS

We thank Dr. Vadivel Ganapathy for stimulating discussion and Min Yuan for help with metabolomic flux analysis. The work was supported by grants from NIH (R01CA124982), DoD (W81XWH-12-1-0613) and Georgia Cancer Coalition Distinguished Scholar Award to H.-F.D. In part, T.L. and X.W. were supported by grants from the National Natural Science Foundation of China (number 31172268 to T.L. and number 81172443 to X.W.) and J.M.A. by NIH grants (5P30CA006516 and 5 P01CA120964).

Received: June 7, 2013
Revised: August 30, 2013
Accepted: October 16, 2013
Published: December 3, 2013

REFERENCES

Adams, C.M. (2007). Role of the transcription factor ATF4 in the anabolic actions of insulin and the anti-anabolic actions of glucocorticoids. J. Biol. Chem. *282*, 16744–16753.

Black, J.C., Van Rechem, C., and Whetstine, J.R. (2012). Histone lysine methylation dynamics: establishment, regulation, and biological impact. Mol. Cell *48*, 491–507.

Cairns, R.A., Harris, I.S., and Mak, T.W. (2011). Regulation of cancer cell metabolism. Nat. Rev. Cancer *11*, 85–95.

Chen, M.-W., Hua, K.-T., Kao, H.-J., Chi, C.-C., Wei, L.-H., Johansson, G., Shiah, S.-G., Chen, P.-S., Jeng, Y.-M., Cheng, T.-Y., et al. (2010). H3K9 histone methyltransferase G9a promotes lung cancer invasion and metastasis by silencing the cell adhesion molecule Ep-CAM. Cancer Res. *70*, 7830–7840.

Cho, H.S., Kelly, J.D., Hayami, S., Toyokawa, G., Takawa, M., Yoshimatsu, M., Tsunoda, T., Field, H.I., Neal, D.E., Ponder, B.A., et al. (2011). Enhanced expression of EHMT2 is involved in the proliferation of cancer cells through negative regulation of SIAH1. Neoplasia *13*, 676–684.

Corkey, B.E., and Shirihai, O. (2012). Metabolic master regulators: sharing information among multiple systems. Trends Endocrinol. Metab. *23*, 594–601.

DeBerardinis, R.J., Lum, J.J., Hatzivassiliou, G., and Thompson, C.B. (2008). The biology of cancer: metabolic reprogramming fuels cell growth and proliferation. Cell Metab. *7*, 11–20.

de Koning, T.J., Snell, K., Duran, M., Berger, R., Poll-The, B.T., and Surtees, R. (2003). L-serine in disease and development. Biochem. J. *371*, 653–661.

Gentleman, R.C., Carey, V.J., Bates, D.M., Bolstad, B., Dettling, M., Dudoit, S., Ellis, B., Gautier, L., Ge, Y., Gentry, J., et al. (2004). Bioconductor: open software development for computational biology and bioinformatics. Genome Biol. *5*, R80.

Grummt, I., and Ladurner, A.G. (2008). A metabolic throttle regulates the epigenetic state of rDNA. Cell *133*, 577–580.

Harding, H.P., Zhang, Y., Zeng, H., Novoa, I., Lu, P.D., Calfon, M., Sadri, N., Yun, C., Popko, B., Paules, R., et al. (2003). An integrated stress response regulates amino acid metabolism and resistance to oxidative stress. Mol. Cell *11*, 619–633.

He, C., and Klionsky, D.J. (2009). Regulation mechanisms and signaling pathways of autophagy. Annu. Rev. Genet. *43*, 67–93.

Herbig, K., Chiang, E.P., Lee, L.R., Hills, J., Shane, B., and Stover, P.J. (2002). Cytoplasmic serine hydroxymethyltransferase mediates competition between folate-dependent deoxyribonucleotide and S-adenosylmethionine biosyntheses. J. Biol. Chem. *277*, 38381–38389.

Huang, W., Sherman, B.T., and Lempicki, R.A. (2009). Systematic and integrative analysis of large gene lists using DAVID bioinformatics resources. Nat. Protoc. *4*, 44–57.

Huang, J., Dorsey, J., Chuikov, S., Pérez-Burgos, L., Zhang, X., Jenuwein, T., Reinberg, D., and Berger, S.L. (2010). G9a and Glp methylate lysine 373 in the tumor suppressor p53. J. Biol. Chem. *285*, 9636–9641.

Kalhan, S.C., and Hanson, R.W. (2012). Resurgence of serine: an often neglected but indispensable amino acid. J. Biol. Chem. *287*, 19786–19791.

Kilberg, M.S., Pan, Y.X., Chen, H., and Leung-Pineda, V. (2005). Nutritional control of gene expression: how mammalian cells respond to amino acid limitation. Annu. Rev. Nutr. *25*, 59–85.

Kilberg, M.S., Shan, J., and Su, N. (2009). ATF4-dependent transcription mediates signaling of amino acid limitation. Trends Endocrinol. Metab. *20*, 436–443.

Kim, J., and Guan, K.L. (2011). Amino acid signaling in TOR activation. Annu. Rev. Biochem. *80*, 1001–1032.

Klionsky, D.J., Abeliovich, H., Agostinis, P., Agrawal, D.K., Aliev, G., Askew, D.S., Baba, M., Baehrecke, E.H., Bahr, B.A., Ballabio, A., et al. (2008). Guidelines for the use and interpretation of assays for monitoring autophagy in higher eukaryotes. Autophagy *4*, 151–175.

Kondo, Y., Shen, L., Ahmed, S., Boumber, Y., Sekido, Y., Haddad, B.R., and Issa, J.-P.J. (2008). Downregulation of histone H3 lysine 9 methyltransferase G9a induces centrosome disruption and chromosome instability in cancer cells. PLoS ONE *3*, e2037.

Kubicek, S., O'Sullivan, R.J., August, E.M., Hickey, E.R., Zhang, Q., Teodoro, M.L., Rea, S., Mechtler, K., Kowalski, J.A., Homon, C.A., et al. (2007). Reversal of H3K9me2 by a small-molecule inhibitor for the G9a histone methyltransferase. Mol. Cell *25*, 473–481.

Kuma, A., Hatano, M., Matsui, M., Yamamoto, A., Nakaya, H., Yoshimori, T., Ohsumi, Y., Tokuhisa, T., and Mizushima, N. (2004). The role of autophagy during the early neonatal starvation period. Nature *432*, 1032–1036.

Lee, T.I., Johnstone, S.E., and Young, R.A. (2006). Chromatin immunoprecipitation and microarray-based analysis of protein location. Nat. Protoc. *1*, 729–748.

Locasale, J.W. (2013). Serine, glycine and one-carbon units: cancer metabolism in full circle. Nat. Rev. Cancer *13*, 572–583.

Locasale, J.W., Grassian, A.R., Melman, T., Lyssiotis, C.A., Mattaini, K.R., Bass, A.J., Heffron, G., Metallo, C.M., Muranen, T., Sharfi, H., et al. (2011). Phosphoglycerate dehydrogenase diverts glycolytic flux and contributes to oncogenesis. Nat. Genet. *43*, 869–874.

Mizushima, N., Yamamoto, A., Hatano, M., Kobayashi, Y., Kabeya, Y., Suzuki, K., Tokuhisa, T., Ohsumi, Y., and Yoshimori, T. (2001). Dissection of autophagosome formation using Apg5-deficient mouse embryonic stem cells. J. Cell Biol. *152*, 657–668.

Mizushima, N., Yoshimori, T., and Levine, B. (2010). Methods in mammalian autophagy research. Cell *140*, 313–326.

Mosammaparast, N., and Shi, Y. (2010). Reversal of histone methylation: biochemical and molecular mechanisms of histone demethylases. Annu. Rev. Biochem. *79*, 155–179.

Narkewicz, M.R., Sauls, S.D., Tjoa, S.S., Teng, C., and Fennessey, P.V. (1996). Evidence for intracellular partitioning of serine and glycine metabolism in Chinese hamster ovary cells. Biochem. J. *313*, 991–996.

Peters, A.H.F.M., Kubicek, S., Mechtler, K., O'Sullivan, R.J., Derijck, A.A.H.A., Perez-Burgos, L., Kohlmaier, A., Opravil, S., Tachibana, M., Shinkai, Y., et al. (2003). Partitioning and plasticity of repressive histone methylation states in mammalian chromatin. Mol. Cell *12*, 1577–1589.

Pfendner, W., and Pizer, L.I. (1980). The metabolism of serine and glycine in mutant lines of Chinese hamster ovary cells. Arch. Biochem. Biophys. *200*, 503–512.

Pollari, S., Käkönen, S.M., Edgren, H., Wolf, M., Kohonen, P., Sara, H., Guise, T., Nees, M., and Kallioniemi, O. (2011). Enhanced serine production by bone metastatic breast cancer cells stimulates osteoclastogenesis. Breast Cancer Res. Treat. *125*, 421–430.

Possemato, R., Marks, K.M., Shaul, Y.D., Pacold, M.E., Kim, D., Birsoy, K., Sethumadhavan, S., Woo, H.K., Jang, H.G., Jha, A.K., et al. (2011). Functional genomics reveal that the serine synthesis pathway is essential in breast cancer. Nature *476*, 346–350.

Rabinowitz, J.D., and White, E. (2010). Autophagy and metabolism. Science *330*, 1344–1348.

Rice, J.C., Briggs, S.D., Ueberheide, B., Barber, C.M., Shabanowitz, J., Hunt, D.F., Shinkai, Y., and Allis, C.D. (2003). Histone methyltransferases direct different degrees of methylation to define distinct chromatin domains. Mol. Cell *12*, 1591–1598.

Roberts, A., Pimentel, H., Trapnell, C., and Pachter, L. (2011). Identification of novel transcripts in annotated genomes using RNA-Seq. Bioinformatics *27*, 2325–2329.

Seo, J., Fortuno, E.S., 3rd, Suh, J.M., Stenesen, D., Tang, W., Parks, E.J., Adams, C.M., Townes, T., and Graff, J.M. (2009). Atf4 regulates obesity, glucose homeostasis, and energy expenditure. Diabetes *58*, 2565–2573.

Shinkai, Y., and Tachibana, M. (2011). H3K9 methyltransferase G9a and the related molecule GLP. Genes Dev. *25*, 781–788.

Stover, P.J., Chen, L.H., Suh, J.R., Stover, D.M., Keyomarsi, K., and Shane, B. (1997). Molecular cloning, characterization, and regulation of the human mitochondrial serine hydroxymethyltransferase gene. J. Biol. Chem. *272*, 1842–1848.

Tachibana, M., Sugimoto, K., Nozaki, M., Ueda, J., Ohta, T., Ohki, M., Fukuda, M., Takeda, N., Niida, H., Kato, H., and Shinkai, Y. (2002). G9a histone methyltransferase plays a dominant role in euchromatic histone H3 lysine 9 methylation and is essential for early embryogenesis. Genes Dev. *16*, 1779–1791.

Teperino, R., Schoonjans, K., and Auwerx, J. (2010). Histone methyl transferases and demethylases; can they link metabolism and transcription? Cell Metab. *12*, 321–327.

Tibbetts, A.S., and Appling, D.R. (2010). Compartmentalization of Mammalian folate-mediated one-carbon metabolism. Annu. Rev. Nutr. *30*, 57–81.

Touroutoglou, N., and Pazdur, R. (1996). Thymidylate synthase inhibitors. Clin. Cancer Res. *2*, 227–243.

Trapnell, C., Pachter, L., and Salzberg, S.L. (2009). TopHat: discovering splice junctions with RNA-Seq. Bioinformatics *25*, 1105–1111.

Valentijn, L.J., Koster, J., Haneveld, F., Aissa, R.A., van Sluis, P., Broekmans, M.E., Molenaar, J.J., van Nes, J., and Versteeg, R. (2012). Functional MYCN signature predicts outcome of neuroblastoma irrespective of MYCN amplification. Proc. Natl. Acad. Sci. USA *109*, 19190–19195.

Vander Heiden, M.G., Cantley, L.C., and Thompson, C.B. (2009). Understanding the Warburg effect: the metabolic requirements of cell proliferation. Science *324*, 1029–1033.

Warburg, O. (1956). On respiratory impairment in cancer cells. Science *124*, 269–270.

Ye, J., Mancuso, A., Tong, X., Ward, P.S., Fan, J., Rabinowitz, J.D., and Thompson, C.B. (2012). Pyruvate kinase M2 promotes de novo serine synthesis to sustain mTORC1 activity and cell proliferation. Proc. Natl. Acad. Sci. USA *109*, 6904–6909.

Yoshida, T., and Kikuchi, G. (1970). Major pathways of glycine and serine catabolism in rat liver. Arch. Biochem. Biophys. *139*, 380–392.

Yuan, X., Feng, W., Imhof, A., Grummt, I., and Zhou, Y. (2007). Activation of RNA polymerase I transcription by cockayne syndrome group B protein and histone methyltransferase G9a. Mol. Cell *27*, 585–595.

Yuan, M., Breitkopf, S.B., Yang, X., and Asara, J.M. (2012). A positive/negative ion-switching, targeted mass spectrometry-based metabolomics platform for bodily fluids, cells, and fresh and fixed tissue. Nat. Protoc. *7*, 872–881.

Zhang, Y., Liu, T., Meyer, C.A., Eeckhoute, J., Johnson, D.S., Bernstein, B.E., Nusbaum, C., Myers, R.M., Brown, M., Li, W., and Liu, X.S. (2008). Model-based analysis of ChIP-Seq (MACS). Genome Biol. *9*, R137.